In vitro Investigation of Metabolism, Bioactivation, and Botanical-Drug Interactions of Licorice

BY

KE HUANG

M.S., University of Minnesota, Minneapolis, MN, 2008

B.S., Peking University, Beijing China, 2005

THESIS

Submitted in partial fulfillment of the requirements

for the degree of Doctor of Philosophy in Medicinal Chemistry

in the Graduate College of the

University of Illinois at Chicago, 2017

Chicago, Illinois

Defense Committee:

Richard B. van Breemen, Chair and Advisor
Joanna E. Burdette
Chun-Tao Che
Donald P. Waller, Biopharmaceutical Sciences
Dejan S. Nikolic

TABLE OF CONTENTS

TABLE OF CONTENTS (continued)

TABLE OF CONTENTS (continued)

LIST OF TABLES

LIST OF FIGURES

LIST OF FIGURES (continued)

LIST OF FIGURES (continued)

LIST OF FIGURES (continued)

LIST OF FIGURES (continued)

LIST OF FIGURES (continued)

Chapter 1 Introduction

1.1 Botanical Dietary Supplements

1.1.1 Botanical Dietary Supplements as Alternative Medicines

The term “botanical”, is usually used to refer a plant or part of a plant that has therapeutic value or natural flavor/color. In the United States, Congress defined “dietary supplement” in the Dietary Supplement Health and Education Act (DSHEA) of 1994. Specifically, a dietary supplement contains ingredients to supplement the diet when taken by mouth, and the ingredients may include: vitamins, amino acids, minerals, herbs or other botanicals.[1]

Based on the National Health and Nutrition Examination Survey, 53% of American adults took at least one dietary supplement from 2003 to 2006, of which vitamins and minerals were most commonly consumed by 39% of all adults, followed by calcium and omega-3 or fish oil supplements. Women were also reported more likely than men to take dietary supplements.[2] The most commonly reported reasons for using supplements were to improve (45%) or maintain (33%) overall health. Women used calcium products for bone health (36%), whereas men were more likely to report supplement use for heart health or to lower cholesterol (18%). Interestingly, only 23% of products were used based on recommendations of a health care provider.[3]

According to U.S. federal law, no evidence of safety or efficacy is required for botanical dietary supplements prior to marketing. Recently, U.S. FDA implemented Good Manufacturing Practice to control the quality of dietary supplements.[4] Although they expect a safe product and anticipate beneficial effects, many consumers are unaware that botanical dietary supplements in the United States are not necessarily tested for either safety or efficacy. Some potential safety issues that are being addressed by implementation of GMP in the botanical dietary supplement industry include mis-identification or mislabeling of the plant species, adulteration with pharmaceutical agents, and contamination with pesticides, herbicides, heavy metals, or microbes.[5] Given the complexity of the many natural products comprising botanicals, obtaining scientific evidence for their efficacy and safety can be challenging and varies widely among species. A wide range of testing including the application of conventional and novel analytical tools as well as preclinical and clinical toxicity and efficacy studies needs to be utilized to establish health benefits as well as risks of botanical dietary supplements.

Recently, national retailers of dietary supplements – GNC, Wal-Mart, Walgreens, and Target were accused by the Attorney General of the State of New York of contamination, substitution and false labeling of herbal products.[6] This investigation relied on DNA bar-coding, an analytical test which identifies botanical ingredients through genetic fingerprinting and comparison with known botanical species.[7,8] This incident has renewed public and regulatory interest in the issue of botanical dietary supplement safety and demonstrates that state-of-the-art analytical methods can have an impact on this field.

The UIC/NIH Center for Botanical Dietary Supplements Research has been evaluating the safety and efficacy of botanicals since 1999. Funded by the National Institutes of Health National Center for Complementary and Integrative Health and Office of Dietary Supplements (grant P50 AT000155), the center's medicinal chemists and pharmacognosists are investigating botanical dietary supplements used by menopausal women as alternatives to hormone therapy. Center researchers have developed innovative analytical approaches to characterize and identify botanical species and their natural product constituents, evaluate biological activity, and determine through preclinical and clinical testing the safety and efficacy of botanicals relevant to women's health. Some of these botanicals include red clover (*Trifolium pratense*), black cohosh (*Cimicifuga racemesa*), hops (*Humulus lupus*), wild yam (*Dioscorea villosa*), and licorice (*Glycyrrhiza glabra*).[9-16]

1.1.2 Licorice

The dried roots of licorice have been consumed for the past 6000 years. Licorice is used as a flavoring and sweetening agent in the western world and as anti-allergic and anti-inflammatory agents in Asian countries including China, Japan and Korea. There are more than 15 species of licorice listed under the genus of *Glycyrrhiza*, of which four are commonly used in botanical dietary supplements: *G. glabra* (licorice or liquorice), *G. uralensis* (Chinese licorice), *G. inflata*, and *G. lepidota* (American licorice). Many licorice constituents have been reported, but only recently has there been progress in

distinguishing secondary metabolite differences among various licorice species. *G. glabra* and *G. inflata* produce similar levels of glycyrrhizin, liquiritin, liquiritin apioside, isoliquiritin, isoliquiritin apioside, and liquiritigenin. However, *G. uralensis* differs from *G. glabra* or *G. inflata* by expressing higher levels of liquiritin, isoliquiritin and liquiritigenin.[17] Glabridin (**Figure 1**), glycycoumarin and licochalcone A are species-specific constituents of *G. glabra*, *G. uralensis*, and *G. inflata*, respectively.[17] Other components that have been isolated from licorice species include triterpenoid saponins, flavonoids, polysaccharides, pectins, simple sugars, amino acids, and mineral salts.[18] Glycyrrhizin is composed of a hydrophilic part, two glucuronic acids, and a hydrophobic fragment, glycyrrhetic acid. It accounts for the sweet taste of licorice root, which is 30–50 times sweeter than sucrose. Glycyrrhizin has been found in *G. glabra*, *G. uralensis*, and *G. inflata* with similar levels.[17] Glabrene, an isoflavene that has been reported only in *G. glabra*, showed estrogen receptor (ER) agonism in different tissues and antimicrobial activity against *Helicobacter pylori in vitro*.[19,20] The yellow color of licorice is due to the flavonoid content, which includes liquiritin, isoliquiritin, and other compounds. In this dissertation, experiments were carried out only using preparations of *G. glabra*, and the remaining background is focused on this species and compounds found therein.

As one of the most widely consumed botanicals, licorice is traditionally used to treat gastric ulcers, constipation, cough, stomachache, cystitis, diabetes, tuberculosis, kidney stones, and polycystic ovary syndrome. It is also reported that different parts of the licorice may be used to treat different diseases.[21] Plenty of *in vitro* and *in vivo* studies have been performed to understand the mechanisms of actions including anti-

inflammatory, anti-microbial, anti-viral, anti-oxidative, and anti-cancer activities. The herb and its constituents have been also studied in central nervous system, cardiovascular, renal, and respiratory diseases.[21,22] Licorice constituents also exhibit hepatoprotective activity by lowering serum liver enzyme levels and improving tissue pathology in hepatitis patients.[23]

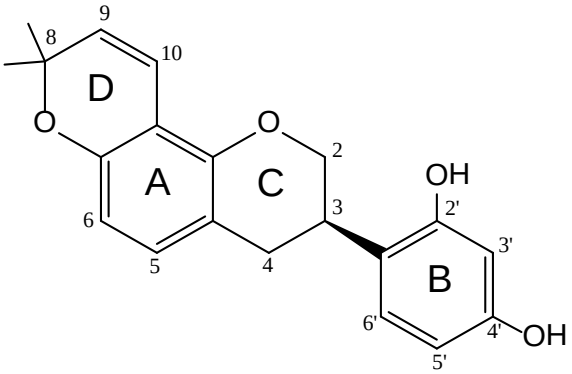

Figure 1. Chemical structure of glabridin, an isoflavan from licorice root.

Overdose of licorice that contains glycyrrhizin and hydrolyzed metabolite glycyrrhetic acid can lead to a syndrome known as apparent mineralocorticoid excess which results from the inhibition of the enzyme 11-ß-HSD and binding to the mineralocorticoid receptor, subsequently increasing in the activity of cortisol.[24] The mineralocorticoid effect can be abated after cessation of intake, adequate potassium replacement and spironolactone therapy.[25] The most published licorice-related complications were hypertension, hypokalemia and other signs of mineralocorticoid excess. Over consumption of glycyrrhizin can also lead to sensitivity to an adrenal hormone due to an acquired reduction in the activity of 11-ß-HSD, which is known as pseudo-hyperaldosteronism, creating secondary side effects of high blood pressure, edema and

more. Pseudo-hyperaldosterionism falls into one type of hyperaldosteronism where suppressed rennin activity and aldosterone level mimic hyperaldosteronism.

Daily consumption of licorice (*G. glabra*) ranges from 3 to 15 g of dried root to 500 mg to 1500 mg of extract.[26-28] In 1991, the European Union proposed a provisional figure of 100 mg/day as the upper limit for ingestion of glycyrrhizin (approximately the amount found in 60–70 g licorice).[29] The content of glycyrrhizin in licorice roots varies from 2 to 25%, depending on the particular species. The typical content of glabridin in licorice is approximately 0.08 to 0.35% of dry weight, and in some licorice extract products, the levels of glabridin reach 1.2 to 11.6%.[30,31] Licorice and its derivatives, including ammoniated glycyrrhizin, are generally recognized as safe (GRAS) for use in foods by the US Food and Drug Administration (FDA). The dietary supplement industry manages the glycyrrhizin toxicity by controlling glycyrrhizin percentage based on FDA guidance for different food categories.[25]

Glycyrrhizin has been shown to inhibit growth and cytopathology of RNA and DNA viruses including hepatitis A and C, *Herpes zoster*, HIV, *Herpes simplex*, and CMV.[32-39] Glycyrrhizin and other licorice components have been reported to inhibit abnormal cell proliferation and tumor formation in breast, liver, and skin cancer.[40-43] Glycyrrhizin and its metabolites inhibit hepatic metabolism of aldosterone and suppress 5-β-reductase. In vitro studies have indicated that glycyrrhizin can inhibit cyclooxygenase activity and prevent prostaglandin formation, as well as indirectly inhibiting platelet aggregation, all factors in inflammatory processes.[44,45] Liquiritigenin was found to be the principle phytoestrogen of the licorice extracts and induced ER-β specific activity in transfection

assays and competitive binding assays. However isoliquiritigen, the precursor chalcone of liquiritigenin, demonstrated significant estrogenic activities but was indifferent for both ER subtypes.[46,47] Flavonoid components of *G. glabra* root extract (glabridin, glabrene, etc.) have been shown to have anti-tumorigenic, anti-microbial, anti-viral, anti-inflammatory, anti-allergic, estrogen-like, and anti-oxidative activities.[19,20,48-51] Estrogenic activities of both glabridin and glabrene have been established by means of competitive ligand biding assays, in vitro cell assays and in vivo animal models.[28,52,53] The glabridin and hispaglabridins A and B from licorice have significant antioxidant activities, and both glabridin and glabrene possess estrogen-like activity.[19,30,54] They inhibit Fe^{3+}-induced mitochondrial lipid peroxidation in rat liver cells.[55] Glabridin has been also shown to inhibit the activity of macrophage NADPH-oxidase, presumably by inhibiting protein kinase C and serotonin re-uptake.[56,57] Glycyrrhizin and glabridin can prevent oxidative DNA fragmentation in UVB-irradiated human keratinocyte cultures.[58] Glabridin was reported to inhibit prostaglandin formation as well as inhibit lipoxygenase and cyclooxygenase.[59] Interestingly, glabridin has been reported to have an anti-obesity effect by inhibiting adipogenesis in 3T3-L1 cells as well as positive effects on cognitive functions and cholinesterase activity in mice.[60,61]

1.2 Drug Metabolism in Drug Discovery and Development

Pharmaceutical companies have invested extensively in drug discovery and development in order to bring effective and safe medicinal agents to market while satisfying healthcare

needs. It is estimated that the average cost of bringing a drug from discovery and development to market is near $1 billion, and most drug candidates fail during this lengthy 8-12 year process. During drug metabolism, lipophilic xenobiotics are transformed by human enzymes to more hydrophilic products for elimination from the body. Drug metabolism connects many aspects of drug discovery and development including pharmacology, medicinal chemistry, candidate optimization, preclinical and clinical development, and toxicology. The importance of drug metabolism and pharmacokinetics (DMPK) is best illustrated as 40% of the drug attrition during development before 1990 was due to undesirable DMPK properties. With more awareness in early development and technology advances, DMPK based drug failure during the clinical development stage was reduced to less 1%, saving billions of dollars for the pharmaceutical industry and the healthcare system.[62,63]

1.2.1 Metabolic Stability

Metabolic stability studies offer a simple way of assessing how rapidly a drug candidate undergoes biotransformation by a defined enzymatic system. Metabolic stability information is used to prioritize lead compounds, optimize drug candidates, and provide preliminary understanding for further drug metabolism studies, such as metabolite characterization and identification of metabolizing enzymes. It is the early stage of evaluation of human systemic exposure for a drug candidate and its related metabolites.

A typical metabolic stability test is conducted in vitro with liver microsomal fractions and cryopreserved hepatocytes. Intrinsic clearance (CLint) and half-life ($t_{1/2}$) indicate the ability of hepatic enzymes to metabolize the drug candidates. The clearance and half-life are calculated by monitoring the rate of disappearance of the drug candidate (change of concentration) before and after incubation with an enzyme system.[64] Time-dependent studies and data fitting with pre-determined models with more than two time points are needed to ensure a reliable estimate when more than 50% of the lead compound is metabolized. An acceptable metabolic stability is expected for lead candidates to have reasonable bioavailability *in vivo*. As most metabolic stability studies use *in vitro* systems, good correlation between in vivo hepatic clearance and *in vitro* results is critical, and this has been well documented for many assay systems.[65,66]

1.2.2 Metabolizing Enzymes and Metabolites

Cytochrome P450 enzymes are a family of heme-monooxygenases located in most types of tissue and concentrated in human liver. They are involved in the oxidation of diverse drugs and xenobiotics and catalyze most phase I metabolism and convert lipophilic xenobiotics into more water soluble products, facilitating their elimination from the body.[67] The common reactions catalyzed by cytochrome P450 enzymes include hydroxylation, heteroatom oxygenation, epoxidation, and oxidation of olefins and acetylenes.[68] The metabolism of xenobiotics usually results in more hydrophilic metabolites that are less pharmacologically active and more rapidly eliminated from the

body. In general, cytochrome P450-catalyzed oxidation causes detoxification, but these enzymes can also convert some xenobiotics to more toxic products. Cytochrome P450 enzymes are therefore responsible for either deactivation or bioactivation of the majority of xenobiotics.[69] Cytochrome P450 enzymes are classified into families, subfamilies and specific enzymes based on amino acid sequence homology. The CYP1, CYP2, and CYP3 families are responsible for the oxidative metabolism of more than 90% of clinically used drugs, while CYP3A4 alone is responsible for almost 50% of drug metabolism followed by CYP2D6 (30%) and CYP2C9 (10%).[70,71]

Other major oxidative enzymes include flavin-containing monooxygenases (FMOs) and monoamine oxidases (MAOs). Like cytochrome P450 enzymes, FMOs are located in the endoplasmic reticulum. FMOs usually catalyze heteroatom oxygenation.[72] MAOs oxidize amines as indicated by their names and are located in the outer mitochondrial membrane of liver and other tissues.[73] After oxidative metabolism introduces or exposes heteroatoms with active hydrogen, conjugation reactions can occur that are catalyzed by enzymes such as UDP-glucuronosyltransferases (UGTs), sulfotransferases (SULTs) and glutathione-S-transferases (GSTs), which are responsible for conjugation of xenobiotics with glucuronic acid, sulfonyl group and glutathione, respectively.[74-76]

Used as an *in vitro* model of drug metabolism, human liver microsomes are fractions of endoplasmic reticulum primarily from hepatocytes with high concentrations of cytochrome P450 enzymes. Human hepatocytes are also used for the investigation of xenobiotic metabolism. Since human hepatocytes contain both phase I and phase II

enzymes as well as their co-factors such as reduced nicotinamide adenine dinucleotide phosphate (NADPH) and uridine diphosphoglucuronic acid (UDPGA), this model is more complete than human liver microsomes for the study of hepatic drug transformation reactions.[77]

cDNA-expressed recombinant cytochrome P450 enzymes provide an alternative *in vitro* system for metabolic stability studies, identification of metabolizing enzymes, and drug interaction investigation. They offer opportunities to study drug metabolism with a specific subtype of CYP enzymes by removing the interfering enzyme activities present in microsomes and other mixed enzyme preparations. The comparability of clearance and enzymatic activities between these recombinant CYPs and human liver microsomes has been evaluated.[78]

Although xenobiotic metabolism is usually a detoxification process rendering drugs and similar molecules more polar and more rapidly excreted, metabolic transformation may result in electrophilic products that are potentially more toxic than their precursors.[79,80] There are many examples of metabolic activation of drugs to electrophiles that covalently bind to macromolecules causing cell damage, and this process is responsible for 60% of instances where drugs had to be withdrawn from the US market or had black box warnings added to their packaging due to hepatotoxicity.[81,82] To address this safety concern, lead compounds are typically evaluated early during drug discovery and development for the formation of reactive metabolites and then chemically modified or abandoned to avoid this potentially toxic pathway.

Like drugs, herbal and dietary constituents may be metabolized by cytochrome P450 enzymes to nontoxic metabolites and excreted from the body, but the formation of toxic metabolites is also possible. In addition, the formation of reactive intermediates by CYP450 enzymes may also lead to the enzymatic inactivation.[83] Although there are many possible mechanisms of herbal toxicity, the formation of reactive species that might covalently bind to cellular proteins and/or DNA resulting in cytotoxicity, oncogene activation, and hypersensitivity should be considered.[84]

Glycyrrhizin is one of the major components of licorice extract and it is reported to be metabolized to 18β-glycyrrhetinic acid by β-glucuronidase of human intestinal bacteria before getting absorbed into the body.[85] Two pathways of glycyrrhizin have been proposed: directly from glycyrrhizin to glycyrrhetinic acid and indirect metabolism via glycyrrhetinic acid-glucuronide.[86] As the main metabolite of glycyrrhizin, glycyrrhetinic acid was also studied for metabolism by human and rat liver microsomes; however, only enzyme kinetic data was reported with Km of 33.4 μM and Vmax of 2.2 nmol/mg proteain/min for human liver microsomes and Km of 24.2 μM and Vmax of 6.9 nmol/mg proteain/min for human liver microsomes.[87] CYP3A4 was likely to be the major metabolizing enzyme for human liver microsomes metabolism of glycyrrhetinic acid while CYP2C9 and CYP2C19 were considerably less active. Isoliquiritigenin, a common chalcone found in licorice and other plants was investigated for metabolism by human liver microsomes. Aromatic hydroxylation and reduction of carbon-carbon double bond and cyclization were reported.[88] CYP2C19 was found to contribute significantly to the

formation of butein from isoliquiritigenin. Very recently, some other bioactive licorice compounds from *G. uralensis* were investigated for *in vivo* metabolism in rats including glycyoumarin, glycyrol, licoflanonol, licoricidin, licoisoflavanone, isoglycycoumarin, semilicoisoflavnoe B, and 3-methoxy-9-hydroxy-pterocarpan.[89-91] Phase II metabolism, glucuronidation and sulfation, were the main metabolic pathways for phenolic compounds while hydroxylation as minor reaction was also observed.[89] Other non-phenolic compounds mostly underwent hydroxylation, hydrogenation, and dehydrogenation.[90,91]

1.2.3 Drug Interactions

Drug interactions occur when a co-administered compound affects the activity of a drug. Such interactions have been observed between drugs, between drugs and foods, and between drugs and herbs.[92,93] Drug interactions can alter various processes in the human body including absorption, distribution, metabolism, and excretion as well as change the pharmacological properties of a drug at the site of action, resulting in toxicity or loss of efficacy. Many drug interactions are due to alterations in drug metabolism during which the drug is biotransformed by metabolizing enzymes such as cytochrome P450s.

Metabolism-based drug interactions are categorized into 1) drug inhibition, where the activity of a drug metabolizing enzyme is decreased by the interfering substance, and 2) drug induction, where drug metabolizing enzyme activity becomes elevated. The

inhibition of drug metabolizing enzymes that act on drugs with a narrow therapeutic window may lead to serious toxicological risk while inductive drug interaction can result in decreased plasma concentration and higher burden of metabolites which may also cause safety issues. The majority of drug-drug interactions result from inhibition of cytochrome P450 enzymes. Inhibition of cytochrome P450 enzymes, especially CYP3A4 which accounts for ~30% of the cytochrome P450 enzymes in human liver and is responsible for the metabolism of ~70% of all drugs,[94] is also responsible for most clinical problems associated with drug-botanical interactions.

Drug transporters are important in facilitating membrane permeation of drugs and affect absorption, excretion, and tissue distribution.[45,95-97] Most transporters have broad substrate acceptance, and multiple transporters can have overlapping substrates. Therefore, many transporter-mediated drug interactions have been reported.[98]

It is critical to estimate the possible interactions with existing drugs when developing new therapeutic agents. The U.S. FDA has published a guidance for industry regarding how to evaluate potential drug interactions during drug discovery and development.[99] This preclinical process includes metabolic phenotyping, drug inhibition evaluation and drug induction evaluation. Major metabolic pathways of the drug of interest are identified during metabolic phenotyping, which allows for specific studies of potential interactions of the drug in the defined pathways. During drug inhibition assessment, the ability of the test agent to inhibit the activities of known metabolizing enzymes for particular metabolic pathways is evaluated. If the substance is an inhibitor or an inducer of a particular

metabolizing enzyme, then the substance will have the potential to affect the metabolism of any drugs that are substrates of that enzyme.

Constituents of botanical dietary supplements may be substrates, inhibitors or inducers of metabolizing enzymes such as CYPs and can affect metabolism and pharmacokinetics of co-administered drugs.[100] Potential interactions depend on the botanical, preparation method and dose. Given the complexity of botanical dietary supplements, evaluating botanical-drug interactions is challenging and is often neglected by industry as such studies are not usually required. Experience has shown that botanical-drug interactions can have significant clinical and toxicological implications, and well-designed studies, based on the FDA guidance for drug-drug interactions, are needed.[100-102] St. John's wort, an herbal medicine for depression, has been reported to interaction with prescribed drugs. Clinical trials have shown that St. John's wort induces CYP3A4, CYP2E1, and CYP2C19.[103-105] It has also been reported that St. John's wort lowers the concentrations of P-glycoprotein substrates, including digoxin, fexofenadine, and talinolol.[106-108]

Licorice root extract (*G. glabra*) was reported to inhibit CYP3A4 in both concentration- and time-dependent manner using 7-benzyloxy-trifluromethylcoumarin O-debenzylation as probe reaction.[109] In another study, inhibitions of CYP3A4 and CYP2D6 were observed by licorice extracts (ethanol and DMSO) with IC_{50} of 129-141 μg/mL and 125-132 μg/mL for CYP3A4 and CYP2D6, respectively.[110] Several licorice compounds have been studied for CYP450 enzyme inhibition *in vitro*. Glycyrrhizin was found inactive for CYP3A4 inhibition in one study[111] while another study[110] reported fairly strong inhibition

of CYP3A4 (IC_{50} 172-175 µg/mL) and CYP2D6 (IC_{50} 153-156 µg/mL). Glycyrrhetinic acid showed mixed inhibition of recombinant CYP3A4 enzyme with an IC_{50} of 7.25 µM, a Km of 4.3 µM, a Ki of 6.4 µM, and a Vmax of 176.8 µg/min/µg protein.[112] Another study reported inhibition of CYP2C9 with an IC_{50} of 32.8 µM and CYP3A4 with IC_{50} of 13.8 µM.[87] Not many flavonoids from licorice have been investigated for CYP450 enzyme inhibition until very recently, and several potent CYP inhibitors have been identified. In 2015, a study revealed that licochalcone A, a common constituent of *G. uralensis* significantly inhibited CYP1A2 (IC_{50} 1.15 µM), 2C8 (IC_{50} 1.22 µM), 2C9 (IC_{50} 0.64 µM), and 3A4 (IC_{50} 2.77 µM).[113] The enzyme kinetics showed competitive inhibition of CYP3A4 and mixed-inhibition of CYP1A2, 2C9, 2C19, and 2C8. In 2016, Glycyrol from *G. uralensis* was also found to competitively inhibit CYP1A2 and CYP2C9 with IC_{50} of 2.2 µM and 0.13 µM.[114] In a more comprehensive study, 40 licorice compounds from *G. uralensis* were tested for enzyme inhibition of CYP1A2, 2C9, 2C19, 2D6, and 3A4.[115] Strong, sub-micromolar IC_{50} values were reported for CYP1A2 (2 compounds) and CYP2C9 (5 compounds). Glabridin was reported to inactivate cytochrome P450 enzyme isoform 3A4 (CYP3A4) and CYP2B6 in a time- and concentration-dependent manner and to competitively inhibit CYP2C9.[109] Incubations with 2,4-dimethylglabridin did not lead to a loss in the enzymatic activity of CYP3A4, suggesting that the two hydroxyl groups on the 2' and 4' positions of the flavonoid B ring of glabridin are needed for CYP3A4 inactivation.[109] These two hydroxyl groups are also believed to be essential for its anti-oxidant activity.[116] However, no mechanism is known for the inhibition of CYP3A4 and CYP2B6 by glabridin.

1.3 Application of Liquid Chromatography-Mass Spectrometry to Drug Discovery and Development

1.3.1 Liquid Chromatography and Mass Spectrometry Instrumentation

High performance liquid chromatography (HPLC) is a common analytical technique with numerous applications in pharmaceutical research and development, including high throughput screening and performance assays in early discovery, drug metabolism and pharmacokinetics studies in preclinical development, and process development and quality control in clinical and commercial manufacturing. In many labs in industry and academia, conventional liquid chromatography and HPLC are still widely used, although the state-of-art in chromatography is now ultrahigh pressure/performance liquid chromatography (UHPLC).

Typical characteristics of UHPLC include higher pressure limits (up to 15,000 psi instead of 6,000 psi for HPLC), fast flow rates (up to 2 mL/min), sub-2 µm sorbent particle sizes, and small dwell volumes (100-200 µL), leading to high throughput, high resolution, high sensitivity, and improved accuracy.[117] Compared with conventional HPLC, UHPLC enables up to 10-fold faster separations without sacrificing resolution. The use of sub-2 µm particles significantly enhances chromatographic separation efficiency with decreased peak width enabling the separation of complex samples such as botanical extracts and other biological materials.

Compatible with on-line UHPLC separations, mass spectrometry adds another analytical dimension to drug discovery and development. Based on the measurement of *m/z* ratios of ions, mass spectrometer analyzers may be categorized by their mechanism of ion separation: beam-type analyzers (magnetic sector and quadrupole), pulsed analyzers (time-of-flight) and ion-trapping mass analyzers (cyclotron, orbitrap, quadrupole traps).[118] Both quadrupole and ion trap mass spectrometers have been extensively used in pharmaceutical industry for detecting small molecules and large proteins. In general, triple-quadrupole tandem mass spectrometry (MS/MS) with multiple scan modes are used for quantitative analysis while ion trap mass spectrometers offer limited scan range but more structural information through MS^n capability.

Techniques that advance with instrumentation development also provide new tools for biomedical research. Stable isotope labeling has been widely used to facilitate identification of molecules of interest among complex mixtures during mass spectrometric analysis.[119] Accurate mass measurements, which provide elemental composition information, are commonly used in the identification of drug metabolites during both *in vivo* and *in vitro* studies.[120] Computer based algorithms enable mass spectrometers to adjust the type of measurements being made while acquiring data in real time. For example, data-dependent acquisition during a survey scan (normal scan, precursor ion scan, or constant neutral scan), can provide information that signals the mass spectrometer system to switch from one type of scan (such as MS) to MS/MS mode (or from one type of MS/MS to another) when pre-defined criteria are met, thereby

maximizing mass spectrometric information within a single run.[121] As another example, mass defect filters have been developed for drug metabolism studies that based on the mass defects (the difference between the exact molecular mass and nominal molecular mass) of common metabolites. Typically within a 50 mDa window, high mass accuracy mass spectrometers can filter out interfering ions with mass defects falling out of the window, significantly increasing the data clarity and improving the operation work flow.[122]

1.3.2 Applications of LC-MS in Drug Discovery and Development

HPLC or UHPLC interfaced with mass spectrometry (LC-MS) are used extensively for drug metabolism studies during drug discovery and development. In the early phase of drug discovery, metabolism studies focus on metabolic stability and metabolic pathways of the lead compounds, where identification of the metabolic soft spots is essential for compound optimization and further development. LC-MS is used to evaluate the rate of disappearance of the compound of interest by detecting its concentration before and after incubation with hepatic enzymes. For example, LC-MS/MS analysis using a linear ion trap mass spectrometer has been used to obtain metabolic stability and metabolite information for an investigation compound within a single run.[123]

Metabolite characterization is central to drug metabolism studies during discovery and preclinical stage development. After hepatic incubation of a compound under

investigation, HPLC separation and MS/MS analysis are performed to characterize and to help identify metabolites. In general, a compound eluting from the HPLC is weighed in the mass spectrometer (MS) and then fragmented to form structurally significant product ions (MS/MS). Most xenobiotic metabolites retain large parts of the parent molecules, enabling the use of precursor ion (PI) scanning of all molecular species in a metabolite mixture to be particularly useful for detecting metabolites that form a common product ion. Sometimes, a xenobiotic compound and its metabolites share a common substructure that may be lost during fragmentation in a tandem mass spectrometer. Constant neutral loss (CNL) scanning may be used to detect such metabolites irrespective of their molecular masses. In particular, phase II conjugated metabolites may be easily identified using this approach. For example, CNL of 176, 129 and 80 u are typical MS/MS fragmentation pathways of glucuronides, glutathione conjugates, and sulfates, respectively.[124]

In addition to stable metabolites, identification of reactive metabolites, if formed, is critical during drug development. Since reactive metabolites have short half-lives and are therefore challenging to isolate or even to detect, in vitro chemical trapping has been used to form stable products that may be analyzed using mass spectrometry and/or nuclear magnetic resonance.[80,125-127] The earliest use of MS/MS as a routine screening tool for GSH conjugates was reported and described by our group in 1999.[127] The trapping experiments typically include the incubation of the test agent with liver microsomes, NADPH and thiol trapping agents such as glutathione (GSH) or *N*-acetylcysteine. GSH is present in all mammalian tissues and serves as a natural scavenger for reactive

metabolites by reacting with a broad range of electrophiles including epoxides, arene oxides, alkyl halides, quinones, and Michael addition acceptors.[128] Fragmentation of GSH conjugates during MS/MS with collision-induced dissociation shows characteristic patterns similar to the dissociation of peptides (**Figure 2**).[124,129,130] GSH conjugates generally undergo a neutral loss of 129 Da (corresponding to pyroglutamic acid) during positive ion tandem mass spectrometry, which enables GSH conjugates to be detected during MS/MS using constant neutral loss (CNL) scanning of 129 Da in positive mode.[124] During negative ion MS/MS product ion scanning of the deprotonated molecule, GSH conjugates form a common fragment anion of *m/z* 272 (deprotonated γ-glutamyl-dehydroalanyl-glycine).

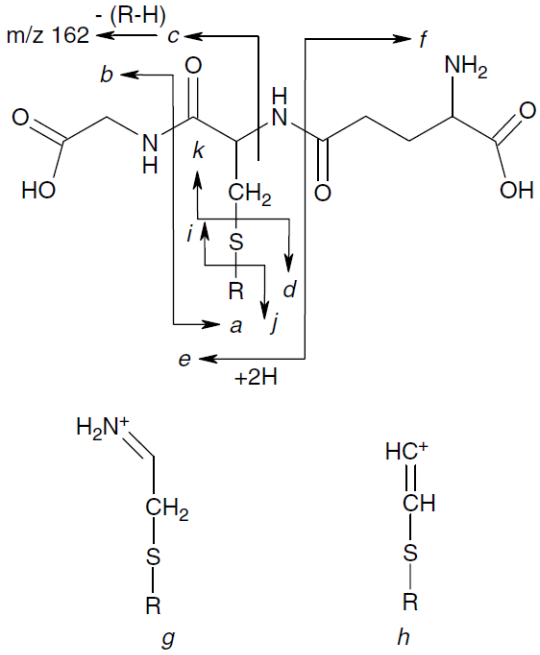

Fragment Ion	*m/z*
a	$MH^+ - 75$
b	76
c	$MH^+ - 146$
c – (R–H)	162
c – H_2O	$MH^+ - 164$
d	$MH^+ - 273$
e	$MH^+ - 129$
e – H_2O	$MH^+ - 147$
f	130
g	$MH^+ - 232$
g – H_2O	$MH^+ - 250$
h	$MH^+ - 249$
i	308
j	$MH^+ - 305/307$
k	274

Figure 2. Characteristic fragment ions of glutathione conjugates during collision-induced dissociation tandem mass spectrometry.

Drug interaction involving metabolizing enzymes is the primary contributor towards adverse clinical events. A new molecular entity (NME) should be evaluated as a potential inhibitor, inducer or substrate of metabolizing enzymes and/or transporters. The U.S. FDA has published a guidance for industry recommending an integrated approach to assess drug interaction potential.[99] The potential of a xenobiotic compound to inhibit CYP enzymes can be evaluated using specific probe substrates incubated with liver microsomes and recombinant CYP enzymes. When the *in vitro* data show that the xenobiotic compound is an inhibitor, in vivo studies are then necessary to assess the significance of the predicted interaction. Major CYP enzymes to be assessed both *in vitro* and *in vivo* include CYP1A2, CYP2C8, CYP2C9, CYP2C19, CYP2D6, and CYP3A4/5. The potential of a xenobiotic compound to induce CYP enzymes can be assessed using human hepatocytes *in vitro* and should begin with studies of CYP1A2, CYP2B6 and CYP3A. If the *in vitro* induction data are positive, then the xenobiotic compound is considered an enzyme inducer and should be evaluated further *in vivo*.

Clinical studies of drug interaction may include simultaneous administration of a mixture of substrates of multiple CYP enzymes and transporters in a single cocktail study. Negative results may eliminate the need for further evaluation of individual CYP enzymes and transporters, significantly reducing the resources spent on the investigation.[99] The cocktail approach has also been implemented in early drug discovery and development to evaluate CYP inhibitory potential.[131] A limitation to the cocktail approach, however, is the possible interaction between substrates as well as the accurate measurement of metabolites with internal standards simultaneously using conventional

LC-MS analysis. Matrix effects resulting in ion suppression or enhancement are also risks for the mass spectrometric-based method. Recently, the applications of UHPLC-MS/MS and/or utilization of stable isotope-labeled internal standards have dramatically increased the speed and accuracy of these measurements with proper selection of CYP probe substrates to avoid interaction.[132-135]

Chapter 2 Investigation of in vitro Metabolism of Glabridin

2.1 Introduction

2.1.1 Background

Metabolism is the biotransformation process of xenobiotics catalyzed by enzymes and usually a detoxification step rendering drugs and similar molecules more polar and more rapidly excreted. Drug metabolism can be roughly divided into two different phases: phase I metabolism where a polar functional group is introduced on the parent molecule and phase II reaction where small polar endogenous molecules are conjugated to the parent molecule. The main types of phase I metabolism are oxidation and hydroxylation by enzymes such as cytochrome P450s and flavin-containing monooxygenases, where cytochrome P450 is considered to have the most significant influence. Phase II metabolism is usually a sequential step following the phase I reaction before excretion in bile or urine. Phase I metabolites are sometimes biologically or pharmacologically active, while phase II conjugates are usually less active or inactive, and they are excreted in urine or bile. Phase II enzymes that are responsible for the conjugate formation include UDP glucuronosyltransferase (UGT), sulfotransferase, *N*-acetyl transferase, and glutathione *S*-transferase, among which UGTs are the most important enzymes involved in elimination of drugs and natural products.[136]

Although most tissues have some metabolizing capacity, the liver is the major site of metabolism for most drugs and xenobiotics. Cytochrome P450 enzymes are a family of heme-monooxygenases located in most types of tissue and concentrated in human liver. Catalyzing most of phase I metabolism, the cytochromes P450 convert lipophilic xenobiotics into more water soluble products, facilitating their elimination from the body.[67] The common reactions catalyzed by cytochrome P450 enzymes include hydroxylation, heteroatom oxygenation, epoxidation, and oxidation of olefins and acetylenes.[68]

During preclinical drug development, the metabolism of drug candidates is studied extensively to ensure their safe administration to humans. Metabolism studies are also needed at the clinical stage of drug development to investigate the compound parameters to understand the safety and efficacy of the drug candidates in human body. To study metabolism parameters, in vitro experiments are particularly useful in that only small quantities of test materials are required. In addition, in vitro studies are fast ways to answer specific questions regarding metabolic stability and potential for drug interaction.

Subcellular fractions from drug-metabolizing tissues such as microsomes, cytosol, and S9 fractions are widely used in drug metabolism studies. Microsomes are the most widely used subcellular fragmented endoplasmic reticulum, and when prepared from hepatocytes, microsomes contain high concentrations of cytochrome P450 enzymes. Microsomal assays have become the default assays that are used for metabolic compound screening.[137] Human hepatocytes are another in vitro model that have been developed for

the investigation of xenobiotics metabolism. Since human hepatocytes contain both phase I and phase II enzymes as well as necessary co-factors such as NADPH and UDPGA, this model is more complete than human liver microsomes for the study of hepatic drug transformation reactions.[77]

Among the constituents identified in common licorice species (*G. glabra*, *G. uralensis*, and *G. inflata*), few have been studied for in vitro metabolism with human cytochrome P450 enzymes. Glycyrrhizin, glycyrrhetinic acid, and isoliquiritigenin from *G. glabra* and several compounds from *G. uralensis* have been investigated for *in vitro* metabolism and are discussed in Section 1.2.2. The metabolism study of these compounds helps with understanding of their potential metabolic pathways in human. On the other hand, Glabridin, a typical flavonoid constituent found in *G. glabra* has not been adequately investigated for metabolism: no *in vitro* metabolism study has been reported. With anti-inflammatory, anti-atherogenic, estrogenic, neuroprotective, and anti-osteoporetic actions[138], glabridin has been included in many cosmetic and food supplement preparations. Therefore, it is important to understand how glabridin is metabolized and if any potential risk exists for consuming too much glabridin.

2.1.2 Applications of LC-MS/MS to Drug Metabolism Studies

Liquid chromatography-tandem mass spectrometry (LC-MS/MS) is a powerful tool for drug metabolism studies, particularly for metabolite identification and quantification.

Triple quadrupole and ion trap mass spectrometers are routinely used in industry and academia for these purposes, while high resolution mass spectrometers (orbitrap and time of flight) are used to provide elemental composition and additional structural information.

The combination of liquid chromatography with mass spectrometry provides an extra dimension of selectivity that simplifies the interpretation and of mass spectra by separating species, especially isomers, prior to mass spectrometric analysis. In addition to acquiring mass spectra and tandem mass spectra, additional data acquisition features such as accurate mass measurement and mass defect filtering may be implemented for further background reduction and signal enhancement. High mass resolution within 5 ppm accuracy is routinely achieved with hybrid quadrupole time-of-flight (Q-ToF), ion trap ToF and Orbitrap mass spectrometers, which significantly improves the specificity of mass measurement and enables elemental compositions to be determined. Mass defect filtering is a function of high resolution mass spectrometers that enables the identification of classes of molecules, such as mixtures of drug metabolites, when they present within complex biological samples. The unique difference between the exact and nominal atomic mass is called the mass defect. Each organic molecule has a unique mass defect based on its elemental composition. Typical phase I and phase II metabolism of xenobiotic compounds involves change of mass defects within 70 mDa. When coupled with liquid chromatography, mass defect filtering with high resolution mass spectrometry is able to differentiate the metabolites of parent drug from other endogenous compounds in the sample.[122]

Constant neutral loss (CNL) and precursor ion (PI) scanning are two common scanning methods in tandem mass spectrometry, especially with triple quadrupole instruments. CNL scanning may be used to search for metabolites with characteristic loss of a neutral fragment, such as 80 Da for sulfates or 176 Da for glucuronides. PI scanning produces a mass spectrum of all precurusor ions that fragment to form the same product ion, and this approach is particularly effective for identifying metabolites forming a common fragment ion. For the detection of glutathione conjugates, PI scanning of fragment ions of *m/z* 272 has been used in the negative ion mode while CNL of 129 Da may be used in the positive ion mode.[139]

Data-dependent product ion scanning is a method based on the ion intensities detected during a standard scan, which triggers acquisition of product ion tandem mass spectra before returning to standard scan mode. This is widely used in ion trap mass spectrometry where both metabolite detection (standard scans) and characterization (product ion scans) are performed in the same run. A limitation of this approach is that the secondary product ion scan is triggered mainly by ion intensity while most of the metabolites exist in relative low abundance. When using ion trap mass spectrometers, multistage scanning (MS^n) may be carried out to obtain fragment ions of fragment ions, thereby providing additional structure information.

2.2 Metabolic Stability of Glabridin

2.2.1 Background and Research Rationale

The metabolic clearance of new compounds is often studied using both *in vitro* and *in vivo* methods. The rapid determination of solubility, permeability, and stability in plasma or liver tissue provides the foundation of oral bioavailability. The *in vitro* metabolism and its kinetic parameters such as V(max), K(m), and half-life ($t_{1/2}$) are often used to predict hepatic clearance.[66] LC-MS/MS has been implemented to measure plasma and liver concentrations of drug candidates to provide a rapid assessment of oral bioavailability. When there is bioavailability problem, a systematic approach is used to isolate the attributes that limit bioavailability, and preventive actions can be taken to slightly modify the chemical structure, adjust the drug formulation, or change the route of administration.

As one of the very first but important assays to predict bioavailability, metabolic stability is tightly linked with other information collected on metabolism and metabolite structure. The initial testing is to determine the stability of the drug candidate in vitro and to identify metabolic soft spots for further compound optimization. After routine metabolic stability screening during candidate optimization, compounds with low metabolic stability are often excluded from further consideration as most therapeutic applications prefer an extended pharmacokinetic half-life. In the recent decades, rapid determination of metabolic stability and profile has been improved dramatically and is now routinely employed.[140] There are no studies in the literature describing the in vitro metabolic stability of glabridin, a licorice constituent specific to *G. glabra*. It is of great interest and

importance to understand more about the metabolic stability of licorice compounds like glabridin in order to understand the biotransformation of licorice in human body.

2.2.2 Materials and Methods

2.2.2.1 Materials

Glabridin, propranolol, ketoconazole, and NADPH were purchased from Sigma-Aldrich (St. Louis, MO). Pooled human liver microsomes (20 mg/mL, 150 donors) were purchased from BD Biosciences (Woburn, MA). HPLC-grade solvents were purchased from Thermo Fisher (Pittsburgh, PA).

2.2.2.2 Microsomal Incubations

Human liver microsomes (1 mg/mL) were incubated with 10 μM glabridin or propranolol (a reference compound that shows medium metabolic stability) in 100 mM phosphate buffer at 37°C in a final volume of 1 mL. NADPH (1 mM final concentration) was added to initiate oxidative metabolism after a 5 min pre-incubation. At 0, 5, 10, 15, 20, 25, 30, 40, 50, and 60 min, 50 μL aliquots were removed and the reaction terminated by the addition of acetonitrile/water/formic acid (86:10:4, v/v/v) containing 5 μM ketoconazole as an internal standard. The samples were vortex mixed for 2 min and centrifuged at

13,000 x *g* at 4°C for 10 min. Aliquots of the supernatant were analyzed using UHPLC-MS/MS to determine the amount of remaining compound.

2.2.2.3 LC-MS/MS Analysis

Quantitative analysis to determine metabolic stability of glabridin was carried using UHPLC-MS/MS with positive ion electrospray, collision-induced dissociation and selected reaction monitoring (SRM) with a Shimadzu (Kyoto, Japan) LCMS-8040 triple quadrupole mass spectrometer and Shimadzu Nexera UHPLC system. UHPLC separations were obtained using a Waters (Milford, MA) Acquity BEH Shield RP18, 2.1×50 mm, 1.7 µm UHPLC column. The mobile phase consisted of a 3.0 min linear gradient from 100% aqueous 0.05% formic acid containing 5 mM ammonium acetate to 100% acetonitrile containing 0.05% formic acid. The flow rate was 0.4 mL/min. The SRM transitions for glabridin were selected using the auto tune feature of the Shimadzu LabSolutions data system followed by manual inspection for confirmation. The SRM transitions selected for glabridin was *m/z* 325.1 to 189.1. The internal standard ketoconazole was monitored using the SRM transition of *m/z* 531.2 to 489.3, and the SRM transition for propranolol was *m/z* 260.1 to 116.1.

The intrinsic clearance of each test compound was estimated based on the substrate disappearance during a 60 min incubation with human liver microsomes. The percentage of substrate remaining was calculated using t=0 as 100%. The slope of the linear regression curve from the natural log of percentage remaining versus incubation time was

used to calculate half-life. The intrinsic clearance was calculated based on the assumptions of 45 mg protein/g liver and 20 g of human liver per kilogram body weight.[141]

2.2.3 Results and Discussion

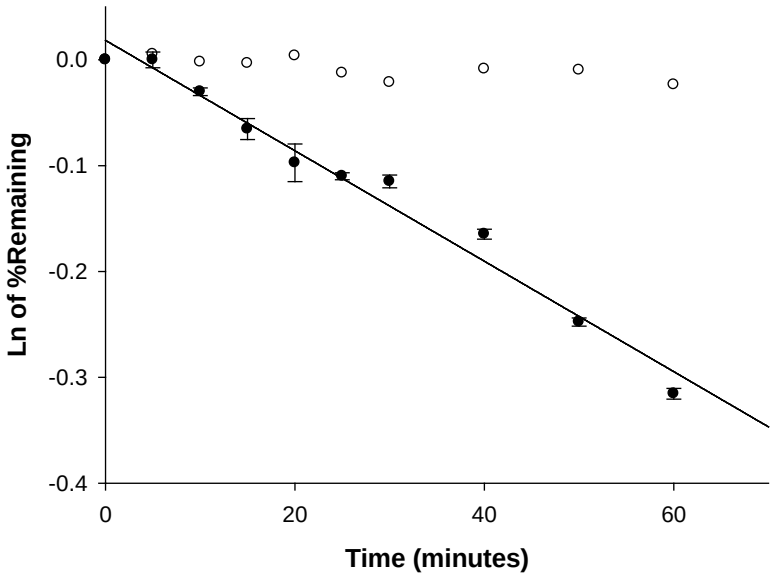

Figure 3. Metabolic stability of glabridin over time during incubation with human liver microsomes. Solid circles: incubations with microsomes, open circles: incubations without microsomes (control). Linear regression gave a slope (elimination constant) of 0.0052 min^{-1}, corresponding to a glabridin half-life of 133 min. Error bars indicate the standard deviation of three replicate experiments.

Glabridin metabolic transformation over time was plotted in **Figure 3** after log transformation of percentage of remaining substrate. Linear regression was performed using SigmaPlot (version 12.0) to give an elimination constant of 0.0052 min^{-1} and half-

life of 133 min. In this experimental system, the half-life of reference compound propranolol was determined to be 21 min. The apparent intrinsic clearances of glabridin and propranolol were calculated to be 5.21 µL/min mg protein and 33 µL/min mg protein (equivalent to 4.69 mL/min/kg body and 29.7 mL/min/kg body by assuming 45 mg protein per g liver and 20 g liver per kg body), respectively. The half-life and intrinsic clearance of propranolol were consistent with literature values.[142] These results indicated that glabridin is much more metabolically stable in vitro than is propranolol. Based on this information and comparison with the literature, the intrinsic clearance of glabridin is similar to those of clozapine, diazepam, dexamethasone, prednisone, ibuprofen, and hexobarbital, all of which are low clearance drugs.[66] The long half-life predicts that glabridin would be eliminated relatively slowly *in vivo* and this was confirmed by the reported 10 hour half-life when pharmacokinetics of glabridin in healthy humans was studied.[143]

2.3 Identification of Glabridin Metabolites

2.3.1 Background and Research Rationale

From discovery through development, drug metabolism studies are conducted to understand the safety and efficacy profiles of drug candidates. *In vitro* studies can provide indirect support for metabolic profiles in humans using *in vitro-in vivo* correlation. Metabolite identification is one of the essential components of drug metabolism studies. In the case of drug development, by comparing the structural

differences between parent compound and metabolites, the metabolic soft spots can be determined to support lead optimization. In the case of natural product constituents of botanical dietary supplements, metabolism studies can provide insights into their safety and efficacy, depending upon the activities or toxicities of the metabolites.

As a unique constituent of *G. glabra*, glabridin has not been investigated for *in vitro* or *in vivo* metabolism. In addition, glabridin was reported to competitively inhibit CYP2C9 and inactivate CYP3A4 and CYP2B6 in a time and concentration dependent fashion.[109] However, incubations with 2, 4-dimethylglabridin did not lead to a loss in CYP3A4 enzyme activity, suggesting that both hydroxyl groups on the flavonoid B ring are required for CYP3A4 inactivation. Metabolism of glabridin by CYP3A4 resulted in destruction of the heme moiety, indicating that reactive metabolites from glabridin metabolism might be the source of licorice-drug interaction.[84] The study of glabridin metabolism and related metabolites may bridge the gap between glabridin and licorice-drug interaction. In this research, phase I metabolism studies of glabridin were conducted *in vitro* with human and rat liver microsomes. *In vitro* metabolism is not studied with hepatocytes due to relatively high cost. Phase II metabolism involves enzyme such as UDP glucuronosyltransferase (UGT), sulfotransferase, *N*-acetyltransferase, and glutathione *S*-transferase. Metabolites from phase II metabolism are often excreted in urine and bile, sometimes at high concentration. Given the phenolic structure of the glabridin molecule and existing literature, glucuronidation and sulfation would be expected as possible important metabolic pathways for glabridin. Not being able to address phase II glabridin metabolism makes the metabolism study incomplete.

2.3.2 Materials and Methods

2.3.2.1 Materials

Glabridin, *meta*-chloroperoxybenzoic acid (*m*CPBA), sodium thiosulfate, horseradish peroxidase, tyrosinase, hydrogen peroxide, and NADPH were purchased from Sigma-Aldrich. Pooled human liver microsomes (20 mg/mL, 150 donors) and rat liver microsomes (20 mg/mL) were purchased from BD Biosciences (Woburn, MA). HPLC-grade solvents were purchased from Thermo Fisher (Pittsburgh, PA).

2.3.2.2 Microsomal Incubation

Human or rat liver microsomes (1 mg/mL) were incubated with 50 µM glabridin in 100 mM phosphate buffer at 37°C in a final volume of 1 mL. NAPDPH (1 mM final concentration) was added to initiate oxidative metabolism after a 5 min pre-incubation. The high glabridin concentration was used due to its relatively low hepatic clearance and long life life. After 60 min, the reaction was terminated by the addition of 3 mL of ice-cold acetonitrile/ethanol (1:1, v/v) followed by 2 min vortex mixing and 10 min centrifugation at 13,000 x *g* and 4°C. The supernatants were removed, evaporated to dryness under nitrogen and reconstituted in 100 µL of acetonitrile/water (20:80, v/v)

before analysis using LC-MS/MS. Control experiments were carried out in parallel that contained no NADPH or no microsomes.

2.3.2.3 Synthesis of Epoxide Metabolites of Glabridin with mCPBA

*m*CPBA (3.2 mM) in 750 µL CH_2Cl_2 was washed 4 times with 1 mL aliquots of 50 mM phosphate buffer (pH 7.4), and then was mixed with 1 mL fresh buffer. Glabridin (3.2 mM) in 250 µL CH_2Cl_2 was added to the *m*CPBA solution, and the reaction mixture was shaken for 2 hours at room temperature. The aqueous layer was removed and organic layer was washed 3 times with 1 mL aliquots of 500 mM sodium thiosulfate. The samples was evaporated under a stream of nitrogen and reconstituted with 200 µL acetonitrile/water 10:90 (v/v) and 50 µL acetic acid immediately before analysis using LC-MS/MS.

2.3.2.4 Enzyme Kinetics Studies

For the determination of enzymatic kinetic parameters, 0.25 mg/mL liver microsomal protein, 1 mM NADPH, and various concentrations of glabridin ranging from 0.5 to 50 µM were incubated in 0.5 mL of 50 mM phosphate buffer (pH 7.4). Incubations were carried out for 10 min, and the reactions were stopped by the addition of 1.5 mL of ice-cold acetonitrile/ethanol (1:1, v/v) followed by 2 min vortex mixing and 10 min centrifugation at 13,000 x *g* and 4°C. The samples were evaporated under nitrogen and reconstituted in 100 µL of acetonitrile/water (10:90, v/v) before analysis using LC-

MS/MS. Kinetic parameters were calculated by nonlinear regression analysis using SigmaPlot (Systat Software, San Jose, CA). Due to lack of synthetic metabolite standards, glabridin was used to build a standard curve for quantitation.

2.3.2.5 Incubation with Horseradish Peroxidase and Tyrosinase

Horseradish peroxidase (20 units/mL with 500 µM hydrogen peroxide) or 0.1 mg/mL tyrosinase were incubated with 100 µM glabridin in 50 mM phosphate buffer (pH 7.4) at 37 °C in a final volume of 1 mL. After 60 min, the reaction was terminated by the addition of 3 mL of ice-cold acetonitrile/ethanol (1:1, v/v) followed by 2 min vortex mixing and 10 min centrifugation at 13,000 x *g* and 4°C. The supernatants were removed, evaporated under nitrogen and reconstituted in 100 µL of acetonitrile/water (10:90, v/v) before analysis using LC-MS/MS.

2.3.2.6 LC-MS/MS Analysis

For the characterization of glabridin metabolites, LC-MS/MS was carried out using data-dependent product ion tandem mass spectrometric analysis on a Shimadzu IT-ToF mass spectrometer equipped with a Prominence UFLCXR system. HPLC separations were obtained using a Waters XTerra C_{18}, 2.1×100 mm, 3.5 µm HPLC column. The mobile phase consisted of a 20 min linear gradient from 100% aqueous 0.05% formic acid containing 2 mM ammonium acetate to 100% acetonitrile containing 0.05% formic acid. The flow rate was 0.3 mL/min. Product ion (positive and negative) scans were recorded

over the range *m/z* 100 to 900 or less depending on the molecular mass of the metabolite. The 20 min gradient might be too fast and could be further optimized.

Quantitative analysis to determine metabolite concentration was carried using UHPLC-MS/MS with positive ion electrospray, collision-induced dissociation (CID) and SRM with a Shimadzu LCMS-8040 triple quadrupole mass spectrometer and Nexera UHPLC system. UHPLC separations were obtained using a Waters Acquity BEH Shield RP18, 2.1×50 mm, 1.7 µm UHPLC column. The mobile phase consisted of a 5.0 min linear gradient from 100% aqueous 0.05% formic acid containing 5 mM ammonium acetate to 100% acetonitrile containing 0.05% formic acid. The flow rate was 0.5 mL/min. The SRM transitions for each metabolite were determined based on tandem mass spectra of the metabolites obtained during metabolite characterization with the IT-ToF mass spectrometer described above. Each metabolite was characterized by its chromatographic retention time and product ion tandem mass spectrum. The internal standard ketoconazole was monitored using the SRM transition of m/z 531.2 to 489.3.

2.3.3 Results and Discussion

2.3.3.1 Incubation with Human Liver Microsomes

In the incubations of glabridin with human liver microsomes, 9 chromatographic peaks were detected during LC-MS analysis and are labeled as Peaks 1, 2, 2', 3, 3', 4, 5, 5', and

6 in **Figure 4**. Accurate mass measurements of Peaks 1, 2', 3', 4, 5, and 6 were within 5 ppm of the elemental composition $C_{20}H_{20}O_5$ which indicates that they contained one more oxygen than did glabridin. Accurate mass measurements of Peak 2 and Peak 3 were both within 2 ppm of the elemental composition $C_{20}H_{22}O_6$ which indicates that they contained one oxygen and two hydrogens (H_2O) more than mono-oxygenated glabridin. Accurate mass measurement of Peak 5' was within 2 ppm of the elemental composition $C_{20}H_{18}O_4$, which was two hydrogens less than glabridin. The retention times of these mono-oxygenated glabridin peaks were 2.9 min (Peak 1, assigned as M1), 3.9 min (Peak 2'), 4.2 min (Peak 3'), 4.4 min (Peak 4, assigned as M4), 4.9 min (Peak 5, assigned as M5), and 5.6 min (Peak 6, assigned as M6), respectively. Peak 2 and Peak 3 with the elemental composition $C_{20}H_{22}O_6$ in **Figure 4A** eluted at the same time as Peak 2' and Peak 3' in **Figure 4B**, leading to the hypothesis that Peak 2' and Peak 3' were in-source dehydration products of Peak 2 (assigned as M2) and Peak 3 (assigned as M3). Similarly, Peak 5' in Figure 4C is proposed as an in-source dehydration product of Peak 5 (M5). Additional supporting evidence is provided as follows.

High resolution ion electrospray CID product ion tandem mass spectra of the deprotonated and protonated molecules of glabridin with proposed fragmentation pathways are provided in **Figures 5 and 6** to assist metabolite structure elucidation. In the negative MS/MS spectrum, *m/z* 201 is most abundant ion $^{1,2}A^-$ and was used for quantitative analysis of glabridin[144-146] while *m/z* 135 is the second abundant fragment ion resulting from retro-Diels–Alder reaction ($^{1,3}B^-$). In the positive MS/MS spectrum, *m/z*

189 and *m/z* 123 are the dominant fragment ions that represent retro-Diels–Alder reaction product ions ($^{1,3}A^{+}$) and $^{1,2}B^{+}$.

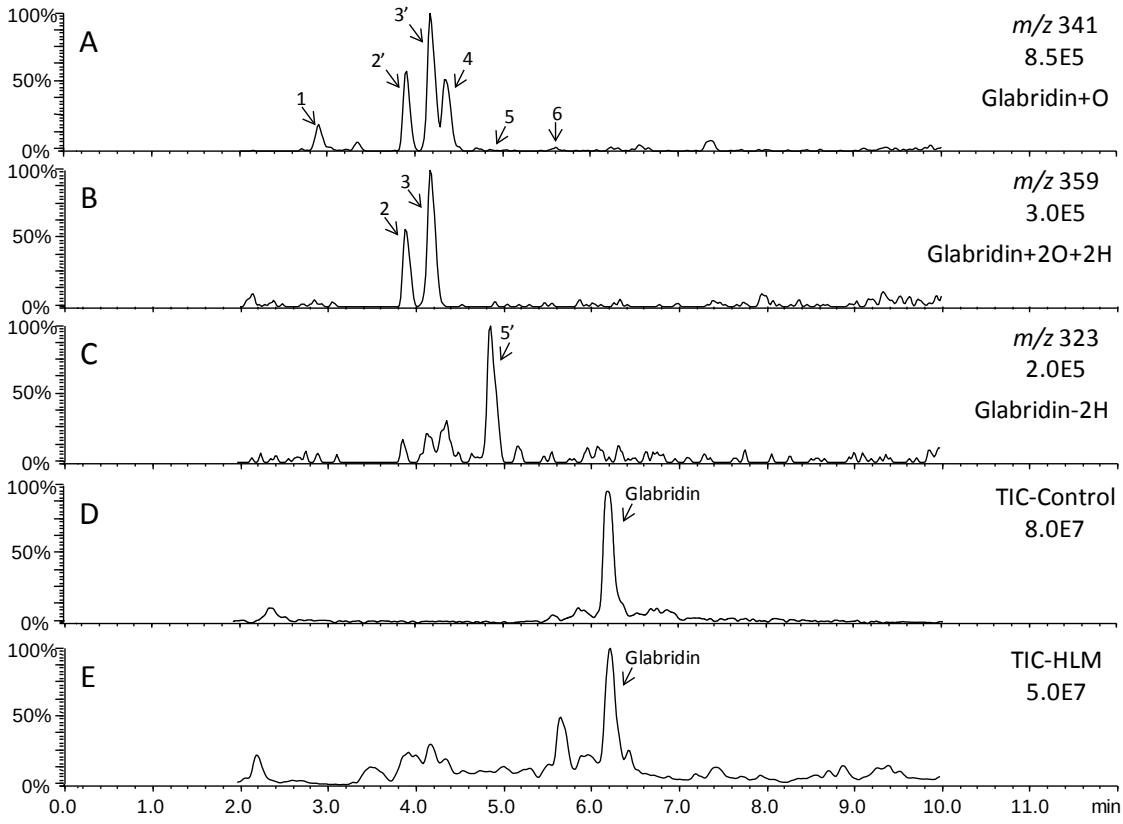

Figure 4. Positive ion electrospray total ion chromatogram (TIC) and computer-reconstructed mass chromatograms of metabolites of glabridin after incubation with human liver microsomes and NADPH (no NADPH for control).

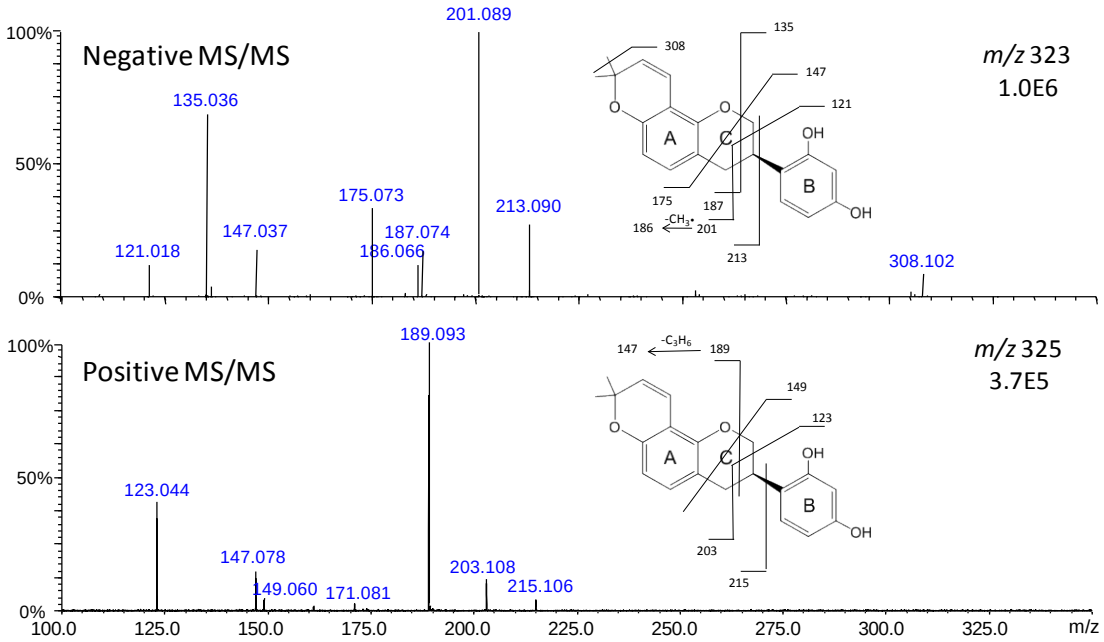

Figure 5. High resolution ion electrospray CID product ion tandem mass spectra of the deprotonated (top) and protonated (bottom) molecules of glabridin eluted at 6.2 min in Figure 4D with proposed fragments.

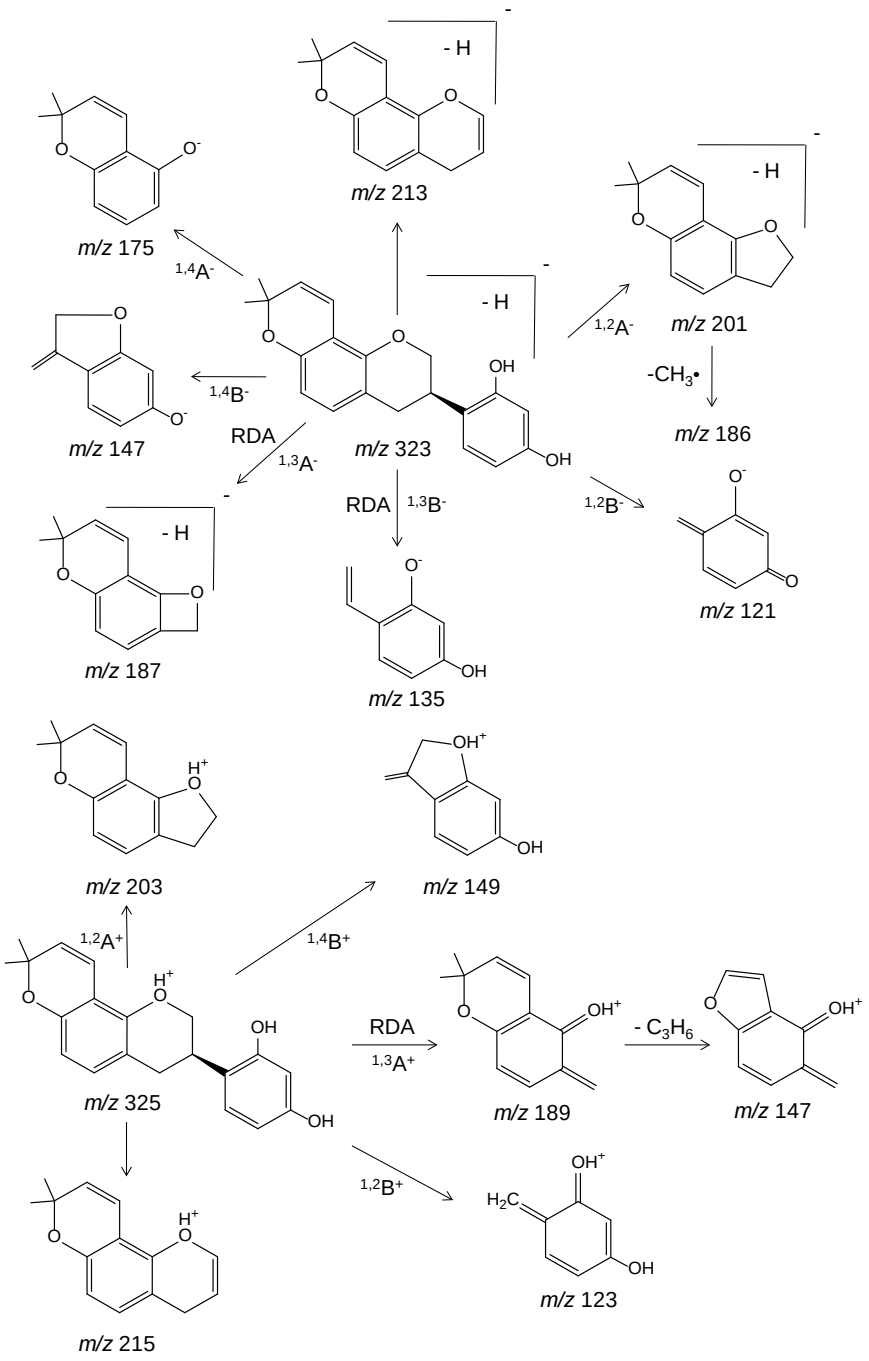

Figure 6. Proposed fragmentation pathways during MS/MS with CID for the deprotonated (top) and protonated (bottom) molecules of glabridin.

The positive MS/MS spectra of Peak 1 has a characteristic *m/z* 205 fragment which corresponds to one additional oxygen to *m/z* 187 from glabridin MS/MS spectra,

indicating the oxygenation position is on A ring, D ring, or 4 position on C ring. The shared *m/z* 123 with glabridin confirms that there is no oxygenation on B ring. The exact oxygenation location could not be determined from these data. In the negative ion chromatogram, no obvious *m/z* 339 corresponding to *m/z* 341 was observed, therefore oxygenation at the end methyl group is proposed as opposed to oxygenation on the A-ring which can easily form a negative ion.

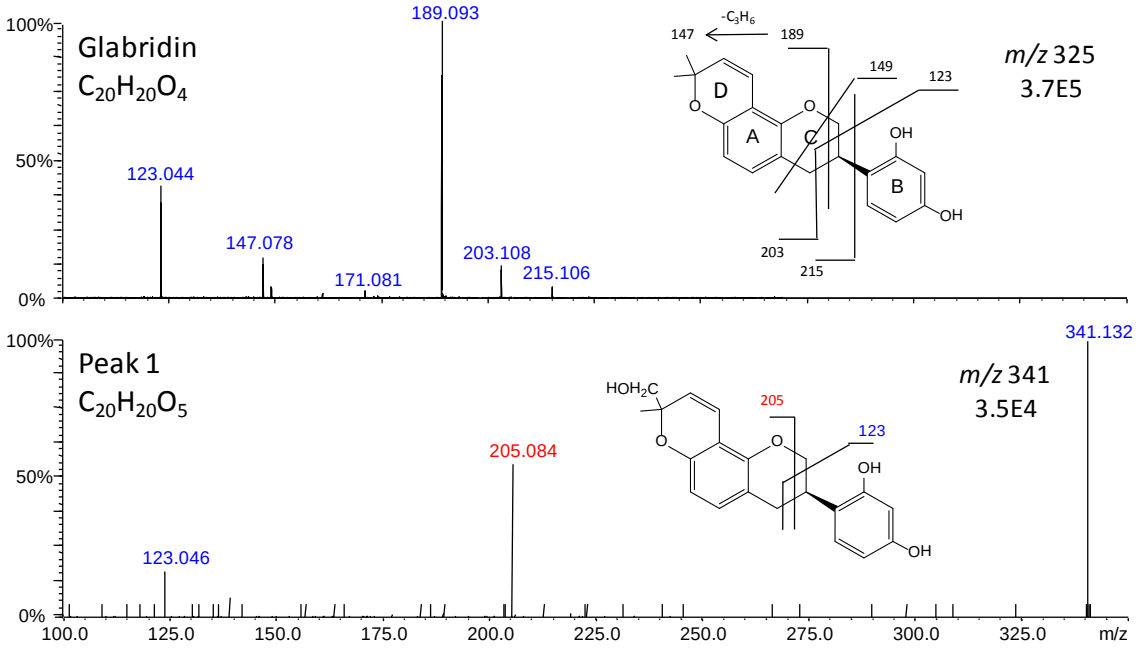

Figure 7. High resolution positive ion electrospray CID product ion tandem mass spectra of the protonated molecules of glabridin (top) and Peak 1 (M1, bottom, retention time at 2.9 min in Figure 4) with proposed structures.

Comparison of the MS/MS spectra of Peak 2' and Peak 3' with those of glabridin (**Figure 8**) indicates that Peak 2' and Peak 3' share the product ion of *m/z* 205 while glabridin had a corresponding product ion of *m/z* 189. This fragmentation pattern confirms that mono-oxygenation of glabridin to form Peak 2' and Peak 3' took place on

the D ring or on the adjacent A ring. Accurate mass product ion tandem mass spectra of Peak 2 and Peak 2' (similar as those of Peak 3' and Peak 3) are shown in **Figure 9**. Peak 2 and Peak 2' shared almost all fragment ions except *m/z* 341, and further sequential MS^3 spectra of *m/z* 341 (the product ion formed from *m/z* 359, Peak 2) produced an tandem mass spectrum that was identical to that of Peak 2', confirming that in-source fragmentation of *m/z* 359 (Peak 2, M1) to *m/z* 341 (Peak 2') corresponded to loss of water. Additional evidence from negative ion chromatogram supports the hypothesis where very strong signal of *m/z* 357 (corresponding to *m/z* 359 in positive mode) was observed, and to the less extent, *m/z* 339 (corresponding to *m/z* 341 in positive mode). The information above combined with two pairs of identical product ion tandem mass spectra of Peak 2/Peak 3 (M2/M3) and Peak 2'/Peak 3', M2 and M3 are proposed to be diol metabolites at 9- and 10-positions that were formed from epoxide ring opening. Peak 2' and Peak 3' might be the corresponding enols, ketones, or stable carbocation intermediate after the diols eliminated water (in Figure 8, enol is shown as an example. M2 and M3 might be a pair of diastereoisomers that are structurally related and formed by the attack of a water molecule on an epoxide intermediate resulting in two hydroxyl groups of opposite confirmations.

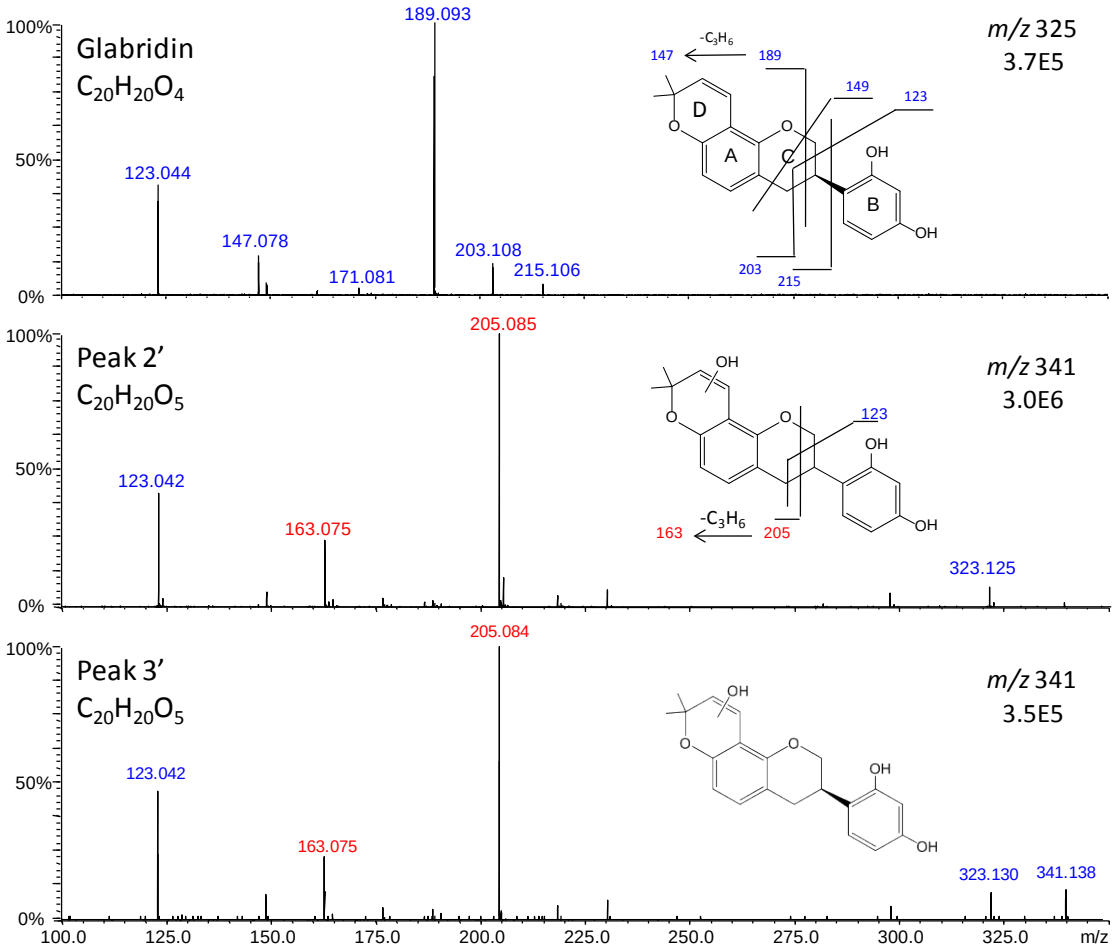

Figure 8. High resolution positive ion electrospray CID product ion tandem mass spectra of the protonated molecules of glabridin (top), Peak 2' (middle, retention time at 3.9 min in Figure 4), and Peak 3' (bottom, retention time at 4.2 min in Figure 4) with proposed structures.

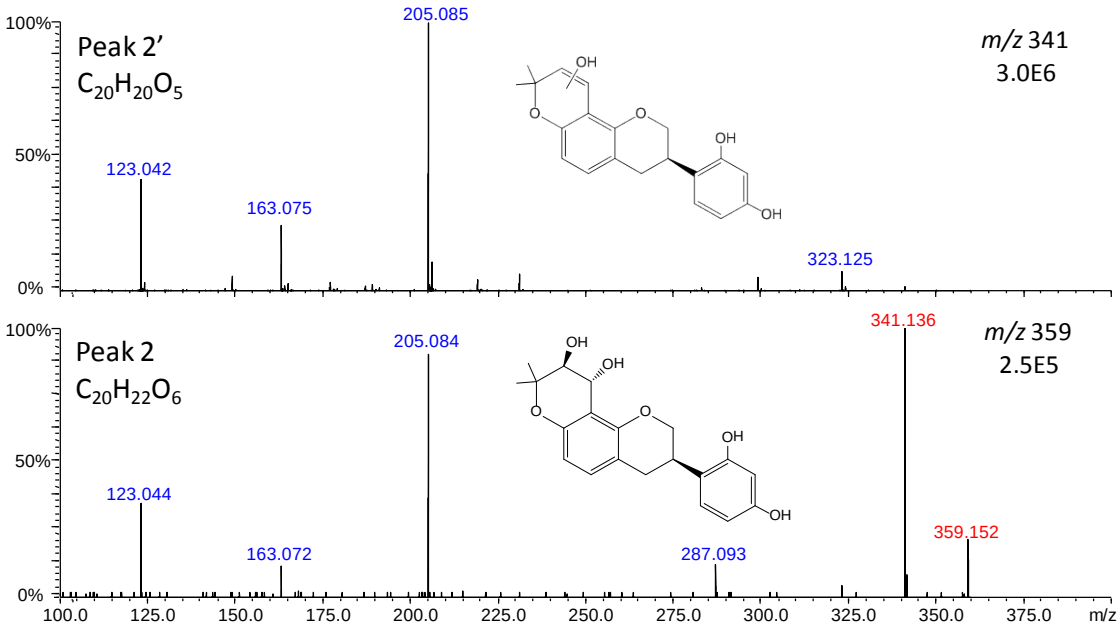

Figure 9. High resolution positive ion electrospray CID product ion tandem mass spectra of the protonated molecules of Peak 2' (top) and Peak 2 (M2, bottom, retention times both at 3.9 min, in Figure 4).

*m*CPBA is a useful reagent for synthesizing epoxides from alkenes while retaining the stereochemistry.[147-149] To confirm that glabridin formed epoxide metabolites that then underwent hydrolysis to diols, glabridin was treated with *m*CPBA and then analyzed using LC-MS/MS. **Figure 10C and 10D** show positive ion electrospray computer-reconstructed mass chromatograms of mono-oxygenated glabridin formed by treatment with *m*CPBA and by incubation with human liver microsomes. Each treatment of glabridin produced two pairs of peaks, Peak 2/Peak 2' and Peak 3/Peak 3', that eluted at 3,9 min for Peak 2/2' and 4.2 min for Peak 3/3'. All four peaks were within 2 ppm of the elemental composition $C_{20}H_{20}O_5$. Although the peak height ratio between Peak 2/Peak 3 and Peak 2'/Peak 3' were different between the *m*CPBA treatment and microsomal incubation of glabridin, these data suggest that glabridin formed unstable epoxide

metabolites that subsequently reacted with water to form diols. The different peak height ratios might be related to different reactivities of *m*CPBA and liver microsomal enzymes.

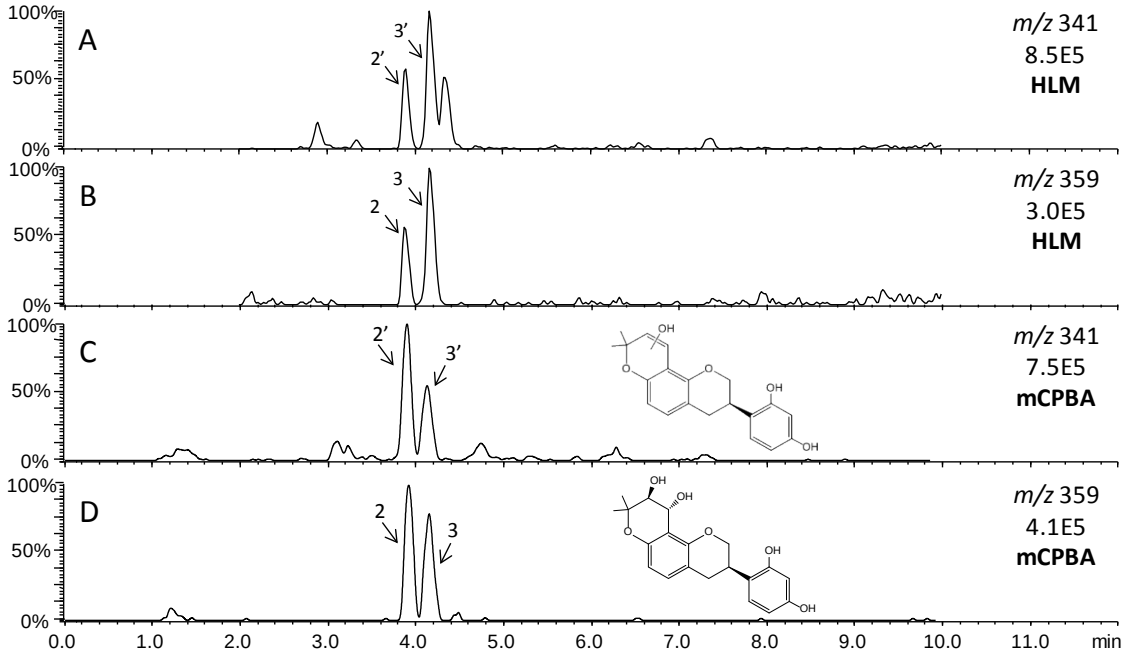

Figure 10. Positive ion electrospray computer-reconstructed mass chromatograms of diol metabolites of glabridin formed during incubation with human liver microsomes (A and B) and diol derivatives of glabridin formed spontaneously after epoxidation using *m*CPBA (C and D).

Potential glabridin metabolite Peak 4 ($C_{20}H_{20}O_5$, **Figure 11 bottom**) at retention time of 4.4 min (**Figure 4**) shared the same fragment ion of *m/z* 205 with Peak 2' and Peak 3', which indicated that the extra oxygen was located on the D-ring, the A-ring, or the 4-position on the C-ring. On the other hand, Peak 4 also had a low abundance fragment ion of *m/z* 189 shared with glabridin, demonstrating that a hydroxyl group could be at the 4-position on the C-ring. Note, if the hydroxyl group were located on the methylene carbon

of the C-ring, the molecule should easily eliminate water to form a double bond at the 3-position. This would also explain the ion of *m/z* 205 and the facile loss of water (from *m/z* 341 to *m/z* 323). The negative MS/MS spectra of *m/z* 339 (assigned as Peak 4', **Figure 11 top**, corresponding to *m/z* 341 in positive MS/MS) was also obtained to compare with that of glabridin (**Figure 5**): the facile loss of water (*m/z* 339 to *m/z* 321) in addition to characteristic retro-Diels–Alder reaction fragments *m/z* 135 ($^{1,3}B^-$) and *m/z* 203 (187+O, $^{1,3}A^-$) also points to the high likelihood of hydroxylation at 4-position on the C-ring. Therefore Peak 4 (M4) is assigned to 4-hydroxy glabridin. The stereochemistry of the 4-hydroxyl metabolite was not determined but is proposed to be in the *trans* position to the B-ring which is less structurally restricted.

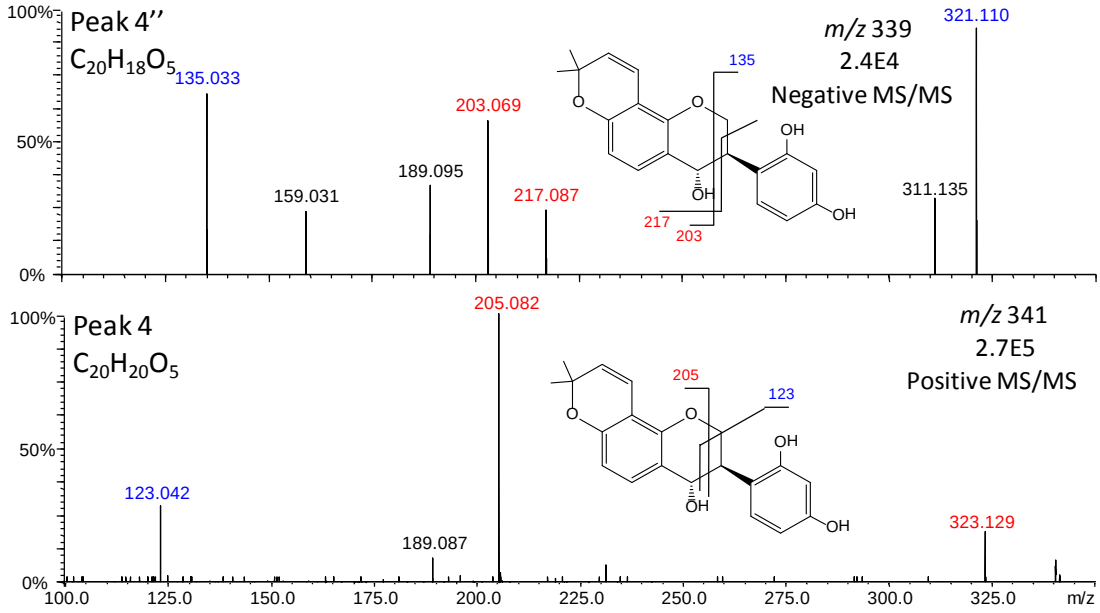

Figure 11. High resolution ion electrospray CID product ion tandem mass spectra of the deprotonated (top) and protonated (bottom) molecules of Peak 4'

(top) and Peak 4 (M4, bottom, retention time at 4.4 min) with proposed fragments.

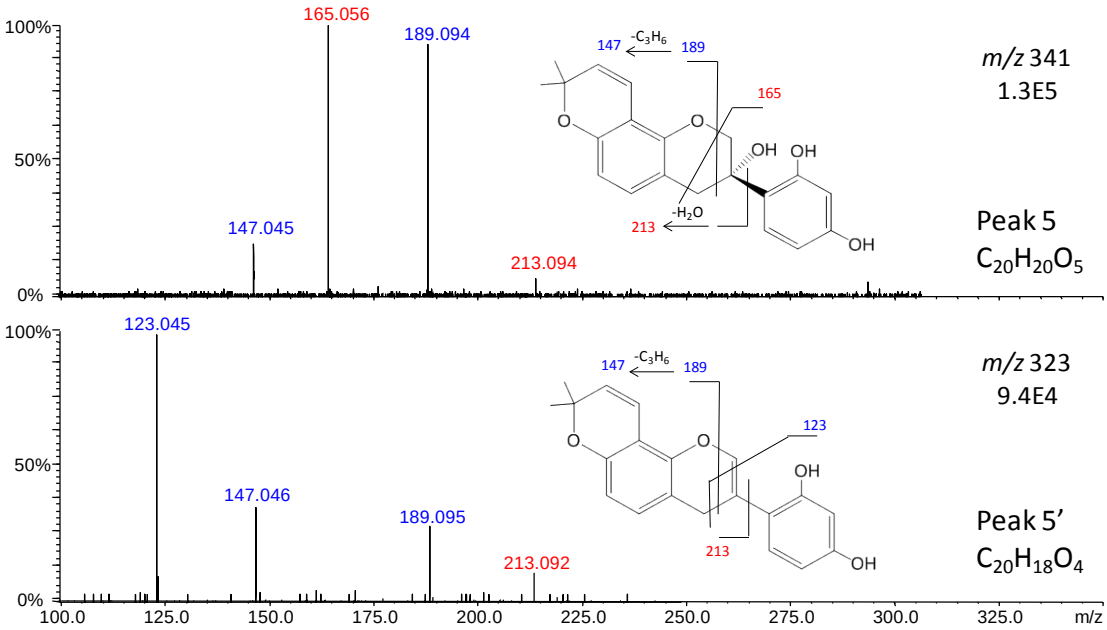

Figure 12. High resolution positive ion electrospray CID product ion tandem mass spectra of the protonated molecules of Peak 5 (top, M5) and Peak 5' (bottom, retention times both at 4.9 min, in Figure 4).

Peak 5' ($C_{20}H_{18}O_4$, **Figure 12**) co-eluted with Peak 5 (M5, $C_{20}H_{20}O_5$, **Figure 12**) at 4.9 min in the chromatograms shown in **Figure 4**) and shared fragment ions of *m/z* 147 and *m/z* 189 with glabridin indicating there was no element change on the A-ring and the D-ring. The unique fragment ion of *m/z* 165 (*m/z* 149 + 16) from Peak 5 confirmed that the hydroxyl group could be on the B-ring or at the 2- or 3- position on the C-ring. The minor fragment ion of *m/z* 213 formed by Peak 5 and Peak 5' (**Figure 12**) and the 18 Da mass different with same retention time points easily to the hypothesis that Peak 5 lose water to form Peak 5' during in-source fragmentation, similar to Peak 2/2' and Peak 3/3', most

likely 3-hydroxy glabridin which lost water during fragmentation to form the structure of Peak 5 which further formed fragment ion of *m/z* 213 as depicted in **Figure 12**. In negative MS/MS spectra, the corresponding *m/z* 339 peak was observed with the dominant product ion *m/z* 321 indicating relatively easy loss of water. Adding to all above, the ions of *m/z* 189 and *m/z* 213 from *m/z* 323 (Peak 5') demonstrated that the elimination of two hydrogens from glabridin would result in formation of a double bond on the C-ring, most likely at the 2-position. Therefore, Peak 5 (M5) is proposed to be hydroxylated glabridin at the 3-position on the C-ring.

Peak 6 (M6, $C_{20}H_{20}O_5$) in **Figure 4** was a minor metabolite from the incubation with human liver microsomes. However, an identical compound was formed as a major metabolite during incubation with horseradish peroxidase and tyrosinase. Therefore, this metabolite and its proposed structure is discussed in the next section 2.3.3.2.

2.3.3.2 Incubation with Rat Liver Microsomes, Horseradish Peroxidase, and Tyrosinase

Rat liver microsomes, horseradish peroxidase, and tyrosinase were used for metabolism incubation to compare with human liver microsomes generated metabolites as they have different enzyme composition, potentially producing different metabolites. In the incubations of glabridin with rat liver microsomes, a metabolite profile was observed that was similar to that produced using human liver microsomes. Among all 9 chromatographic peaks in **Figure 4**, 6 were identified with rat liver microsome

incubation: Peak 2, Peak 2', Peak 3, Peak 3', Peak 4, and Peak 5 in **Figure 13**. Compared with human liver microsomes (**Figure 4**), all human liver microsomal metabolites except for M1 and M6 were produced by rat liver microsomes. The accurate mass measurements and retention times of the peaks observed in **Figure 13** were identical to the corresponding peaks in **Figure 4**. Based on the chromatographic peak area, under the same incubation condition, rat liver microsomes produced 3x to 4x more Peak 2 and Peak 3 compared with human liver microsomes. Similarly, Peak 2 (M2) and Peak 3 (M3) from rat liver microsomal incubation had 3x to 4x larger peak areas compared with M2 and M3 from human liver microsomes. However, rat liver microsomes produced significantly less M4 (30%) and M5 (20%) than did human liver microsomes. These observations indicated that rat liver microsomes differed slightly from human liver microsomes with respect to metabolic activity.

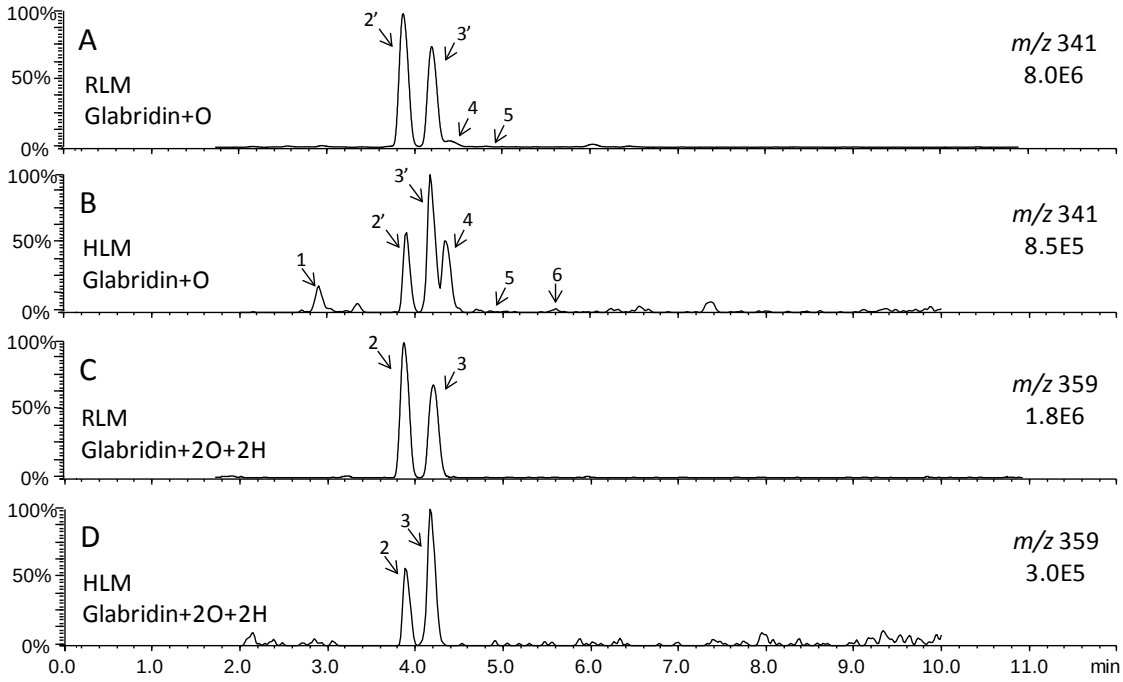

Figure 13. Positive ion electrospray computer-reconstructed mass chromatograms of metabolites of glabridin formed by incubation with rat liver microsomes (RLM, Panel A and C) and NADPH compared to incubation with human liver microsomes (HLM, Panel B and D).

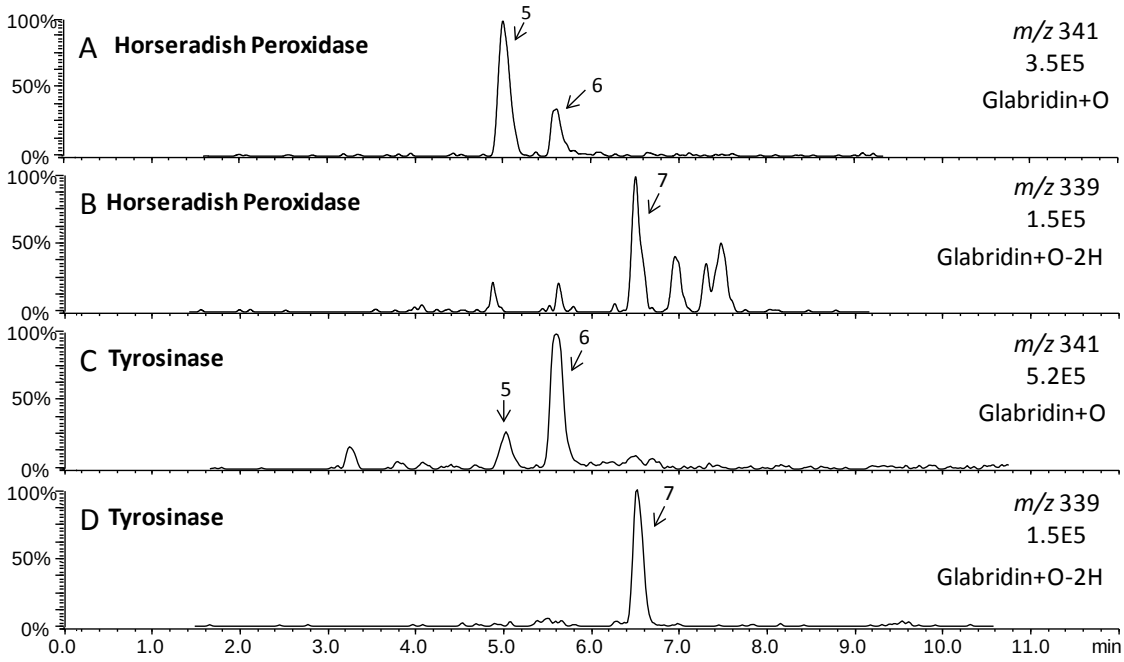

Figure 14. Positive ion computer-reconstructed mass chromatograms of metabolites of glabridin after incubation with horseradish peroxidase (A and B) and tyrosinase (C and D).

Incubations of glabridin with horseradish peroxidase or tyrosinase produced different metabolite profiles than did incubations with liver microsomes (**Figure 4**), or *m*CPBA, as only metabolites Peak 5 (M5), Peak 6 (M6) and a new metabolite Peak 7 (assigned as M7, retention time at 6.6 min) were formed (**Figure 14**). M5 and M6 were both within 2 ppm of the elemental composition $C_{20}H_{20}O_5$ which was one oxygen more than the glabridin

formula while M7 was within 2 ppm elemental composition $C_{20}H_{18}O_5$, two hydrogen less than M5 and M6 formula. In addition to the new metabolite M7, horseradish peroxidase and tyrosinase produced more M5 (20x) and M6 (10x) than did liver microsomes when incubated under the same incubation conditions. Horseradish peroxidase formed more M5 than M6 and more M6 than M5 was observed from the incubation with tyrosinase. These differences were the result of polyphenol oxidases in horseradish peroxidase and tyrosinase that do not catalyze epoxide formation.[150,151]

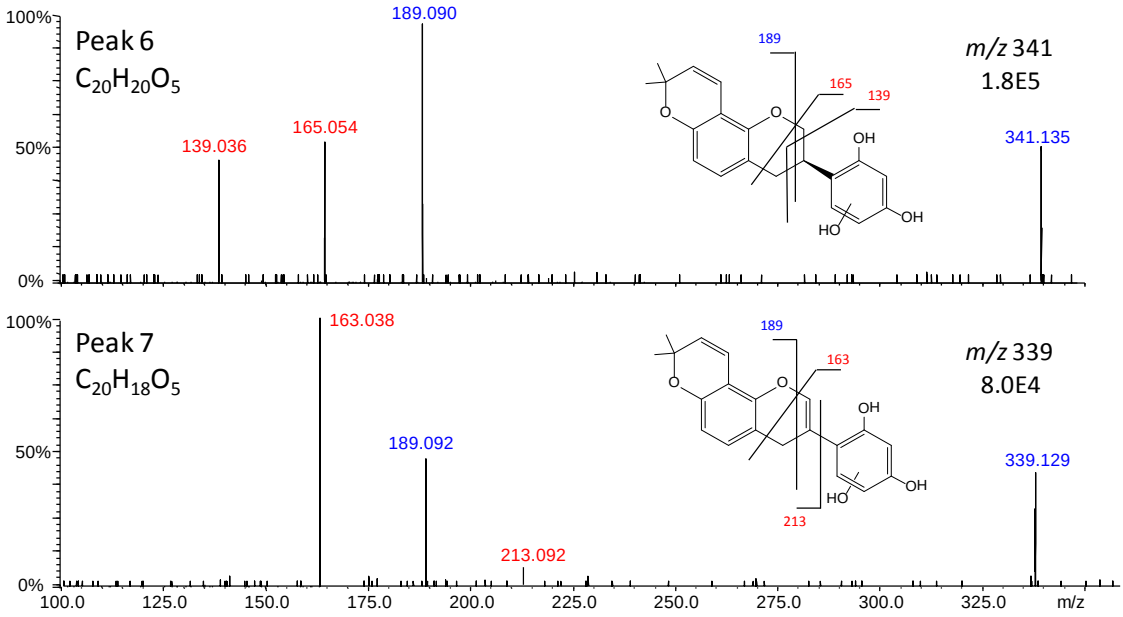

Figure 15. Positive ion electrospray CID product ion tandem mass spectra and proposed chemical structures of the protonated molecules of rat (and human) liver microsomal mono-oxygenated glabridin metabolites Peak 6 (M6) and Peak 7 (M7) with retention times of 5.6 min and 6.6 min (**Figure 14**), respectively.

Similar to M4 and M5, Peak 6 (M6, **Figure 15**) showed the same product ion of *m/z* 189 as did glabridin (**Figure 7**) but formed a different fragment ion of *m/z* 165 which was 16

units higher than the corresponding *m/z* 149 fragment ion formed by glabridin. This fragment was also observed in Peak 5 hinting that the extra oxygen was also located on the B-ring or 2-/3- position on the C-ring. However, the tandem mass spectrum of M6 did not show facile loss of water (unlike M4 fragmentation of *m/z* 341 to *m/z* 323, **Figure 11**) indicating that the hydroxyl group was not likely on the 2- or 3- position of the C-ring but instead on the B-ring (**Figure 15**). In negative MS/MS spectra, the corresponding *m/z* 339 peak was observed with no *m/z* 321 (loss of water) indicating the hydroxyl group could be more likely on C-ring (aromatic ring). The exact chemical structure of the glabridin metabolite M6 has not been determined, but it might be one of several possible hydroxylated metabolites that have a hydroxyl group at the 2'-, 4'-, or 5'- position, with the 4'-hydroxyl metabolite being sterically and electrophile-favored.

The positive ion electrospray product ion tandem mass spectrum of Peak 7 (M7) is shown in **Figure 15**. Peak 6 shared the same fragment ions of *m/z* 189 and *m/z* 213 with M5 (**Figure 12**) indicating the structures of the two compounds were the same with respect to the D-ring, the A-ring, and the C-ring. The fragment ion of *m/z* 163 was two hydrogens less than the *m/z* 165 fragment from M6 (**Figure 15**) which confirmed the position of the double bond (2-position) on the C-ring as well as the extra oxygen on the B-ring as a hydroxyl group. Like M6, the hydroxylation position was not determined but might be at the 2'-, 4'-, or 5'- position, with the 4'-hydroxyl metabolite being sterically and electronically favored.

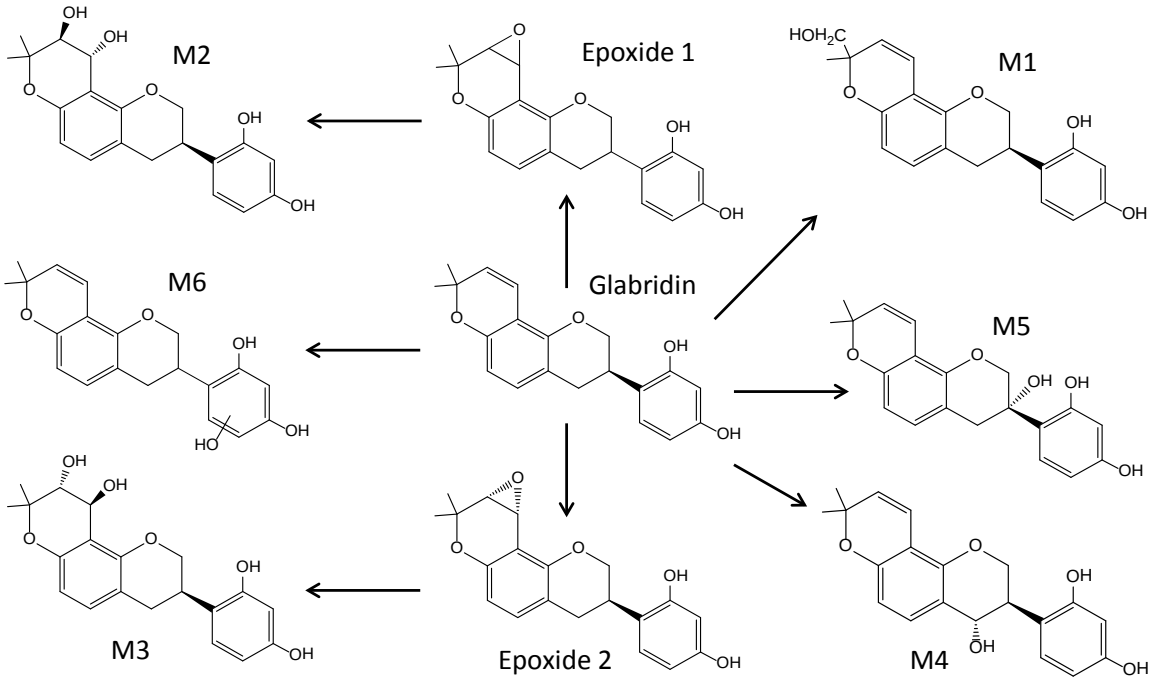

Figure 16. Summary of proposed glabridin metabolites and metabolic pathways.

A total of seven glabridin metabolites were observed from the incubations with human liver microsomes, rat liver microsomes, horseradish peroxidase, and tyrosinase. The proposed metabolic pathways of glabridin with liver microsomes (the seventh metabolite was not observed with human liver microsomes) are summarized in **Figure 16**. Based on the chromatographic peak areas of the glabridin metabolites in **Figure 4**, the diol metabolites comprised approximately 66% of the total metabolite mass (22% and 44% for M2 and M3, respectively) while phenolic metabolites (M4, M5, and M6) only contributed about 22% of the total metabolite mass. As proposed, the M2 and M3 are secondary metabolites formed from epoxides (Epoxide 1 and Epoxide 2 in **Figure 16**) that are unstable and easy to hydrolyze to diols by enzymes such as microsomal epoxide hydrolase. The exact stereochemistry relationship between Epoxide 1 and Epoxide 2 vs M2 and M3 were not determined. Therefore epoxide/diol metabolites are predicted to be

the major metabolic pathway for glabridin *in vivo* based on liver microsomal data. Epoxide/diol metabolites are more likely than other metabolites to cause toxicity issues as reactive epoxide/diol metabolites in general have been associated with increased mutation frequency and toxicity, leading to DNA damage.[152-154] However, given the reactivity of epoxide/diol, we would also predict the half-lives *in vivo* for the epoxide/diol metabolites to be relatively short compared with phenolic metabolites (particularly for diol metabolites) with limited negative pharmacological impact *in vivo*.

2.3.3.3 Enzymatic Kinetics Studies

The kinetics of the formation of glabridin metabolites M2 to M5 catalyzed by P450 enzymes in liver microsomes were determined and are shown in **Table 1** and **Figure 15**. The kinetics parameters were calculated using a nonlinear regression fit to the Michaelis-Menten equation. The *Km* values for the metabolism of glabridin to M2 to M5 were 6.0, 5.6, 21.1, and 8.9 μM, respectively. M2 and M3 have similar *Km* values, but the maximum initial enzyme velocity, *Vmax* for M3 formation was approximately 30% higher than that for M2 formation. M5 had the slowest *Vmax* (1/4 of that of M3 formation) while M4 had *Vmax* values similar to M2.

For comparison, the epoxidation and hydroxylation kinetics of carbamazepine and resveratrol were determined. Carbamazepine is a commonly prescribed anticonvulsive drug; its major metabolite is carbamazepine-10,11-epoxide. Many studies on *in vitro* carbamazepine epoxide formation have reported data from incubations with human liver

microsomes and purified and reconstituted CYP3A4. Both hyperbolic and sigmoidal dependencies of the reaction rate on the substrate concentration have been observed.[155] cDNA-expressed CYP3A4 was reported to catalyze 10,11-epoxidation of carbamazepine with *Km* of 442 μM.[156] In another study, carbamazepine was incubated with human liver microsomes and *Km* of 71.6 μM was reported.[157] Although the exact experimental conditions were not the same, the *Km* values of 6.0 and 5.6 μM (M2 and M3) indicated that cytochrome P450 mediated glabridin epoxide/diol metabolite formation had higher enzyme affinity than carbamazepine epoxidation. Similar *Km* values were reported for epoxidation of anandamide, eicosapentaenoic acid, arachidonic acid, and ezlopitant alkene.[158-160]

Resveratrol, a natural product present in mulberries, peanuts and grapes, has been studied for metabolism in human liver microsomes where the apparent *Km* was found to be 21 μM for piceatannol (mono-hydroxylated metabolite of resveratrol).[161] Xanthohumol, a major flavonoid in hop extracts was reported to have a *Km* of 246 μM for its B-ring mono-hydroxylated metabolite.[162] According to Guo *et al*., 8-prenylnaringenin, also a prenylated flavanone in hops, produced prenyl-oxylated metabolites with *Km* of 14.8 μM and 16.8 μM for the CYP2C19 isozyme and *Km* of 3.7 μM for the CYP2C8 isozyme.[10] The *Km* value of mono-hydroxylated metabolites of glabridin (21.1 μM for M4) was comparable to that of the resveratrol mono-hydroxylated metabolite and CYP2C19 mediated 8-prenylnaringenin metabolite but much smaller than that of xanthohumol, indicating similar cytochrome P450 enzyme affinity between glabridin mono-hydroxylation and resveratrol mono-hydroxylation.

TABLE I. ENZYMATIC CONSTANTS OF GLABRIDIN METABOLISM

Metabolite	Vmax (pmol/min/mg microsomal protein)	Km (μM)
M2	324.2 ± 12.6	6.0 ± 0.7
M3	425.7 ± 14.9	5.6 ± 0.6
M4	306.7 ± 23.7	21.1 ± 3.5
M5	117.8 ± 9.6	8.9 ± 2.0

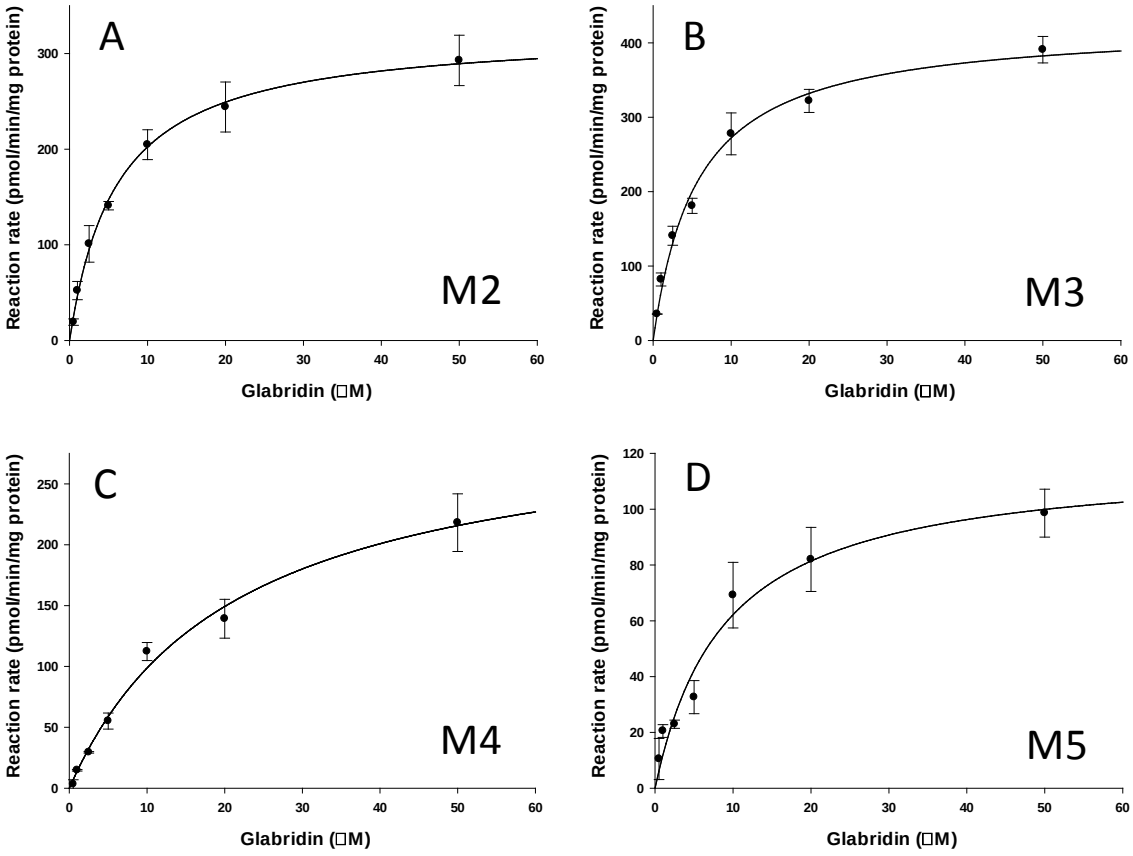

Figure 17. Michaelis-Menten plot of glabridin metabolite formation (A: M2, r^2 = 0.98, B: M3, r^2 = 0.98, C: M4, r^2 = 0.98, and D: M5, r^2 = 0.94). Error bars represent the mean ± S.D., n = 3.

2.4 Enzymes Responsible for the Metabolism of Glabridin

2.4.1 Background and Research Rationale

Xenobiotics undergo phase I and phase II metabolism in liver, intestine, and kidney, contributing to the overall systemic clearance of the compounds. The identification of xenobiotic metabolizing enzymes is also known as reaction phenotyping. By identifying the enzyme(s) responsible for the metabolism of a xenobiotic compound, potential interactions with the metabolism of drugs may be predicted, when those drugs are substrates of the same enzyme(s).

To identify relative contributions of specific P450 enzymes in human liver that are responsible for the formation of major metabolites of licorice compounds, incubations are usually carried out using either monoclonal antibodies (mAbs)[163-165] or chemical inhibitors that selectively inhibit specific cytochrome P450 enzymes.[166-168] Incubations with individual cDNA-expressed recombinant P450 enzymes can be used to confirm the results of the inhibition studies.[101,169,170]

Among the constituents identified in licorice species, only a few have been studied for in vitro metabolism with human cytochrome P450 enzymes. Occurring in all licorice species used in botanical dietary supplements (*Glycyrrhiza glabra*, *Glycyrrhiza uralensis*, and *Glycyrrhiza inflata*), glycyrrhetinic acid has been reported to be metabolized primarily by CYP3A4 and, to a lesser extent, by CYP2C9 and CYP2C19 in human liver

microsomes.[87] A unique constituent of *Glycyrrhiza glabra*, the metabolism of glabridin has not been investigated *in vitro* or *in vivo*. After determining the structures of some glabridin metabolites and proposing the structures of others based on tandem mass spectrometry with accurate mass measurement, enzymes responsible the formation of these metabolites were identified. According to Sections 1.1.2 and 2.1.1, phase I metabolism would therefore be a minor metabolic pathway. Studies of phase II metabolism of glabridin should therefore be investigated next.

2.4.2 Materials and Methods

2.4.2.1 Materials

Glabridin and NADPH were purchased from Sigma-Aldrich. Pooled human liver microsomes (20 mg/mL, 150 donors) and cDNA-expressed recombinant P450 enzymes (CYP1A2, 2A6, 2B6, 2C8, 2C9, 2C19, 2D6, 2E1, and 3A4) were purchased from BD Biosciences (Woburn, MA). HPLC-grade solvents were purchased from Thermo Fisher (Pittsburgh, PA).

2.4.2.2 Incubation with Recombinant P450 Enzymes

The CYP450 enzymes involved in the formation of the most abundant glabridin metabolites were identified using the cDNA-expressed human recombinant enzymes CYP1A2, 2A6, 2B6, 2C8, 2C9, 2C19, 2D6, 2E1, and 3A4. A 50 µM solution of glabridin

in 0.2 mL of 100 mM phosphate buffer at pH 7.4 was incubated with 1 pmol of each recombinant P450 enzyme and 1 mM NADPH for 60 min at 37 °C after a 5 min pre-incubation. Incubations were terminated by the addition of 10 µL 10% trichloroacetic acid to precipitate proteins followed by 2 min vortex mixing and 15 min centrifugation at 13,000 x *g* and 4 °C. The supernatants were removed, evaporated to dryness under a stream of nitrogen and reconstituted in 100 µL of acetonitrile/water (20:80, v/v) before analysis using UHPLC-MS/MS.

2.4.2.3 LC-MS/MS Analysis

Quantitative analysis to determine metabolite identity and concentration was carried using UHPLC-MS/MS with positive ion electrospray, CID and SRM with a Shimadzu LCMS-8040 triple quadrupole mass spectrometer and Nexera UHPLC system. UHPLC separations were obtained using a Waters Acquity BEH Shield RP18 (2.1×50 mm, 1.7 µm) UHPLC column. The mobile phase consisted of a 5.0 min linear gradient from 100% aqueous 0.05% formic acid containing 5 mM ammonium acetate to 100% acetonitrile containing 0.05% formic acid. The flow rate was 0.5 mL/min. The SRM transitions for each metabolite were determined based on tandem mass spectra of the metabolites during metabolite characterization using IT-TOF MS/MS analysis as stated above. Each metabolite was identified by its chromatographic retention time and tandem mass spectrum.

2.4.3 Results and Discussion

To investigate the roles of individual human cytochrome P450 enzymes in the metabolism of glabridin, incubations were carried out using cDNA-expressed recombinant enzymes. The formation of metabolites obtained from individual incubations with recombinant cytochrome P450 enzymes were multiplied by the mean specific content of the corresponding P450 enzyme in human liver microsomes to normalize the contribution of each P450 enzyme (**Figure 18**).[170] After normalization for the relative hepatic abundances of the cytochrome P450 isozymes, CYP1A2, CYP2C9, and CYP3A4 were found to be the major enzymes (>60% contribution) in the formation of the diol metabolites M2 and M3, while CYP2B6 and CYP2D6 contributed approximately 4 to 7% to their formation. The similar patterns of individual cytochrome P450 isozyme contributions to the formation of M2 and M3 confirmed that the diol metabolites were produced through the same pathway of oxidation likely followed by epoxide hydrolase catalyzed transformation. The slightly affinity difference between M2 and M3 might result from steric cooperativity in oxidation reaction with the enzyme.[171]

M4, the metabolite with a proposed hydroxyl group at the 4-carbon on the C-ring, was produced differently from M2 and M3. CYP3A4 and CYP2C9 were the primary enzymes responsible for M4 formation, with approximately equal contributions from each accounting for 40-50% of M4 production. CYP1A2, CYP2C8, CYP2C19, and CYP2D6 each catalyzed about 5% of M4 formation (**Figure 18**). M5 is proposed to be a dehydrogenation product at the 2-carbon position on the C-ring, and the data in **Figure 18** indicate that CYP2C9 and CYP3A4 were the predominant enzymes responsible for its

formation (combined 50% of total metabolite formation). CYP2C8, CYP2A6 and CYP2E1 contributed approximately 10%, 5%, and 5%, respectively, to the formation of metabolite M5. Other cytochrome P450 enzymes combined contributed less than 20% to the formation of M5.

In the literature, CYP1A2, CYP2C9, and CYP3A4 are reported in regards of epoxide/diol metabolite formation. Rabbit liver cytochrome P450 1A2 was found to catalyze the 5, 6-epoxidation of α-naphthoflavone, 1-hydroxylation of pyrene, and the subsequent 6-, 8-, and other hydroxylations of 1-hydroxypyrene.[171] Human CYP1A1 and CYP1A2 were reported to produce the epoxidation product of 3-methylindole, 3-methyloxindole.[172] Evidence from human liver microsomes also demonstrated that CYP1A2 has a major role in metabolism of resveratrol to form its hydroxylated metabolite.[161] CYP3A4 and/or CYP2C9 have also been reported to catalyze expoxide/diol metabolite formation from carbamazepine, linoleic acid, arachidonic acid, eicosapentaenoic acid, simvastatin, and ezlopitant alkene.[156,159,160,173,174]

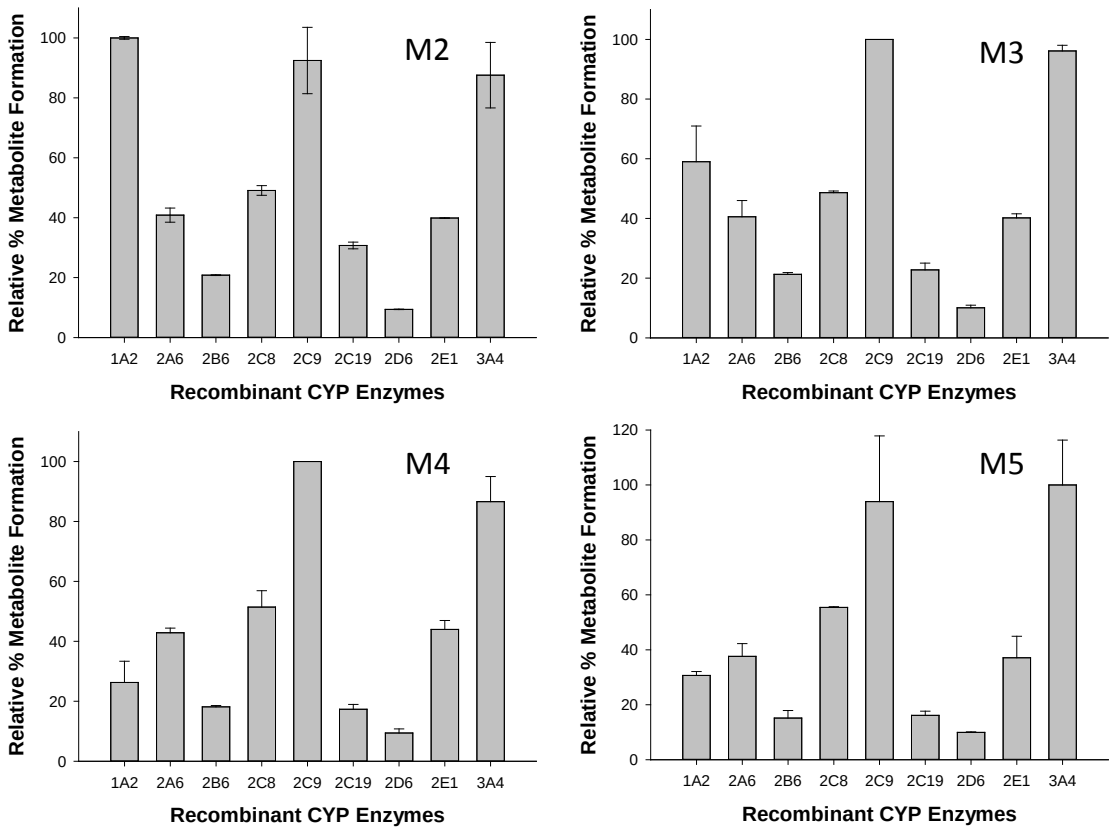

Figure 18. Relative contributions of recombinant CYP450 isozymes to the formation of M2, M3, M4, and M5

Chapter 3 Investigation of Reactive Metabolites Formed from Licorice

Most of this dissertation chapter has been published previously in *Analytical Chemistry* as follows:

Huang K, Huang L, van Breemen R. Detection of reactive metabolites using isotope-labeled glutathione trapping and simultaneous neutral loss and precursor ion scanning with ultra-high-pressure liquid chromatography triple quadruple mass spectrometry, *Anal Chem.* **2015**, *87*, 3646-3654

3.1 Introduction

Although xenobiotic metabolism is usually a detoxification process rendering drugs and similar molecules more polar and more rapidly excreted, metabolic transformation may result in electrophilic products that are potentially more toxic than their precursors. There are many examples of metabolic activation of drugs to electrophiles that covalently bind to macromolecules causing cell damage, and this process is responsible for 60% of instances where drugs had to be withdrawn from the US market or had black box warnings added to their packaging due to hepatotoxicity.[81] To address this safety concern, lead compounds are typically evaluated early during drug discovery and development for the formation of reactive metabolites and then chemically modified or abandoned to avoid this potentially toxic pathway.[175]

Since reactive metabolites have short half-lives and are therefore challenging to isolate or even to detect, in vitro chemical trapping has been used to form stable products that may be analyzed using mass spectrometry and/or nuclear magnetic resonance.[80,125,126] These experiments typically include the incubation of liver microsomes with NADPH and thiol trapping agents such as glutathione (GSH) or *N*-acetylcysteine. GSH is present in all mammalian tissues and serves as a natural scavenger for reactive metabolites by reacting with a broad range of electrophiles including epoxides, arene oxides, alkyl halides, quinones, and Michael addition acceptors.[128]

To overcome these limitations, a fast triple quadrupole mass spectrometer-based approach was developed that can detect positively and negatively charged GSH conjugates in a single analysis without the need for advance knowledge of the elemental compositions of potential conjugates and while avoiding false positives. This approach utilized UHPLC instead of HPLC to shorten separation time and enhance sensitivity, incorporated stable-isotope labeled GSH to avoid false positives, and used fast polarity switching electrospray MS/MS to detect GSH conjugates that form positive and/or negative ions.

Like drugs, herbal and dietary constituents may be metabolized by cytochrome P450 enzymes to nontoxic metabolites and excreted from the body, but the formation of toxic metabolites is also possible. In addition, the formation of reactive intermediates by CYP450 enzymes may also lead to the inactivation of the enzymes.[83] Although there are many possible mechanisms of herbal toxicity, the formation of reactive species that might

covalently bind to cellular proteins and/or DNA resulting in cytoxicity, oncogene activation, and hypersensitivity should be considered.[84] The general new method was used to test the licorice dietary supplement *Glycyrrhiza glabra* which was found to form multiple GSH conjugates upon metabolic activation.

3.2 Development of UHPLC-MS/MS Method for Detecting Reactive Metabolites

3.2.1 Background and Research Rationale

Tandem mass spectrometric fragmentation of GSH conjugates during collision-induced dissociation shows characteristic peptide product ions.[127,129,130] For example, GSH conjugates generally undergo a neutral loss (NL) of pyroglutamic acid (weighing 129 Da) during positive ion electrospray tandem mass spectrometry (MS/MS), which enables GSH conjugates to be detected with considerable selectivity using constant NL scanning of 129 Da (**Figure 19**).[127,176] Unfortunately, not all GSH conjugates produce abundant positive ion signals, and some that do ionize in positive mode do not produce a NL of 129 Da during collision-induced dissociation.[177] Another major drawback of this approach is false positive results due to interference from endogenous compounds. To overcome such false positives, Yan and Caldwell[178] used an equimolar mixture of GSH and isotope-labeled GSH ([$^{13}C_2{}^{15}N$]glycine) (**Figure 19**) to trap reactive drug metabolites from liver microsomal incubations for detection using HPLC-MS/MS with constant NL scanning. This method produced unambiguous doublet isotopic peaks with a mass difference of 3

Da for GSH conjugates that formed positive ions during electrospray, but those conjugates that did not form positive ions or eliminate 129 Da remained undetected.

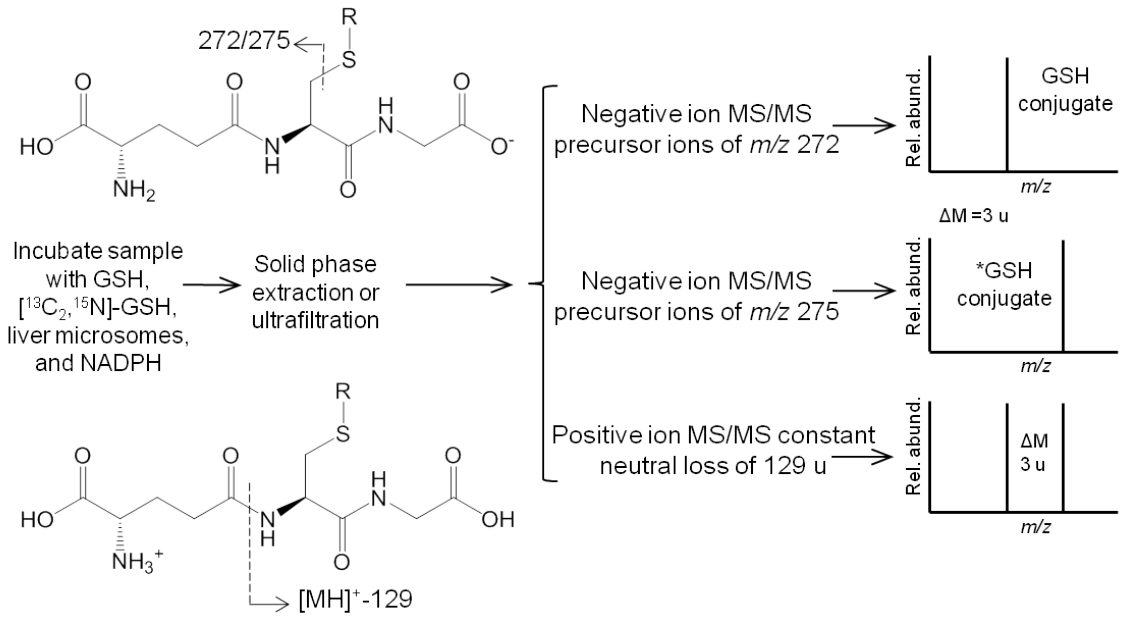

Figure 19. UHPLC-MS/MS approach to screening for GSH conjugates.

When deprotonated GSH conjugates are formed, negative ion MS/MS product ion scanning usually shows fragment ions of *m/z* 272 corresponding to deprotonated γ-glutamyl-dehydroalanyl-glycine (**Figure 19**). Therefore, precursor ion (PI) scanning of *m/z* 272 in negative ion mode is an approach to detect GSH conjugates that do not form positive ions while being less prone to false positive results.[175,177] To reduce false negative results and to characterize the detected GSH conjugates, Wen, *et al.*,[179] used polarity switching during HPLC-MS/MS to combine PI scanning of *m/z* 272 of GSH conjugates in negative ion mode with positive ion MS/MS product ion scanning. This approach to the detection and characterization of GSH conjugates worked well for the

subset of GSH conjugates forming both product ions of *m/z* 272 during negative ion electrospray as well as protonated molecules in positive ion mode.

Another MS-based approach for detecting GSH conjugates is mass defect filtering.[180,181] Using high resolution mass spectrometry with accurate mass measurement, GSH conjugates can be detected by applying a mass defect filter, which takes into account the unique fractional mass (the mass to the right of the decimal point) of a GSH conjugate. In its original form, this approach requires that the approximate elemental composition of the GSH conjugate be known in advance. Then, a mass defect range could be calculated and applied to the high resolution mass spectra such that those ions with mass defects within the predicted range are determined to be GSH conjugates. Recognizing that mass defect filtering cannot be used to screen for GSH conjugates of unknown compounds (as in the case of botanical dietary supplements), Ruan and Zhu[181] revised the approach to test for the negative ion electrospray GSH fragment ion of exact mass *m/z* 272.0888. Of course, mass defect filtering that is limited to negatively charged GSH conjugates will miss those that form only positive ions. Furthermore, mass defect filtering requires access to high resolution mass spectrometers capable of accurate mass measurement.

In the present study, selected features from several previous methods for GSH conjugate detection were combined with new approaches that included constant NL MS/MS scanning,[130] stable isotope labeled GSH,[177] polarity switching,[178] PI MS/MS scanning,[177] and the new features of ultra-high pressure liquid chromatography (UHPLC) and fast-scanning triple quadrupole mass spectrometry. False positive results were avoided by

using a 1:1 ratio of GSH and stable isotope labeled GSH to trap reactive metabolites. Fast positive ion NL MS/MS scanning of 129 Da was alternated on-line with negative ion PI MS/MS scanning of *m/z* 272 (unlabeled GSH) and *m/z* 275 (labeled GSH) for the unambiguous detection of GSH conjugates that formed either positive or negative ions (**Figure 19**). Compared with our previous GSH screening assay based on HPLC-MS/MS,[179] UHPLC-MS/MS reduced analysis time from 30 min to less than 8 min.

The utility of this new approach was verified using 7 compounds known to form reactive metabolites (acetaminophen, ticlopidine, diclofenac, *p*-cresol, 4-ethylphenol, amodiaquine, and 17α-ethinylestradiol) and 4 compounds do not form reactive metabolites as negative controls (dextromethorphan, testosterone, midazolam, and tolbutamide) (**Figure 20**).

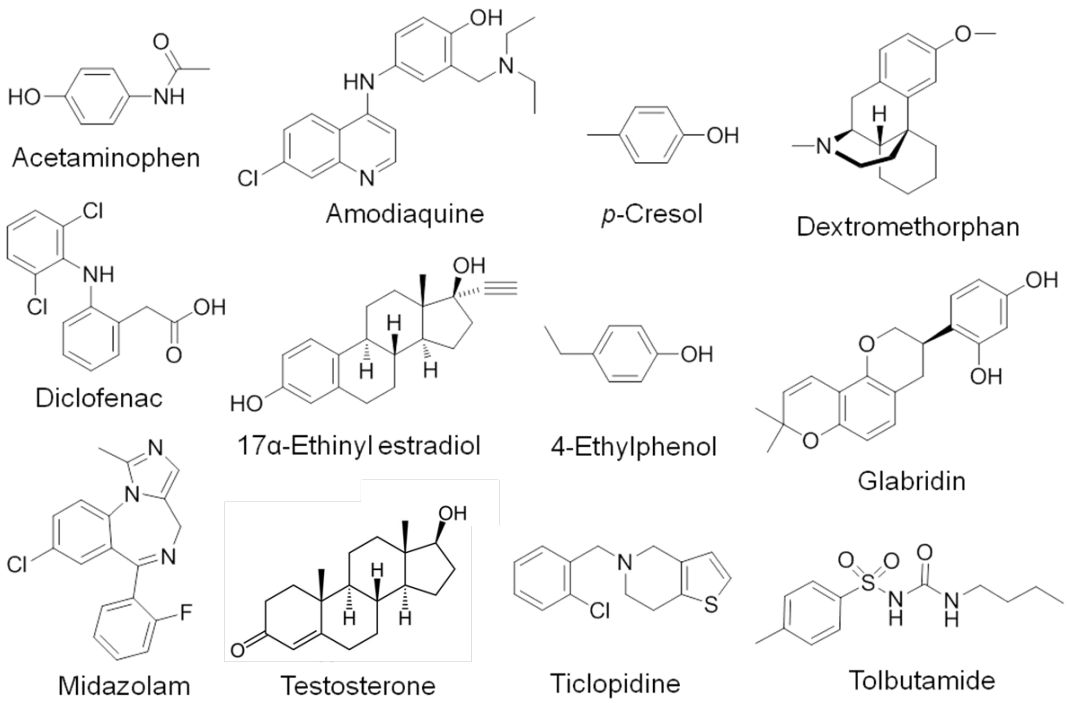

Figure 20. Structures of compounds tested for metabolic activation to electrophilic metabolites.

3.2.2 Materials and Methods

3.2.2.1 Materials

Acetaminophen, diclofenac, *p*-cresol, ticlopidine, amodiaquine, 17α-ethinyl estradiol, dextromethorphan, testosterone, midazolam, tolbutamide, reduced GSH, ([$^{13}C_2{}^{15}N$]-glycine) GSH (**Figure 19**, **Figure 20**), β-nicotinamide adenine dinucleotide 2'-phosphate reduced tetrasodium salt (NADPH), and trichloroacetic acid were purchased from Sigma-Aldrich (St. Louis, MO). Pooled human liver microsomes (20 mg/mL, 150 donors) were purchased from BD Biosciences (Woburn, MA). Bond Elute C_{18} solid phase extraction cartridges (3 mL, 200 mg sorbent) were purchased from Agilent Technologies (Santa Clara, CA), and HPLC-grade solvents were purchased from Thermo Fisher (Pittsburgh, PA).

3.2.2.2 Microsomal Incubations

Human liver microsomes (0.5 mg/mL) and 1 mM GSH (equimolar unlabeled GSH and labeled GSH) were incubated separately with each test compound (10 to 50 µM) or extract (500 µg/mL) in 100 mM phosphate buffer (pH 7.4) at 37 °C in a final volume of 1 mL. NADPH (1 mM) was added to initiate oxidative metabolism after a 5 min pre-

incubation. Control experiments were carried out without microsomes, NADPH, test compound or GSH. After 60 min, the reactions were terminated by the addition of 100 µL of trichloroacetic acid (10%) followed by 15 min centrifugation at 12,000 *g* and 4 °C. Supernatants (1 mL) of each were removed and loaded onto solid phase extraction cartridges.

3.2.2.3 Solid Phase Extraction

Sample preparation was carried out using C_{18} solid phase extraction cartridges that were pre-washed with 1 mL of methanol and then conditioned with 1 mL of water. After loading a supernatant from a microsomal incubation, the cartridge was washed with 2 mL water and then eluted with 2 mL of methanol. The methanol eluate was evaporated to dryness under a stream of nitrogen and reconstituted in 100 µL of acetonitrile/water (10:90, v/v) before analysis using UHPLC-MS/MS.

3.2.2.4 Mass Spectrometry

A Shimadzu (Kyoto, Japan) LCMS-8050 triple quadrupole mass spectrometer equipped with a Shimadzu Nexera UHPLC system was used with a Waters (Milford, MA) Acquity UPLC BEH Shield RP18, 2.1×50 mm, 1.7 µm column for UHPLC-MS/MS analyses. The UHPLC mobile phase A was 5 mM ammonium acetate in water containing 0.1% formic acid, and mobile phase B was acetonitrile containing 0.1% formic acid. The gradient elution profile consisted of a 3.5 min linear gradient from 5% B to 100% B. The column

was re-equilibrated with 5% B for at least 1 min between analyses. The UHPLC flow rate was 0.4 mL/min, the column temperature was 40 °C, and the injection volume was 10 µL.

Electrospray was used for ionization during UHPLC-MS/MS while the following cycle of MS/MS scans was carried out: negative ion PI scanning for *m/z* 272 (unlabeled GSH conjugates); negative ion PI scanning for *m/z* 275 (labeled GSH conjugates); and positive ion constant NL scanning for loss of 129 Da (labeled and unlabeled GSH conjugates). The scan range was *m/z* 400-700 at unit resolving power, the polarity switching speed was 5 ms, and each scan was recorded over 0.12 s. Additional mass spectrometer parameters included an electrospray voltage of 4.0 kV (positive ion) and -4.5 kV (negative ion), Q3 voltage of -17 V (positive ion) and 13 V (negative ion), collision energy -13 V (positive ion) and 12 V (negative ion), nebulizing gas flow 2 L/min, heating gas flow 10 L/min, drying gas flow 10 L/min, interface temperature 300 °C, desolvation line temperature 250 °C, and a heat block temperature of 400 °C.

As part of the method validation (although not required for routine GSH conjugate screening), each sample was also analyzed using high resolution accurate mass measurement with data-dependent product ion MS/MS on a Shimadzu LCMS-IT-TOF hybrid mass spectrometer equipped with a Shimadzu Prominence UFLC-XR HPLC system. Separations were obtained using a Waters XTerra C_{18}, 2.1×100 mm, 3.5 µm HPLC column. The mobile phase consisted of a 20 min linear gradient from 2 mM ammonium acetate in water containing 0.1% formic acid to acetonitrile containing 0.1% formic acid. The flow rate was 0.3 mL/min, and the column temperature was 30 °C. In

the electrospray source, the nitrogen nebulizing gas flow was 1.5 L/min, the heating gas flow 10 L/min, the interface temperature 300 °C, the desolvation line 200 °C, and the heat block 300 °C. Positive ion electrospray mass spectra and product ion tandem mass spectra were recorded from *m/z* 100-700. Product ion mass spectra were recorded in 0.411 sec using unit resolution selection in the ion trap and a resolving power of 14,000 in the time-of-flight (TOF) sector. Ion accumulation times in the ion trap were 0.02 s for MS and 0.015 s for MS/MS. During collision-induced dissociation in the ion trap, the collision energy was set to 80%, the collision gas was 80%, and the frequency was 0.251 (45 kHz). The detector voltage was 1.65 kV.

The MS/MS conditions for GSH conjugate detection were optimized using 1 μM GSH prior to the analysis of the GSH conjugates. By varying the concentration of formic acid from 0 to 0.2%, it was determined that 0.1% formic acid was optimum for the formation of abundant protonated GSH during positive ion electrospray as well as abundant deprotonated GSH during negative ion electrospray. The optimum CE values for MS/MS (-13 V for positive ion and 12 V for negative ion) that were determined using GSH were confirmed to be valid for GSH conjugates such as those of acetaminophen. Even though the triple quadrupole mass spectrometer that was used was capable of 0.01 s per scan over the selected mass range, scans of 0.10 s to 0.15 s produced tandem mass spectra with superior signal-to-noise in both NL and PI modes. Subsequently, 0.12 s per scan was used for all GSH conjugate screening.

3.2.3 Results and Discussion

3.2.3.1 Acetaminophen

Cytochrome P450 enzymes in human liver catalyze the oxidation of acetaminophen to several metabolites including the electrophile *N*-acetyl-*p*-benzoquinone imine.[125] **Figure 21** shows NL and PI MS/MS chromatograms of acetaminophen metabolites after incubation with human liver microsomes, cofactor NADPH, unlabeled GSH, and [$^{13}C_2$,^{15}N]-GSH. Two peaks were detected eluting at 1.75 min and 1.86 min in all 3 chromatograms using our new approach, indicating that these were GSH conjugates of acetaminophen.

The positive ion electrospray constant NL (129 Da) MS/MS chromatogram of the acetaminophen GSH conjugate eluting at 1.75 min showed two protonated molecules of equal abundance at *m/z* 473 and *m/z* 476 (**Table 2**), corresponding to conjugation with unlabeled and labeled GSH, respectively, and confirming that this peak was not a false positive result. The corresponding deprotonated molecules of *m/z* 471 and *m/z* 474 at equal abundance observed during negative ion PI scanning (**Table 2**) also indicated that this peak was a GSH conjugate. This compound is consistent with a previously reported mono-oxygenated acetaminophen quinone imine that forms a GSH conjugate (acetaminophen +O –2H +GSH).[179]

The most intense peak (retention time 1.86 min; **Figure 21**) showed protonated molecules of *m/z* 457 and *m/z* 460 at equal abundance during positive ion NL scanning and also formed the corresponding deprotonated molecules of *m/z* 455 and *m/z* 458 at approximately equal abundance during negative PI scanning of *m/z* 272 (**Table 2**). These masses are consistent with the reaction of GSH with an *N*-acetyl-*p*-benzoquinone imine metabolite of acetaminophen (acetaminophen –2H +GSH) as reported previously.[178,180]

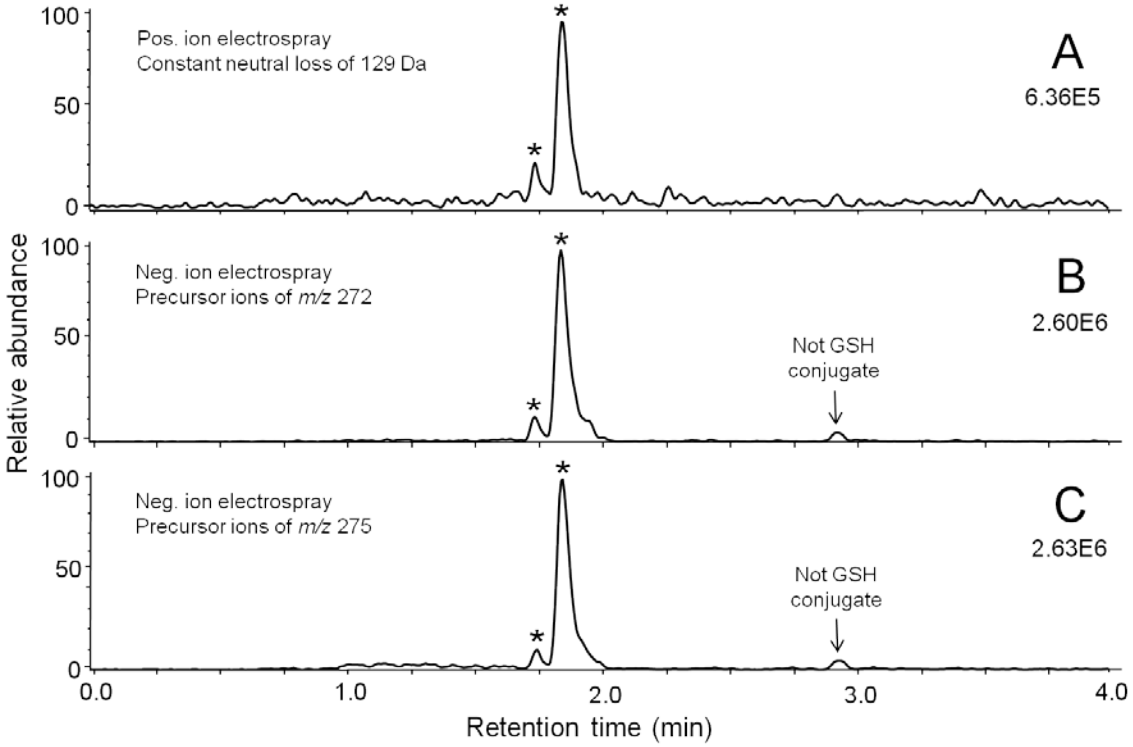

Figure 21. UHPLC-MS/MS chromatograms of GSH conjugates formed during incubation of acetaminophen with human liver microsomes, NADPH, GSH, and [$^{13}C_2$,^{15}N]-GSH. A) Positive ion electrospray neutral loss MS/MS scanning of 129 Da; B) negative ion electrospray MS/MS scanning for precursors of *m/z* 272 (unlabeled GSH); and C) negative ion electrospray MS/MS precursor ion scanning for precursors of *m/z* 275 (labeled GSH). *Denotes GSH conjugate.

For method validation, positive ion electrospray HPLC-MS/MS analyses with product ion scanning of the ions of *m/z* 473, *m/z* 476, *m/z* 457 and *m/z* 460 were carried out using a high resolution hybrid mass spectrometer. For example, accurate mass measurements of the ions of *m/z* 457 and *m/z* 460 were within 5 ppm of expected formula $C_{18}H_{24}N_4O_8S$, and both conjugates shared a common fragment ion of *m/z* 382 (**Figure 22**), which represented the loss of labeled/unlabeled glycine from the GSH moiety. Another common fragment ion of *m/z* 182 corresponded to cleavage of the S-peptide bond with loss of the GSH residue and retention of the positive charge on the unlabeled acetaminophen metabolite. Other abundant fragment ions of *m/z* 328 (unlabeled) and *m/z* 331 (labeled) originated from the loss of a GSH-characteristic pyroglutamate (129 Da) group, and ions of *m/z* 311 and *m/z* 314 corresponded to loss of unlabeled amino-pyroglutamate (146 Da) from the protonated molecules (**Figure 22**). Therefore, this new screening assay correctly detected and characterized the known quinoid GSH conjugates of acetaminophen oxidative metabolites.

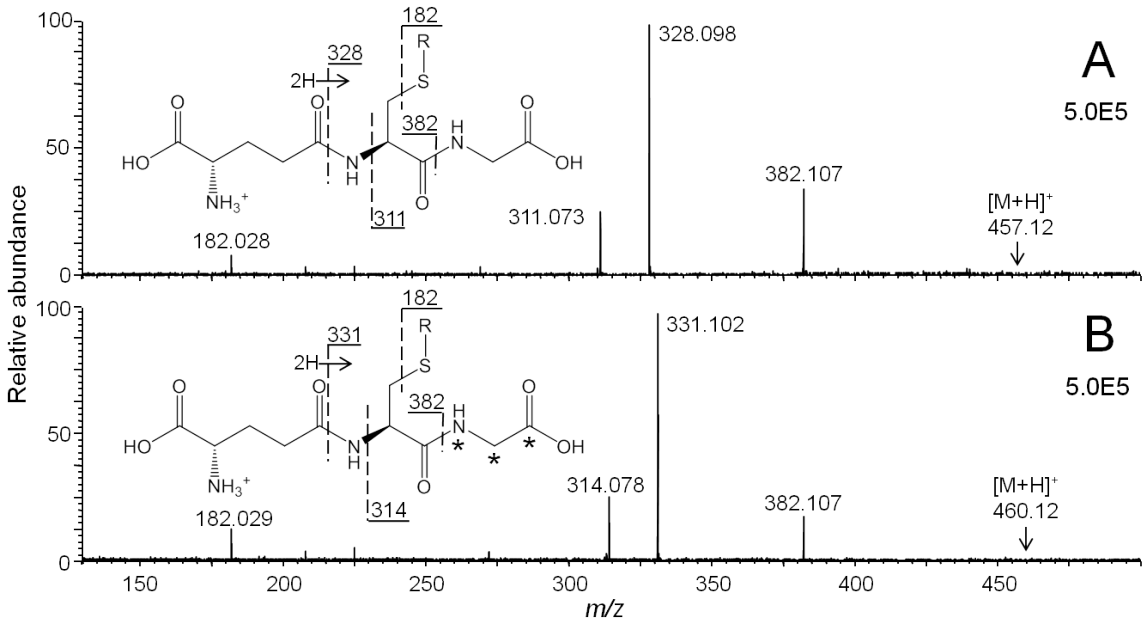

Figure 22. High resolution product ion MS/MS spectra of protonated molecules of acetaminophen GSH conjugates eluting at a retention time of 1.86 min in Figure 19 containing A) unlabeled GSH (*m/z* 457); and B) isotope-labeled GSH (*m/z* 460).

A minor chromatographic peak was observed at a retention time of 2.95 min only in the negative ion PI scanning chromatogram (**Figure 21**). The corresponding precursor ion scans indicated ions of *m/z* 443.0 and *m/z* 445.5 (ΔM = 2) (**Table 2**) which are inconsistent with GSH conjugates differing by 3 u. Also, the relative abundances of these two signals were 40% and 100%, respectively (**Table 2**), which are also inconsistent with the expected equal abundances of conjugates formed by reaction of an acetaminophen metabolite with equimolar GSH and labeled GSH. Therefore, the signal detected at 2.95 min may be dismissed as a false positive without the need for any additional experimentation.

3.2.3.2 p-Cresol

Three GSH conjugates of *p*-cresol metabolites were detected during UHPLC-MS/MS at retention times 2.93 min, 3.21 and 3.39 min, respectively (**Figure 23**, **Table 2**). The peak eluting at 2.93 min formed a pair of protonated molecules of *m/z* 414/417 of equal abundance during positive ion NL MS/MS and a pair of deprotonated molecules of *m/z* 412/415 during negative ion PI MS/MS, which confirmed that this was a GSH conjugate. The molecular mass of this compound (413 u) corresponded to a known quinone methide of *p*-cresol (*p*-cresol –2H +GSH).[180,182] The peaks eluting at 3.21 min and 3.39 min were isomeric GSH conjugates as indicated by the pairs of protonated and deprotonated molecules of equal relative abundance at *m/z* 430/433 and *m/z* 428/431, respectively (**Table 2**). With a molecular mass of 429 u, these two isomers corresponded to GSH conjugates of known catechol metabolites of *p*-cresol (*p*-cresol +O –2H +GSH).[180,182]

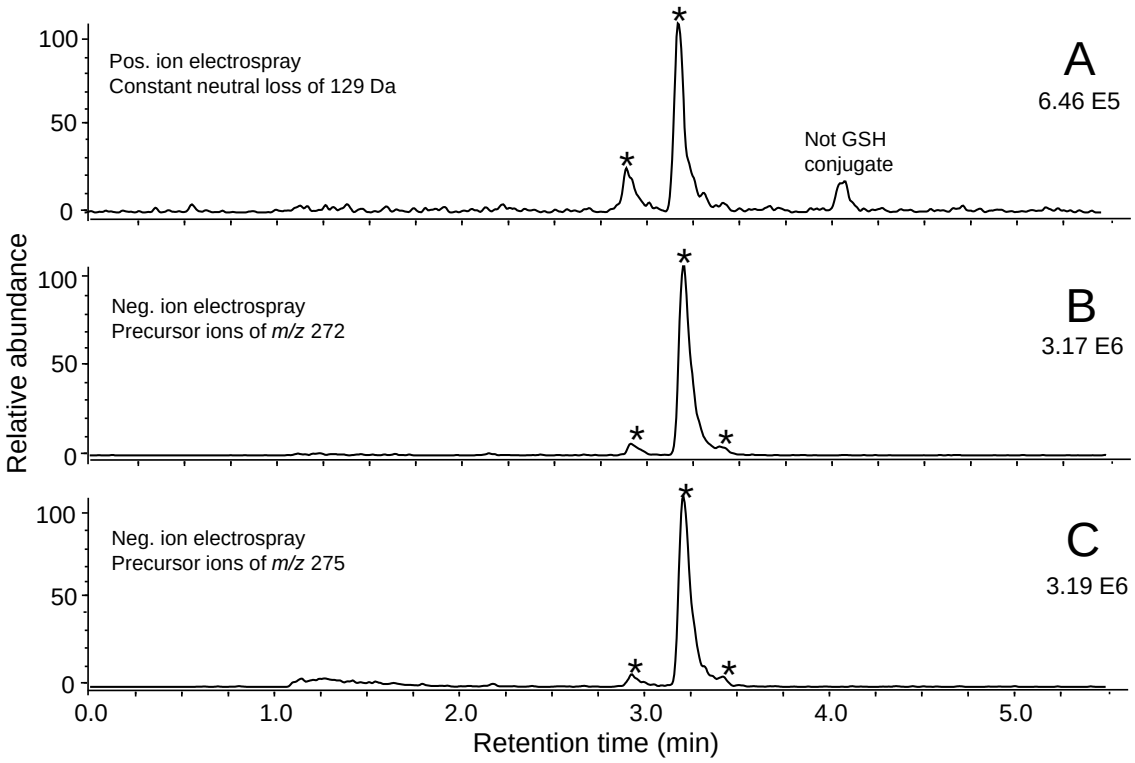

Figure 23. UHPLC-MS/MS chromatograms of GSH conjugates formed during incubation of *p*-cresol with human liver microsomes, NADPH, GSH, and [$^{13}C_2$,^{15}N]-GSH. A) Positive ion electrospray neutral loss MS/MS scanning of 129 Da; B) negative ion electrospray MS/MS scanning for precursors of *m/z* 272 (unlabeled GSH); and C) negative ion electrospray MS/MS precursor ion scanning for *m/z* 275 (labeled GSH). A peak eluting at 4.11 min was detected only during positive ion UHPLC-MS/MS NL analysis of *p*-cresol metabolites (Table 2). Although there were signals corresponding to precursor ions differing by 3 u (*m/z* 444.5 and *m/z* 447.2), the relative abundances of these two signals were 12% and 100%, respectively, which is inconsistent with GSH conjugates formed by reaction of an electrophilic metabolite with equimolar unlabeled and labeled GSH (Table 2). Therefore, the signal detected at 4.11 min was not a GSH conjugate. *Denotes GSH conjugate.

3.2.3.3 Diclofenac

After incubation of diclofenac with human liver microsomes, NADPH and GSH, seven peaks were detected during UHPLC-MS/MS with positive ion NL and negative ion PI scanning (**Figure 24**, **Table 2**). The peak eluting at 4.00 min was confirmed as a GSH conjugate by the precursor ions of equal abundance at *m/z* 583 and *m/z* 586 during positive ion NL scanning and the corresponding doublet of *m/z* 581 and *m/z* 584 observed during negative ion PI scanning (**Table 2**). This GSH conjugate corresponds to a previously reported metabolite of molecular mass 582 formed by mono-oxygenation of diclofenac, loss of HCl and addition of GSH (diclofenac +O –HCl +GSH).[179,180,183,184] Peaks eluting at 4.14 min, 4.27 min and 4.60 min during UHPLC-MS/MS produced protonated molecules of equal abundance of *m/z* 617/620 during positive ion NL scanning and of *m/z* 615/618 during negative ion PI scanning (**Table 2**), which confirmed that they were isomeric diclofenac GSH conjugates (diclofenac +O –2H +GSH) as had been reported previously.[179,180,183,184]

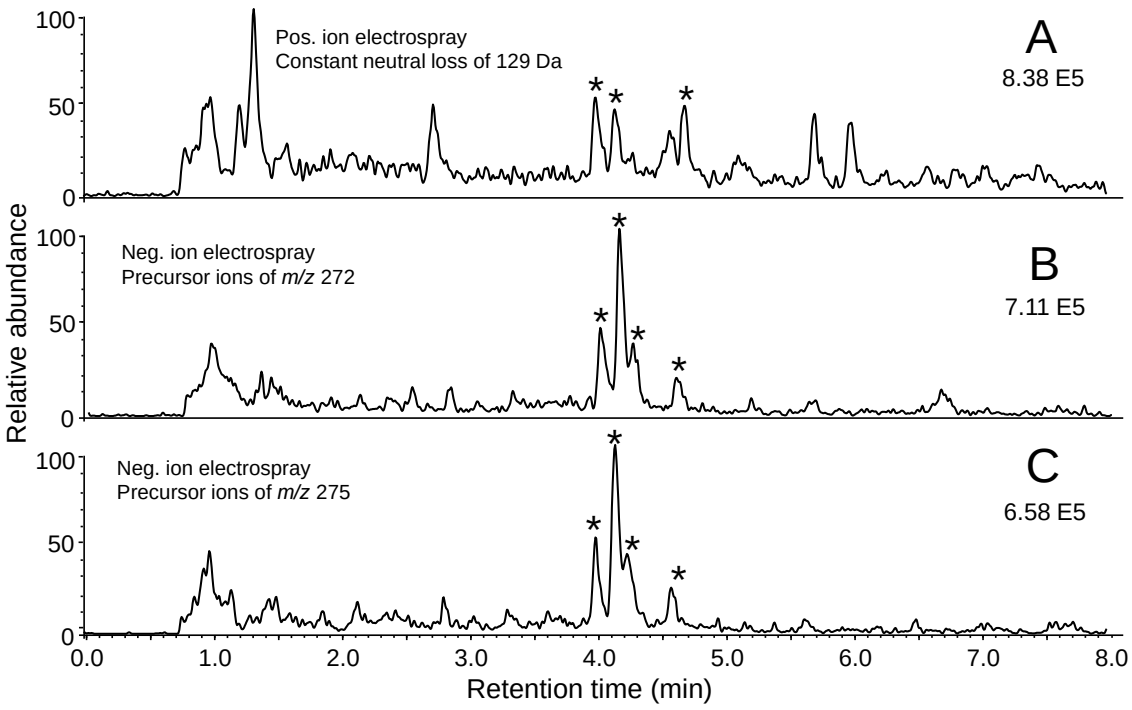

Figure 24. UHPLC-MS/MS chromatograms of GSH conjugates formed during incubation of diclofenac with human liver microsomes, NADPH, GSH, and [$^{13}C_2$,^{15}N]-GSH. A) Positive ion electrospray neutral loss MS/MS scanning of 129 Da; B) negative ion electrospray MS/MS scanning for precursors of *m/z* 272 (unlabeled GSH); and C) negative ion electrospray MS/MS precursor ion scanning for *m/z* 275 (labeled GSH). Peaks with retention times of 2.75, 5.71 and 5.89 min, observed only during positive ion NL scanning, could be excluded from consideration as GSH conjugates, as they did not show signals of equal abundance corresponding to unlabeled and labeled GSH (Table 2). As part of method validation, the elemental compositions of all peaks were determined using high resolution mass spectrometry, and the presence of GSH was also confirmed using UHPLC-MS/MS with product ion scanning.

3.2.3.4 Ticlopidine

During analysis of the ticlopidine incubation mixture, two peaks were detected at retention times 1.83 min and 2.02 min in the UHPLC-MS/MS chromatograms (**Figure 25**; **Table 2**). Pairs of precursor ions (ΔM = 3) of equal abundance were detected in both positive mode (*m/z* 587/590) and negative mode (*m/z* 585/588) for each peak corresponding to conjugates with light and heavy GSH, respectively. These isomeric compounds were formed by mono-oxygenation of ticlopidine followed by conjugation with GSH (ticlopidine +O +GSH). GSH conjugates of mono-oxygenated ticlopidine have been reported previously.[179]

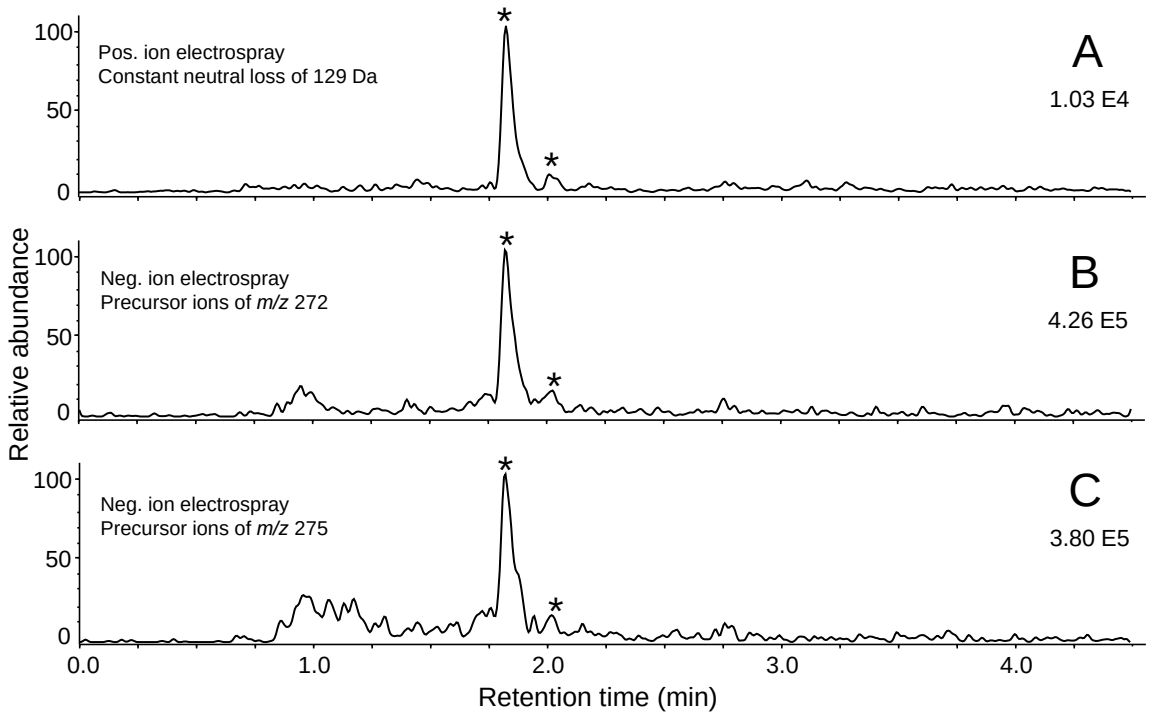

Figure 25. UHPLC-MS/MS chromatograms of GSH conjugates formed during incubation of ticlopidine with human liver microsomes, NADPH, GSH, and

[$^{13}C_2$,^{15}N]-GSH. A) Positive ion electrospray neutral loss MS/MS scanning of 129 Da; B) negative ion electrospray MS/MS scanning for precursors of *m/z* 272 (unlabeled GSH); and C) negative ion electrospray MS/MS precursor ion scanning for *m/z* 275 (labeled GSH).

3.2.3.5 Amodiaquine

As reported previously,[184] two GSH conjugates of electrophilic metabolites of amodiaquine (retention times 3.63 and 3.84 min) were detected during negative ion electrospray UHPLC-MS/MS PI scanning, and one peak eluting at 3.84 min was detected during positive ion UHPLC-MS/MS NL scanning (**Figure 26**; **Table 2**). The peak eluting at 3.63 min corresponded to a GSH conjugate of amodiaquine that had undergone oxidative *N*-deethylation (amodiaquine -C_2H_6 +GSH). The presence of a pair of ions of equal abundance that differed by 3 u (*m/z* 632/635) confirmed that this peak was a GSH conjugate (**Table 2**). The abundant peak eluting at 3.84 min corresponded to an amodiaquine quinonimine that had reacted with GSH (amodiaquine –2H +GSH). Pairs of ions of equal abundance differing by 3 u in positive mode (*m/z* 662/665) and in negative mode (*m/z* 660/663) confirmed that this compound was a GSH conjugate (**Table 2**).

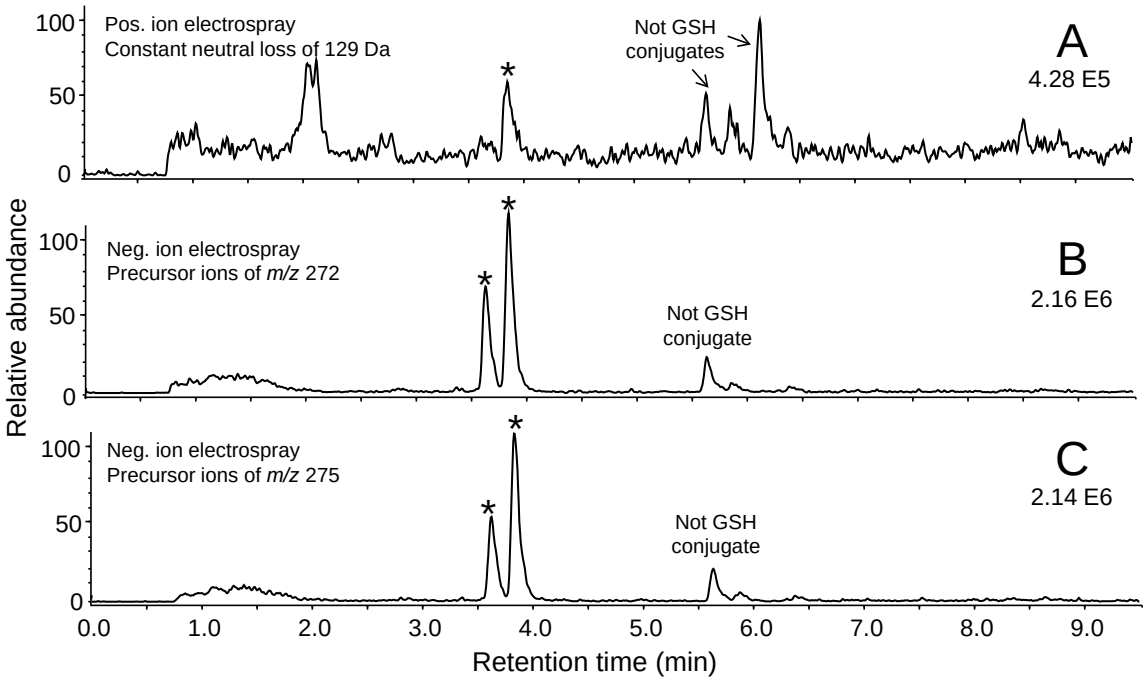

Figure 26. UHPLC-MS/MS chromatograms of GSH conjugates formed during incubation of amodiaquine with human liver microsomes, NADPH, GSH, and [$^{13}C_2$,^{15}N]-GSH. A) Positive ion electrospray neutral loss MS/MS scanning of 129 Da; B) negative ion electrospray MS/MS scanning for precursors of *m/z* 272 (unlabeled GSH); and C) negative ion electrospray MS/MS precursor ion scanning for *m/z* 275 (labeled GSH).

Although the peak observed at 5.69 min formed ion of *m/z* 576.4/579.4) during positive ion NL MS/MS and negative ions of *m/z* 574.0/577.5 during PI MS/MS, the relative abundances of each pair of ions were unequal. Therefore, this compound was not a GSH conjugate. Finally, the peak detected at 6.12 min during positive ion NL MS/MS was not a GSH conjugate, since its precursor ions did not differ by 3 u or show equal abundances (**Table 2**).

3.2.3.6 4-Ethylphenol

UHPLC-MS/MS analysis of metabolites of 4-ethylphenol after incubation with human liver microsomes, NADPH, and labeled and unlabeled GSH showed five peaks (**Figure 27**), and each of these five peaks showed signals separated by 3 u corresponding to the isotope signatures for labeled and unlabeled GSH (**Table 2**). The peak eluting at 3.31 min corresponded to a previously reported quinone methide metabolite of 4-ethylphenol that eliminated 2H atoms before reacting with GSH (4-ethylphenol –2H +GSH).[180] The most abundant GSH conjugate (retention time 3.85 min) has also been reported previously[180] and consisted of a catechol metabolite of 4-ethylphenol that was oxidized to an *ortho*-quinone before reacting with GSH (4-ethylphenol +GSH –2H +O). The GSH conjugate eluting at 4.14 min (**Table 2**) was a previously unreported minor isomer of the *ortho*-quinone conjugate.

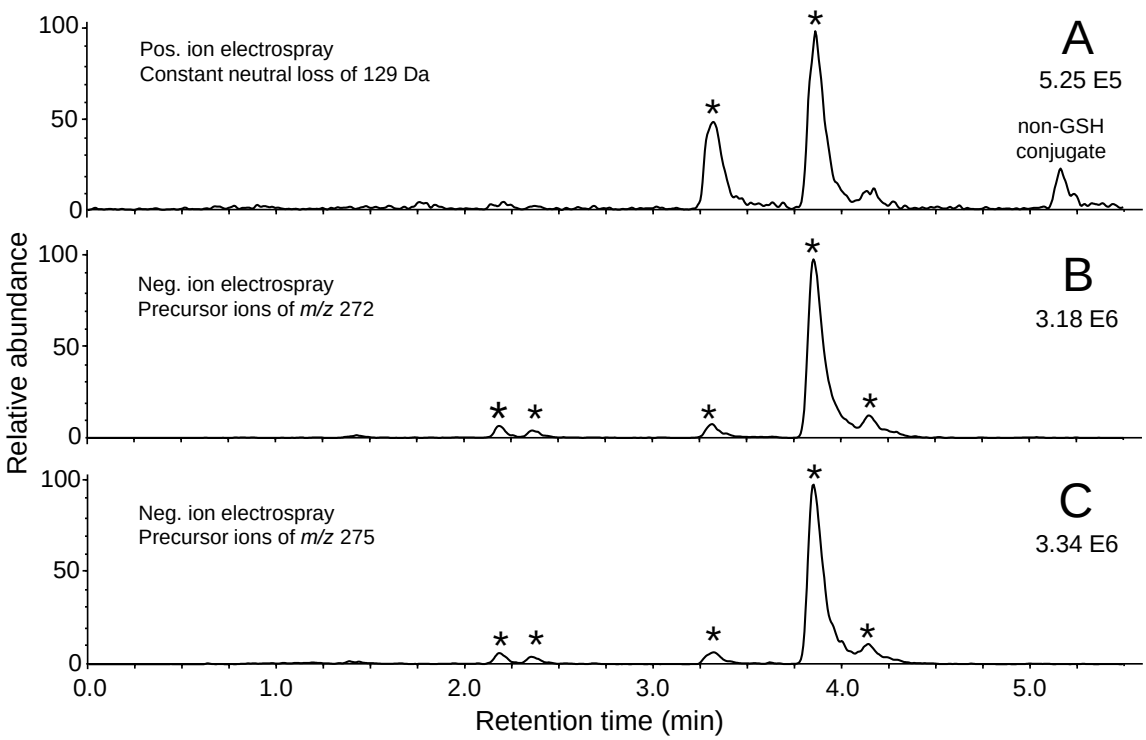

Figure 27. UHPLC-MS/MS chromatograms of GSH conjugates formed during incubation of 4-ethylphenol with human liver microsomes, NADPH, GSH, and [$^{13}C_2$,^{15}N]-GSH. A) Positive ion electrospray neutral loss MS/MS scanning of 129 Da; B) negative ion electrospray MS/MS scanning for precursors of *m/z* 272 (unlabeled GSH); and C) negative ion electrospray MS/MS precursor ion scanning for precursors of *m/z* 275 (labeled GSH).

The peaks eluting at 2.18 min and 2.38 min (**Figure 27**) corresponded to previously unreported isomeric GSH conjugates of 4-ethylphenol metabolites which had gained 2 oxygen atoms and lost 2 hydrogen atoms (4-ethylphenol +2O –2H +GSH). These two peaks were only observed in negative PI scan mode, which emphasizes the need for measuring negative ions and not just positively charged GSH conjugates. A peak was detected at 5.24 min during positive ion NL screening but not during negative ion PI

screening, and without any additional experimentation, it could be determined that this peak was not a GSH conjugate. Although the positive ion constant neutral loss ion scanning indicated ions of both *m/z* 458.3 and *m/z* 461.2 (ΔM = 3), the relative abundances of these two signals were 100% and 48%, respectively (**Table 2**), which is inconsistent with the equal abundances of conjugates that would be formed by reaction of an electrophilic metabolite with equimolar GSH and labeled GSH.

3.2.3.7 17α-Ethinyl estradiol

Five GSH conjugates were detected during positive ion NL and/or negative ion PI MS/MS scanning of the liver microsomal metabolites of 17α-ethinyl estradiol (**Figure 28**, **Table 2**). Each of these peaks was confirmed as a GSH conjugate by the presence of ions differing by 3 u that corresponded to the isotope signatures for labeled and unlabeled GSH (**Table 2**). The precursor ions for the peaks eluting at 3.82, 4.00 and 4.13 min were *m/z* 618/621 in positive ion mode (NL) and *m/z* 616/619 in negative mode (PI), which corresponded to an unlabeled molecular mass of 617 (17α-ethinyl estradiol +O –2H +GSH). This mass is consistent with the known *ortho*-quinone metabolite of 17-α-ethinyl estradiol.[185]

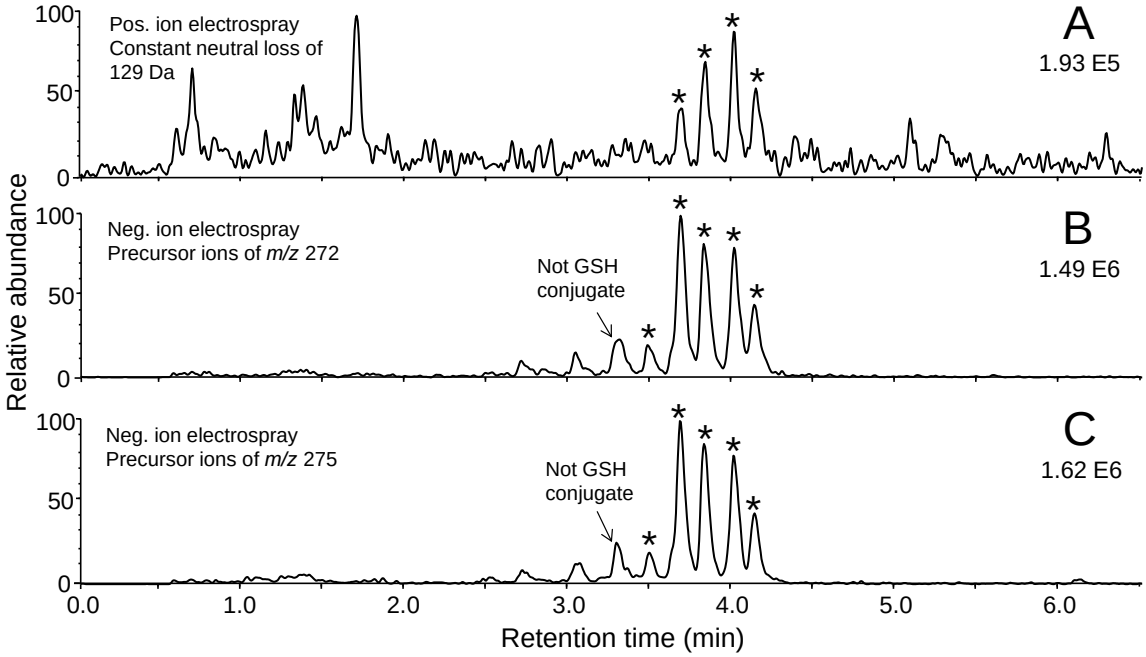

Figure 28. UHPLC-MS/MS chromatograms of GSH conjugates formed during incubation of 17α-ethinyl estradiol with human liver microsomes, NADPH, GSH, and [$^{13}C_2$, ^{15}N]-GSH. A) Positive ion electrospray neutral loss MS/MS scanning of 129 Da; B) negative ion electrospray MS/MS scanning for precursors of *m/z* 272 (unlabeled GSH); and C) negative ion electrospray MS/MS precursor ion scanning for precursors of *m/z* 275 (labeled GSH).

The precursor ions of the peaks eluting at 3.47 min and 3.68 min (**Figure 28**) showed doublet ions of equal abundance at *m/z* 634 and *m/z* 637 during positive ion NL scanning and at *m/z* 632 and *m/z* 635 during negative ion PI scanning (**Table 2**), which indicated that these peaks corresponded to GSH conjugates. Previously unreported GSH conjugates of 17α-ethinyl estradiol, these isomers corresponded to the addition of two oxygen atoms and loss of two hydrogen atoms before conjugation with GSH (17α-ethinyl estradiol +2O –2H +GSH). Although a peak was observed at 3.29 min during negative ion PI, it was

inconsistent with a GSH conjugate since the precursor ions of *m/z* 632.1 and *m/z* 636.0 differed by 4 u instead of 3 u as would be expected for conjugates containing unlabeled and labeled GSH, respectively (**Table 2**).

3.2.3.7 Dextromethorphan, Midazolam, Testosterone, and Tolbutamide

Since dextromethorphan, midazolam, testosterone, and tolbutamide have not been reported to form electrophilic metabolites or GSH conjugates,[178] these compounds were used as negative controls to validate the UHPLC-MS/MS method. As expected, no GSH conjugates were detected using either positive ion NL scanning or negative ion PI scanning, indicating that the new GSH conjugate screening approach is highly accurate at preventing false positive results.

3.2.4 Conclusion

To validate this new GSH screening assay, seven compounds known to form electrophilic intermediates and GSH conjugates and four compounds that do not form such metabolites were tested. All of these positive control and negative control compounds produced the expected results. In addition to the detection of known metabolites, three new GSH conjugates of 4-ethyl phenol and two new GSH conjugates of 17α-ethinyl estradiol were detected. This indicated that the new GSH screening assay is extremely sensitive.

Since some GSH conjugates might produce only positive ion signals while others might form only negation ions, our approach to measuring GSH conjugates using both positive ion and negative ion MS/MS in a single assay provides both higher throughput and consumes less sample than two separate analyses. This approach also detects more GSH conjugates than would UHPLC-MS/MS screening using only positive ion or only negative ion electrospray. For example, GSH conjugates of 17α-ethinyl estradiol eluting at 3.47 min and amodiaquine eluting at 3.63 min (**Table 2**) were detected only when using negative ion electrospray PI MS/MS.

In addition to the 2-fold enhancement of throughput by combining negative ion and positive ion MS/MS into a single analysis, the use of UHPLC instead of HPLC increases the throughput of the assay from ~30 min[186] to <8 min per injection. The incorporation of labeled and unlabeled GSH eliminates the need for subsequent measurements to determine if a peak is actually a GSH conjugate or a false positive result and thereby enhances throughput by at least another 2-fold. Therefore, by using fast polarity switching, fast MS/MS, and UHPLC instead of HPLC, this new approach increases the throughput of GSH screening by >10-fold.

TABLE II. GSH CONJUGATES (MODEL COMPOUNDS) AND CORRESPONDING PRECURSOR IONS DETECTED DURING UHPLC-MS/MS WITH POSITIVE ION ELECTROSPRAY CONSTANT NEUTRAL LOSS (NL) SCANNING AND WITH NEGATIVE ION ELECTROSPRAY PRECURSOR ION (PI) SCANNING.

Compound	GSH conjugate	Retention time (min)	NL[a] 129 Da (+) GSH	NL[a] 129 Da (+) [$^{13}C_2$,^{15}N]-GSH	PI[b] *m/z* 275/278 (-) GSH	PI[b] *m/z* 275/278 (-) [$^{13}C_2$,^{15}N]- GSH
Acetaminopher	Y	1.75	473.3[c] (100)[d]	476.2 (92)	471.6 (91)	474.5 (100)
	Y	1.86	457.3 (100)	460.3 (94)	455.5 (100)	458.6 (90)
	N	2.95	-	-	443.0 (40)	445.5 (100)
Amodiaquine	Y	3.63	-	-	631.7 (100)	634.7 (95)
	Y	3.84	661.5 (98)	664.5 (100)	659.7 (100)	662.7 (97)
	N	5.69	576.4 (35)	579.4 (100)	574.0 (100)	577.5 (55)
	N	6.12	441.4 (100)	445.0 (32)	-	-
***p*-Cresol**	Y	2.93	414.2 (100)	417.2 (91)	412.6 (100)	415.7 (86)
	Y	3.21	430.2 (100)	433.2 (95)	428.6 (100)	431.4 (95)
	Y	3.39	430.4 (100)	433.5 (98)	428.6 (100)	431.6 (84)
	N	4.11	444.5 (12)	447.2 (100)	-	-
Diclofenac	Y	4.00	583.5 (89)	586.4 (100)	581.6 (87)	584.5 (100)
	Y	4.14	617.5 (97)	620.4 (100)	615.6 (100)	618.6 (92)
	Y	4.27	617.4 (96)	620.4 (100)	615.2 (100)	618.3 (97)
	Y	4.60	617.3 (84)	620.4 (100)	615.3 (92)	618.4 (100)
	N	2.75	454.3 (100)	457.1 (11)	-	-
	N	5.71	465.7 (100)	468.4 (17)	-	-
	N	5.89	466.0 (100)	469.5 (35)	-	-
17*α*-Ethinyl estradiol	Y	3.47	-	-	632.8 (100)	635.8 (88)
	Y	3.68	634.5 (100)	637.5 (83)	632.8 (100)	636.0 (88)
	Y	3.82	618.4 (100)	621.3 (88)	616.8 (95)	619.8 (100)
	Y	4.00	618.4 (100)	621.4 (75)	616.8 (100)	619.6 (73)
	Y	4.13	618.2 (100)	621.3 (85)	616.8 (100)	619.8 (91)
	N	3.29	-	-	632.1 (100)	636.0 (82)
4-Ethylphenol	Y	2.18	460.3 (100)	463.4 (88)	458.6 (100)	461.6 (95)
	Y	2.38	460.4 (95)	463.1 (100)	458.6 (98)	461.7 (100)
	Y	3.31	428.3 (100)	431.2 (89)	426.6 (100)	429.6 (88)
	Y	3.85	444.3 (90)	447.3 (100)	442.6 (96)	445.6 (100)
	Y	4.14	444.3 (100)	447.2 (97)	442.5 (100)	445.6 (98)
	N	5.24	458.3 (100)	461.2 (48)	-	-
Ticlopidine	Y	1.83	587.2 (82)	590.3 (100)	585.8 (100)	588.7 (77)
	Y	2.02	587.3 (88)	590.2 (100)	585.7 (100)	588.5 (85)

[a] Constant neutral loss scanning MS/MS (NL)
[b] Precursor ion scanning MS/MS (PI)
[c] Apparent *m/z* value of precursor ion
[d] (Relative abundance)

3.3 Metabolic Activation of Licorice Constituents

3.3.1 Background and Research Rationale

When investigating the formation of stable metabolites produced by cytochrome P450 enzymes, it is also important to check if any reactive metabolites are produced during *in vitro* incubations. The potential of botanical compounds to be metabolized to electrophilic and possibly toxic metabolites has been evaluated based on ultrafiltration HPLC-MS/MS assays developed in this laboratory and described thoroughly in the literature.[127,186-188]

Licorice (*Glycyrrhiza glabra*) has been studied for in vitro metabolism in Chapter 2 of this work and expoxide/diol metabolites have been observed as major phase I metabolism products. The following section examines whether licorice constituents can be bioactivated to produce electrophilic metabolites. Glabridin is known to inactivate CYP3A4 and CYP2B6 in a time-dependent manner,[109] but no reactive metabolites have yet been reported. Study of potential reactive metabolites of glabridin might also help facilitate understanding of its inhibition of some CYP450 enzymes. As a general approach, GSH trapping using UHPLC-MS/MS requires no advanced knowledge of the compounds that might form GSH conjugates. To demonstrate its suitability for testing complex botanical extracts, a methanolic extract of the botanical dietary supplement licorice root (*Glycyrhiza glabra*) was tested. Licorice is used as a dietary supplements as well as a flavoring agent and has been reported to inhibit the drug metabolizing enzyme CYP3A4.[109]

3.3.2 Materials and Methods

3.3.2.1 Materials

Glabridin, isoliquiritigenin, reduced GSH, ([$^{13}C_{2,}$ ^{15}N]-glycine) GSH (**Figure 3**, **Figure 4**), β-nicotinamide adenine dinucleotide 2'-phosphate reduced tetrasodium salt (NADPH), and trichloroacetic acid were purchased from Sigma-Aldrich (St. Louis, MO). Pooled human liver microsomes (20 mg/mL, 150 donors) were purchased from BD Biosciences (Woburn, MA). Bond Elute C_{18} solid phase extraction cartridges (3 mL, 200 mg sorbent) were purchased from Agilent Technologies (Santa Clara, CA), and HPLC-grade solvents were purchased from Thermo Fisher (Pittsburgh, PA).

3.3.2.2 Microsomal Incubations

Microsomal incubations were carried out as described above in section 3.2.2.2.

3.3.2.3 Solid Phase Extraction

Sample preparation was carried out as described above in section 3.2.2.3.

3.3.2.4 Mass Spectrometry

Mass spectrometric analyses were carried out as described above in section 3.2.2.4.

3.3.3 Results and Discussion

A large number of peaks were detected during UHPLC-MS/MS analysis (**Figure 29**; **Table 3**), and all were GSH conjugates except for the peak eluting at 3.0 min, which showed ions of *m/z* 511/514 that were not of equal abundance (100% and 68%, respectively).

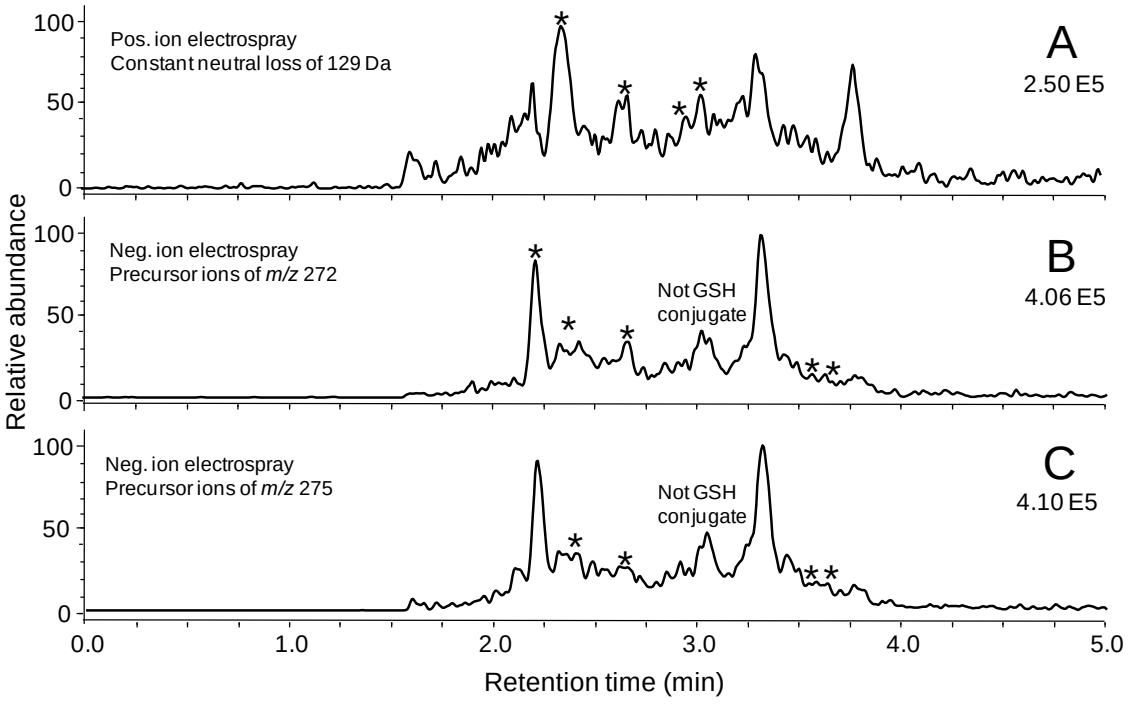

Figure 29. UHPLC-MS/MS chromatograms of GSH conjugates formed during incubation of a methanolic extract of licorice root (*Glycyrrhiza glabra*) with human liver microsomes, NADPH, GSH, and [$^{13}C_2$, ^{15}N]-GSH. A) Positive ion

electrospray neutral loss MS/MS scanning of 129 Da; B) negative ion MS/MS scanning for precursors of *m/z* 272 (unlabeled GSH); and C) negative ion MS/MS scanning for precursors of *m/z* 275 (labeled GSH).

Based on dereplication of the measured masses using NAPRALERT, SciFinder, and Reaxys, we hypothesized that at least some of the conjugates were formed through reaction of GSH with metabolites of the isoflavan glabridin and with the chalcone isoliquiritigenin and its metabolites. These peaks were observed at retention times 2.38, 2.65, 2.95, 3.05, 3.55, and 3.62 min (**Figure 29**, **Table 3**). An electrophilic α,β-unsaturated ketone, isoliquiritigenin has been reported to form a GSH adduct without metabolic activation,[189] and a peak of *m/z* 564/567 corresponding to unchanged isoliquiritigenin plus GSH was observed at 2.38 min in all incubations including control incubations of licorice extract without liver microsomes or without NADPH (data not shown). The peak eluting at 2.65 min was a GSH conjugate of isoliquiritigenin after mono-oxygenation and loss of two hydrogen atoms (isoliquiritigenin +O –2H +GSH) and was observed only in the presence of GSH, liver microsomes and NADPH. Separate incubation of purified isoliquiritigenin confirmed the formation of the GSH conjugates eluting at both 2.38 min and 2.65 min (**Figure 30**, **Table 3**).

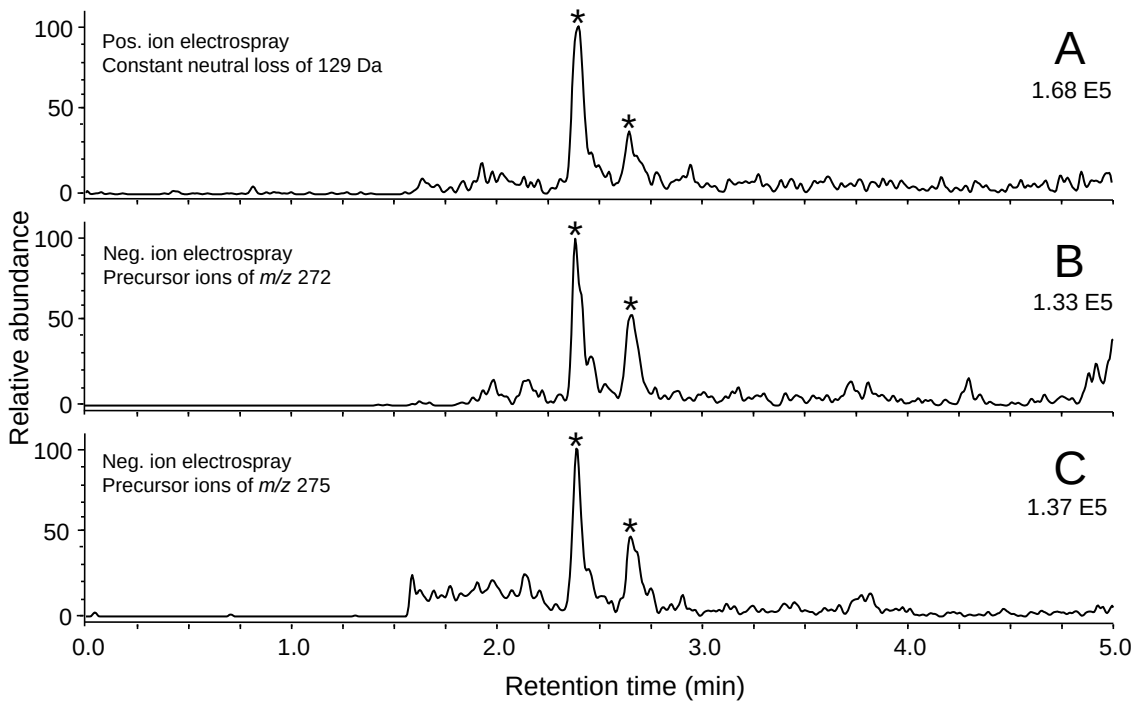

Figure 30. UHPLC-MS/MS chromatograms of GSH conjugates formed during incubation of isoliquiritigenin with human liver microsomes, NADPH, GSH, and [$^{13}C_2$,^{15}N]-GSH. A) Positive ion electrospray neutral loss MS/MS scanning of 129 Da; B) negative ion electrospray MS/MS scanning for precursors of *m/z* 272 (unlabeled GSH); and C) negative ion electrospray MS/MS precursor ion scanning for *m/z* 275 (labeled GSH).

The natural product glabridin from licorice can irreversibly inhibit CYP3A4, although no reactive metabolites of glabridin have yet been reported.[18] UHPLC-MS/MS analysis of a glabridin incubation mixture after incubation with human liver microsomes showed peaks at retention times of 2.95 min and 3.05 min only in the positive ion NL MS/MS chromatogram (**Figure 31**, **Table 3**). The precursor ions of each peak corresponded to a pair of ions of equal abundance at *m/z* 630 and *m/z* 633 ($\Delta M = 3$) (**Table 3**). Therefore, these peaks, which were also present in the licorice extract incubation (**Figure 31**), were

confirmed as isomeric GSH conjugates. Accurate mass measurements of these peaks were within 5 ppm of the elemental composition $C_{30}H_{35}N_3O_{10}S$ (glabridin –2H +GSH, ΔM 4.05 ppm) which is consistent with a quinone methide of glabridin that had reacted with GSH to form two isomers. To confirm these glabridin GSH conjugates, product ion scanning of the ions of *m/z* 630 was carried out using a high resolution data dependent LCMS-IT-TOF hybrid mass spectrometer. Accurate mass measurements of the ion of *m/z* 630 (**Figure 32**) produced fragment ions of *m/z* 555, *m/z* 501, and *m/z* 323, which represented the loss of glycine (-75 Da), the loss of pyroglutamate (-129 Da), and the loss of GSH (-307 Da), respectively as typical MS/MS fragments of GSH conjugates. Note that these glabridin GSH conjugates were observed only during positive ion PI MS/MS scanning, which emphasizes the need for measuring positive ions as well as negative ions.

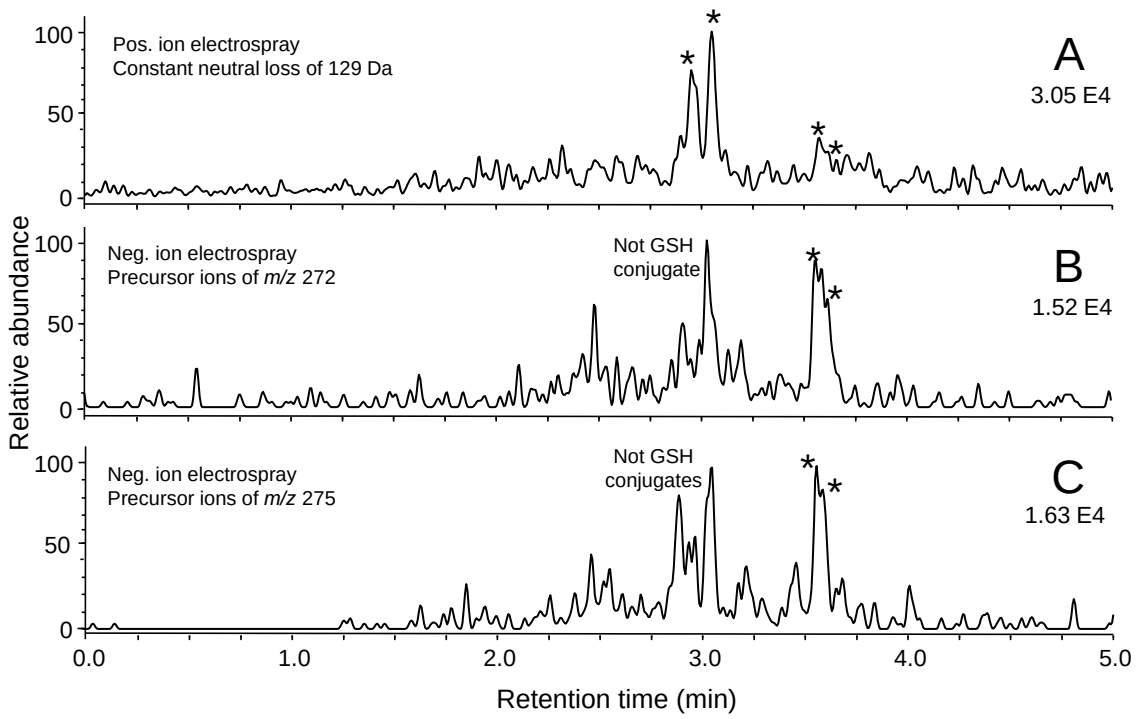

Figure 31. UHPLC-MS/MS chromatograms of GSH conjugates formed during incubation of glabridin (50 µM) with human liver microsomes, NADPH, GSH, and [$^{13}C_2$,^{15}N]-GSH. A) Positive ion electrospray neutral loss MS/MS scanning of 129 Da; B) negative ion electrospray MS/MS scanning for precursors of *m/z* 272 (unlabeled GSH); and C) negative ion electrospray MS/MS precursor ion scanning for *m/z* 275 (labeled GSH).

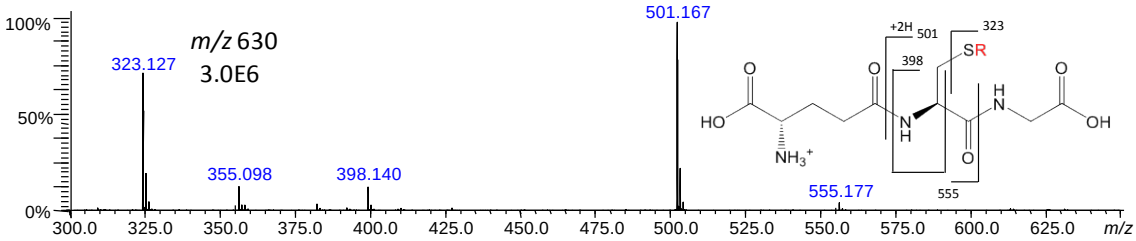

Figure 32. High resolution product ion MS/MS spectrum of protonated molecule of glabridin GSH conjugate $C_{30}H_{35}N_3O_{10}S$ (*m/z* 630) eluting at 2.95 min in the

UHPLC-MS/MS chromatogram shown in Figure 31A. The product ion tandem mass spectrum of the peak eluting at 3.05 min was identical (data not shown).

GSH conjugates of mono-oxygenated glabridin were detected at 3.55 min and 3.62 min during both positive ion NL and negative ion PI MS/MS scanning of the glabridin incubation mixture as well as the licorice extract incubation mixture (**Figure 31**, **Figure 31**). Pairs of precursor ions of approximately equal abundance were observed for both peaks, confirming that they were GSH conjugates (**Table 3**). With a molecular mass of 645 Da and an elemental composition of $C_{30}H_{35}N_3O_{11}S$ (ΔM 3.45 ppm), the compound eluting at 3.55 min corresponded to a conjugate of GSH with either a mono-oxygenated glabridin quinone methide or a mono-oxygenated glabridin *ortho*-quinone (glabridin +O –2H +GSH). To confirm this glabridin GSH conjugate, product ion scanning of the ions of *m/z* 646 was carried out using a high resolution data dependent LCMS-IT-TOF hybrid mass spectrometer. Accurate mass measurements of the ion of *m/z* 646 (**Figure 33**) produced major fragment ions of *m/z* 517 (and subsequent loss of H_2O to form *m/z* 499), *m/z* 339, and *m/z* 414, which represented the loss of pyroglutamate (-129 Da), the loss of GSH (-307 Da), and the loss of pyroglutamic acid, glycine residues and CO (-232 Da), respectively, as typical MS/MS fragments of GSH conjugates.

The compound eluting at 3.62 min (**Figure 29**) had a molecular mass of 643 Da and an elemental composition of $C_{30}H_{33}N_3O_{11}S$ (ΔM 3.35 ppm), which corresponded to a GSH conjugate of mono-oxygenated glabridin that had eliminated 4H atoms (glabridin +O -4H +GSH). To confirm this glabridin GSH conjugate, product ion scanning of the ions of *m/z* 646 was carried out using a high resolution data dependent LCMS-IT-TOF hybrid mass

spectrometer. Accurate mass measurements of the ion of *m/z* 644 (**Figure 34**) produced major fragment ions of *m/z* 515 (and subsequent loss of H_2O to form *m/z* 497) and *m/z* 569, which represented the loss of pyroglutamate (-129 Da) and the loss of glycine (-75 Da) respectively as typical MS/MS fragments of GSH conjugates.

The observation of four GSH conjugates formed from at least three different glabridin metabolites supports the hypothesis that electrophilic metabolites of glabridin were generated which may not be observed through conventional in vitro microsomal metabolism studies. Finally, note that the peak eluting at 3.00 min (**Figure 29**; **Figure 31**) in the glabridin and licorice UHPLC-MS/MS chromatograms was not a GSH conjugate based on the absence of a pair of ions (ΔM = 3) of equal abundance (**Table 3**).

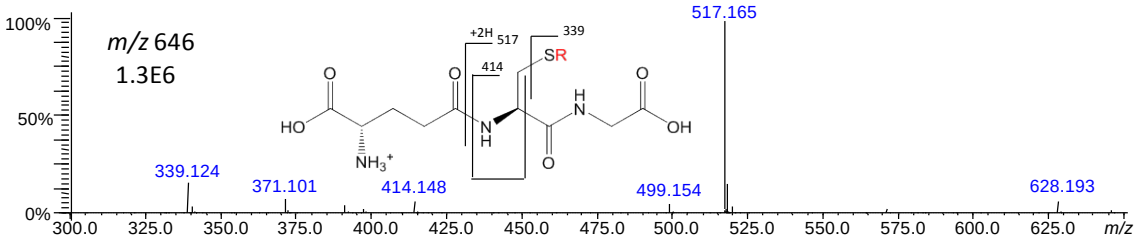

Figure 33. High resolution product ion MS/MS spectrum of protonated molecule of glabridin GSH conjugate $C_{30}H_{35}N_3O_{11}S$ (*m/z* 646)

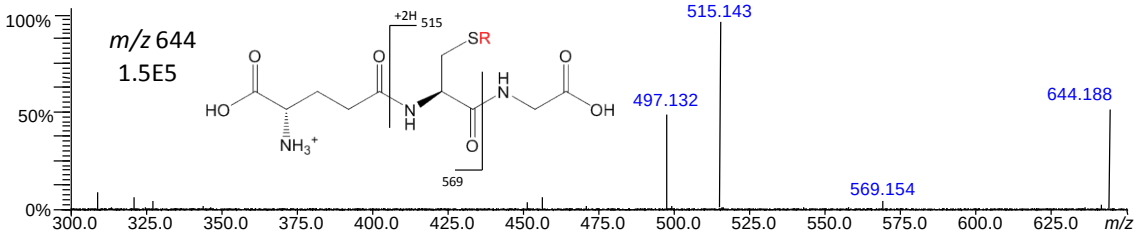

Figure 34. High resolution product ion MS/MS spectrum of protonated molecule of glabridin GSH conjugate $C_{30}H_{33}N_3O_{11}S$ (*m/z* 644) corresponding the peak eluting at 3.62 min in the UHPLC-MS/MS chromatogram shown in Figure 29.

TABLE III. GSH CONJUGATES (LICORICE EXTRACT, ISOLIQUIRITIGENIN, AND GLABRIDIN) AND CORRESPONDING PRECURSOR IONS DETECTED DURING UHPLC-MS/MS WITH POSITIVE ION ELECTROSPRAY CONSTANT NEUTRAL LOSS (NL) SCANNING AND WITH NEGATIVE ION ELECTROSPRAY PRECURSOR ION (PI) SCANNING.

Compound	GSH conjugate	Retention time (min)	NL[a] 129 Da (+) GSH	NL[a] 129 Da (+) [$^{13}C_2$,^{15}N]-GSH	PI[b] *m/z* 275/278 (-) GSH	PI[b] *m/z* 275/278 (-) [$^{13}C_2$,^{15}N]- GSH
***G. glabra* extract**	Y	2.24	528.4[c] (100)[d]	531.4 (96)	526.4 (98)	529.4 (100)
	Y	2.38	564.3 (100)	567.3 (94)	562.3 (91)	565.3 (100)
	Y	2.65	578.3 (100)	581.2 (88)	576.4 (100)	579.5 (95)
	Y	2.95	630.3 (100)	633.3 (91)	-	-
	N	3.00	-	-	511.2 (100)	514.2 (68)
	Y	3.05	630.3 (88)	633.3 (100)	-	-
	Y	3.35	664.3 (97)	667.4 (100)	662.3 (100)	665.3 (95)
	Y	3.55	-	-	644.5 (100)	647.3 (85)
	Y	3.62	-	-	642.3 (100)	645.5 (90)
	Y	3.77	602.5 (98)	605.4 (100)	600.3 (100)	603.3 (82)
Isoliquiritigenin	Y	2.38	564.3 (100)	567.3 (98)	562.3 (100)	565.3 (96)
		2.65	578.3 (94)	581.2 (100)	576.4 (100)	579.5 (96)
Glabridin	Y	2.95	630.3 (94)	633.3 (100)	-	-
	N	3.00	-	-	647.2 (100)	649.2 (25)
	Y	3.05	630.3 (87)	633.3 (100)	-	-
	Y	3.55	646.5 (100)	649.5 (96)	644.5 (100)	647.5 (92)
	Y	3.62	644.3 (92)	647.3 (100)	642.3 (87)	645.3 (100)

[a] Constant neutral loss scanning MS/MS (NL)
[b] Precursor ion scanning MS/MS (PI)
[c] Apparent *m/z* value of precursor ion
[d] (Relative abundance)

3.3.4 Conclusion

Licorice had been reported to inactivate CYP3A4 but had not been reported previously to form electrophilic metabolites. To demonstrate how the new method may be applied to complex mixtures without advanced knowledge of elemental compositions of possible

conjugates, the general new method was used with licorice dietary supplement *Glycyrrhiza glabra*.

Metabolites of glabridin, the licorice chalcone isoliquiritigenin, and one metabolite of isoliquiritigenin were found to form multiple GSH conjugates upon metabolic activation, including previously reported isoliquiritigenin GSH conjugates[189]. Glabridin is known to inactivate CYP3A4 and CYP2B6 in a time-dependent manner,[109] although no reactive metabolites have yet been reported. This study confirmed that licorice contains compounds capable of forming electrophilic metabolites that react with biological nucleophiles.

3.4 Summary and Future Direction

A fast triple quadrupole mass spectrometer-based approach was developed that can detect positively and negatively charged GSH conjugates in a single analysis without the need for advance knowledge of the elemental compositions of potential conjugates and while avoiding false positives. This approach utilized UHPLC instead of HPLC to shorten separation time and enhance sensitivity; incorporated stable-isotope labeled GSH to avoid false positives, and used fast polarity switching electrospray MS/MS to detect GSH conjugates that form positive and/or negative ions. The method was used to study the bioactivation of a licorice extract from *Glycyrrhiza glabra*, which was found to form multiple GSH conjugates, including previously reported GSH conjugates with the

chalcone isoliquiritigenin[189] as well as new conjugates with the isoflavan glabridin. Glabridin is known to inactivate CYP3A4 and CYP2B6 in a time-dependent manner,[109] although no reactive metabolites have yet been reported.

The immediate next step for future research is to apply this validated method to the analysis of other botanical dietary supplements such as the licorice species *Glycyrrhiza uralensis* and *Glycyrrhiza inflata*, and hops (*Humulus lupulus*). Isolated natural products from a variety of dietary supplement and food sources should be also screened with this fast method to evaluate the risk of reactive metabolite formation. Further investigations should also characterize any unknown reactive metabolites of glabridin and isoliquiritigenin (metabolism study has been published) as well as their corresponding GSH conjugates, which would be also supplemental to the study of botanical-drug interactions of licorice in chapter 4 of this dissertation.

Chapter 4 Evaluation of Botanical-Drug Inhibition by Glabridin, Licorice, and Hops

4.1 Introduction

Co-administration of multiple drugs to a patient is common in medical practice. A recent survey showed that more than 81% of individuals who are taking medications take at least one of these drugs in a given week and more than 25% take at least 5 medications.[190] It is known that drug-drug interactions may have serious, sometimes fatal consequences, which have led to half of the recent US market withdrawals of approved drugs and to some non-approvals of new molecular entities.[191] A major mechanism of adverse drug-drug interactions involves the inhibition of the metabolizing enzymes or transporters of a drug by a co-administered drug, resulting in increased drug exposure and toxicity. On the other hand, induction of metabolizing enzymes or transporters can lead to a reduced concentration of a drug and loss of efficacy.[191] Therefore, estimating the potential for drug-drug interactions is a critical step during drug development and has become a regulatory requirement for new drug applications to the US FDA.

The consumption of medicinal herbs is high in developing countries and is increasing in the United States where they are known as botanical dietary supplements. These supplements are often taken in combination with conventional drugs, usually without consultation with medical professionals. Since constituents in botanical preparations may be substrates, inhibitors or inducers of cytochrome P450 enzymes, there is significant

potential that co-administered drugs may be metabolized by these same enzymes.[100] There are already many known botanical-drug interactions in which the botanical constituents inhibit or induce CYP450 enzymes. Examples include constituents of St. John's wort, grapefruit, garlic, and ginseng, and botanical natural products including piperine, flavonoids, triterpenoids, anthraquinones, polyphenols, resveratrol, and alkaloids.[100,192-198] Grapefruit juice has been reported to inhibit CYP3A4 leading to increase of bioavailability of most dihydropyridines, terfenadine, cyclosporine, and midazolam.[92,199-201] Resveratrol, a promising cancer chemopreventive agent, has been reported to inhibit phase I enzymes and to induce phase II enzymes.[202,203]

4.2 Inhibition of Cytochrome P450 Enzymes by Licorice and Glabridin

4.2.1 Background and Research Rationale

Inhibition of cytochrome P450 (CYP450) enzymes is the most commonly studied drug-interaction and can occur through two pathways, reversible inhibition and time-dependent inhibition. Reversible CYP inhibition is further categorized as competitive, noncompetitive, uncompetitive, or mixed inhibition. Evaluation of reversible inhibition of CYP enzymes is often based on Michaelis-Menten kinetics. Time-dependent inhibition is kinetically defined as a compound that exhibits inhibition when incubated with enzyme before substrate is added. Mechanism-based inhibition is a type time-dependent inhibition which usually involves permanent inactivation of enzyme during the reaction.

Enzyme inhibition is usually expressed as an IC_{50} value, which is defined as the concentration of the inhibitor causing 50% of the maximum inhibition at a certain substrate concentration.

Assays using recombinant CYP enzymes are both convenient and rapid for evaluating the inhibitory potential of a drug, natural product or botanical extract. These inhibition assays utilize probe substrates of specific CYP enzymes that form metabolites that can be measured by using HPLC-UV or HPLC-MS/MS. Assays using liver microsomes are used more often than recombinant enzymes for the evaluation of CYP enzyme inhibition. The CYP isoform-specific substrates are incubated with liver microsomes and test agents followed by quantitative analysis of the metabolites. More expensive but more accurate hepatocyte-based inhibition assays, also using probe substrates, are typically used to confirm inhibition predicted using recombinant CYP enzymes or human liver microsomes.

Glycyrrhiza glabra and *Glycyrrhiza uralensis* have been reported to inhibit CYP3A4, however the mechanism of this interaction is unknown.[109-111] It has also been reported that an alcoholic extract of *Glycyrrhiza glabra* moderately inhibited CYP3A4, and its flavonoid constituent glabridin inhibited the activities of CYP2B6, CYP2C9 and CYP3A4.[109] No thorough study has been conducted to investigate the botanical-drug interactions of licorice with all the major CYP450 enzymes including CYP1A2, CYP2A6, CYP2B6, CYP2C8, CYP2C9, CYP2C19, CYP2D6, CYP2E1, and CYP3A4.

Although most CYP450 inhibition assays typically evaluate inhibition of one CYP isoform by one test agent at a time, the US FDA recommends that at least seven CYP isoforms should be investigated for possible inhibition (at least for studies of drug-drug interactions).[99] To expedite these multiple assays, a rapid, selective, and sensitive assay using UHPLC-MS/MS was developed as part of this dissertation and used to monitor the appearance of marker metabolites of probe substrates of multiple CYP450 enzymes. This was an updated assay based on a previous HPLC-MS/MS method that our laboratory had developed and validated previously.[204] The current method was used able to separate and detect metabolites of nine probe substrates in a single analysis with the implementation of UHPLC instead of HPLC to shorten separation time and enhance sensitivity, and fast polarity switching electrospray MS/MS to detect signal in both positive and negative modes. Following the FDA drug interaction studies guidance,[99] possible inhibition interactions with nine major cytochrome P450 enzymes were investigated (CYP1A2, CYP2A6, CYP2B6, CYP2C8, CYP2C9, CYP2C19, CYP2D6, CYP2E1, and CYP3A4).

Several in vitro methods have been used to study botanical-drug interactions and have included incubations with liver microsomes or hepatocytes. The incubation of liver microsomes and cofactors with botanical compounds is suitable for the production of most major metabolites through phase I and II reactions. Hepatocytes are particularly useful in that they produce all necessary cofactors for xenobiotic metabolism, express drug transporter proteins, and enable functional enzyme assays or mRNA measurements of enzyme up- or down-regulation.[205-207] In contrast, liver microsomal incubations must be supplemented with expensive cofactors such as β-nicotinamide adenine dinucleotide

phosphate (NADPH), uridine 5'-diphosphoglucuronic acid (UDPGA) and 3-phosphoadenosine 5-phosphosulfate (PAPS), and up/down-regulation measurements or studies of drug transporters are not possible.

4.2.2 Materials and Methods

4.2.2.1 **Materials**

Phenacetin was purchased from Tokyo Chemical Industry (Tokyo, Japan). Acetaminophen, coumarin, bupropion hydrochloride, tolbutamide, dextrorphan, chlorzoxazone, 6β-hydroxytestosterone, ticlopidine hydrochloride, quercetin, sulfaphenazole, quinidine, ketoconazole, and NADPH were purchased from Sigma-Aldrich (St. Louis, MO). 1'-Hydroxymidazolam and 6-hydroxychlorzoxazone were purchased from Cayman Chemical (Ann Arbor, MI). Dextromethorphan hydrobromide was obtained from MP Biomedicals (Santa Ana, CA), and 7-hydroxycoumarin was purchased from Indofine Chemical (Hillsborough, NJ). Hydroxybupropion and [d_6]-hydroxybupropion were purchased from Santa Cruz Biotechnology (Dallas, TX), and midazolam and testosterone were obtained from Cerilliant Corporation (Round Rock, TX). [d_5]-7-Hydroxycoumarin, [d_7]-6β-hydroxytestosterone and [$^{13}C_3$]-1'-hydroxymidazolam were purchased from BD Gentest (Woburn, MA). Amodiaquine, *N*-desethylamodiaquine hydrochloride, [d_5]-*N*-desethylamodiaquine, (*S*)-mephenytoin, [d_4]-acetaminophen, [d_2]-6-hydroxychlorxazone, hydroxytolbutamide, [d_9]-4-

hydroxytolbutamide, 4-hydroxymephenytoin, [d_3]-4-hydroxymephenytoin, and [d_3]-dextrorphan were obtained from Toronto Research Chemicals (Toronto, Canada). Pooled human liver microsomes (20 mg/mL, 150 donors) and cDNA-expressed recombinant P450 enzymes (CYP1A2, 2A6, 2B6, 2C8, 2C9, 2C19, 2D6, 2E1, and 3A4) were purchased from BD Biosciences (Woburn, MA).

All organic solvents were HPLC grade or better and were purchased from Thermo Fisher (Pittsburgh, PA). Water was prepared using an Elga Purelab Ultra (Siemens Water Technologies, Woodridge, IL) water purification system. An extract of licorice root (*Glycyrrhiza glabra*) was prepared from botanically authenticated plant material provided by Dr. Charlotte Simmler at the UIC/NIH Center for Botanical Dietary Supplements Research. The licorice root was extracted with 90% ethanol, 5% isopropanol, 5% water (*v/v/v*) (weight root powder (g) / volume solvent (mL): 1:15).

4.2.2.2 Incubation with Recombinant CYP Enzymes

For studies using recombinant cytochrome P450 enzymes, incubation mixtures contained 2 pmol each of recombinant CYP450 enzyme, 1 mM NADPH, licorice extract (1 or 20 µg/mL), and cytochrome P450 substrate (**Table 4**) in 100 mM potassium phosphate buffer at pH 7.4 in the total volume of 100 µL. After pre-incubation at 37 °C for 2 min, the reactions were initiated by the addition of NADPH. Enzymatic reactions were carried out under conditions (**Table 4**). After incubation, each reaction was terminated by the addition of acetonitrile/water/formic acid (86:10:4, v/v/v) containing the appropriate

corresponding stable isotope-labeled internal standard (**Table 5**). The samples were vortexed for 2 min and centrifuged at 13,000 x *g* and 4 °C for 10 min. After centrifugation, 5 µL of each supernatant was injected onto a column for analysis using UHPLC-MS/MS as described below. Negative control incubations contained solvent vehicle (acetonitrile, <0.5% v/v of the total incubation mixture) but no inhibitor. Incubations were carried out in duplicate.

TABLE IV. EXPERIMENTAL CONDITIONS FOR ASSAYS OF SPECIFIC ISOFORMS OF CYTOCHROME P450 ENZYMES IN HUMAN LIVER MICROSOMES WITH KM VALUES IN THE LITERATURE

CYP	Substrate	Substrate Concentration (µM)	Incubation Time (min)	Km (µM)
1A2	Phenacetin	50	20	1 – 115[208-212]
2A6	Coumarin	2	10	0.4 – 2.4[212-214]
2B6	Bupropion	80	20	70 – 130[212]
2C8	Amodiaquine	2	10	1.9 – 3.5[212]
2C9	Tolbutamide	150	10	70 – 580[212,215]
2C19	S-(+)-Mephenytoin	100	40	18 – 340[211,212,216-218]
2D6	Dextromethorphan	5	15	2 – 10[211,212,219]
2E1	Chlorzoxazone	75	20	40 – 160[211,212,220]
3A4	Midazolam	2	10	2 – 12[212,221]
	Testosterone	50	10	30 – 210[211,212,222-224]

4.2.2.3 UHPLC-MS/MS

All metabolites and surrogate standards were analyzed in a single run using UHPLC-MS/MS on a Shimadzu (Kyoto, Japan) Nexera UHPLC and LCMS-8040 triple quadrupole mass spectrometer. The 10 metabolites of the probe substrates and their

corresponding isotope-labeled surrogate standards were separated on a Waters (Milford, MA) Acquity BEH Shield RP18, 2.1×50 mm, 1.7 μm UHPLC column using a 3-min gradient from 20% to 75% acetonitrile in water containing 0.1% formic acid. The flow rate was 0.5 mL/min, and the column oven temperature was 40 °C. Metabolites were detected using electrospray with polarity switching, collision-induced dissociation, and selected reaction monitoring (SRM) tandem mass spectrometry as summarized in **Table 5**. The dwell time was 20 ms/ion, and the polarity switching time was 15 ms. The mass spectrometer source parameters were as follows: desolvation line temperature 300°C, spray voltage 3500 V, nebulizing gas flow 3 L/min, and drying gas flow 20 L/min. The simultaneous analysis of each probe substrate metabolite and the corresponding internal standard was carried out within 3 min using UHPLC-MS/MS as listed in **Table 5**. A stable isotope labeled analog of the metabolite (1 μM) was added to each sample as internal standard after incubation with human liver microsomes to control for sample losses during handling, instrument variations between analyses, and matrix effects that might cause ion suppression or enhancement. These internal standards co-eluted or nearly co-eluted with their respective metabolites during UHPLC-MS/MS.

TABLE V. TANDEM MASS SPECTROMETER PARAMETERS FOR THE SELECTION OF PRECURSOR AND PRODUCT IONS OF PROBE SUBSTRATE METABOLITES AND SURROGATE STANDARDS

CYP Enzyme	Metabolite	SRM (*m/z*)	Polarity	EV[a]	CE[b]	CCL4[c]
		Metabolite				
1A2	acetaminophen	152.0>109.9	+	22	-23	-16
2A6	7- hydroxycoumarin	162.9>106.7	+	28	-32	-16
2B6	hydroxybupropion	256.0>238.0	+	28	-18	-16
2C8	desethylamodiaquine	328.0>282.6	+	19	-29	-22
2C9	hydroxytolbutamide	285.0>186.1	-	-19	22	10
2C19	4-hydroxymephenytoin	233.1>190.1	-	-25	22	25
2D6	dexthorphan	258.1>157.1	+	24	-35	-26
2E1	6-hydroxychlorzoxazone	183.9>120.0	-	-19	14	10
3A4	1'-hydroxymidazolam	341.9>324.0	+	16	-22	-20
	6β-hydroxytestosterone	305.0>269.2	+	20	-17	-8
		Internal Standard				
1A2	[d_4]-acetaminophen	156.0>113.9	+	22	-23	-16
2A6	[d_5]-7-hydroxycoumarin	168.1>111.6	+	28	-32	-16
2B6	[d_6]-hydroxybupropion	262.0>244.0	+	28	-18	-16
2C8	[d_5]-desethylamodiaquine	333.3>282.6	+	19	-29	-22
2C9	[d_9]-hydroxytolbutamide	294.1>186.1	-	-19	22	10
2C19	[d_3]-4-hydroxymephenytoin	236.1>193.1	-	-25	22	25
2D6	[d_3]-dextrorphan	261.1>157.1	+	24	-35	-26
2E1	[d_2]-6-hydroxychlorzoxazone	186.0>122.1	-	-19	14	10
3A4	[$^{13}C_3$]-1'-hydroxymidazolam	344.9>327.0	+	16	-22	-20
	[d_7]-6β-hydroxytestosterone	312.2>276.2	+	20	-20	-25

[a] EV = interface entrance voltage
[b] CE = collision energy
[c] CCL4 = electrode voltage of collision cell lens 4

4.2.2.4 IC50 Determination

When significant inhibition (> 50%) of any cytochrome P450 enzyme was observed for 20 µg/mL licorice extract, follow-up assays were conducted to determine the IC_{50} value for that specific enzyme using 12 concentrations ranging over at least 4 orders of magnitude. The initial substrate concentrations were within the range of their respective K_m values. Incubations with recombinant CYP enzymes were carried out using individual substrates as described above. Comparison was made with negative control incubations containing no inhibitor but solvent, and activity was expressed as the percentage of control activity remaining. Known CYP inhibitors recommended by the FDA were used at 12 different concentrations as follows: 0.05-500 µM ticlopidine for CYP2B6 and CYP2C19, 0.01-200 µM quercetin for CYP2C8, 0.05-500 µM sulfaphenazole for CYP2C9, and 0.005-100 µM ketoconazole for CYP3A4/5.[99] Quantitative UHPLC-MS/MS data were analyzed using Shimadzu LabSolutions software (Kyoto, Japan). The IC_{50} values were determined using the Enzyme Kinetics module of SigmaPlot (Systat Software, San Jose, CA).

4.2.3 Results and Discussion

4.2.3.1 **Probe Substrates and UHPLC-MS/MS**

Ten probe substrates specific to nine CYP isoforms (**Table 4**) were selected based on U.S. FDA recommendation, specificity of the enzymatic reaction, sensitivity of analytical detection, and availability of the stable isotope-labeled surrogate standard of the

corresponding metabolites.[99] The SRM transitions for all ten metabolites and their corresponding isotope-labeled internal standards were selected based on the most abundant fragment ions of each protonated or deprotonated molecule and are listed in **Table 5**. The elution profiles of all metabolites and internal standards detected during UHPLC-MS/MS are shown in **Figure 35**. Note that all compounds eluted within 3 min.

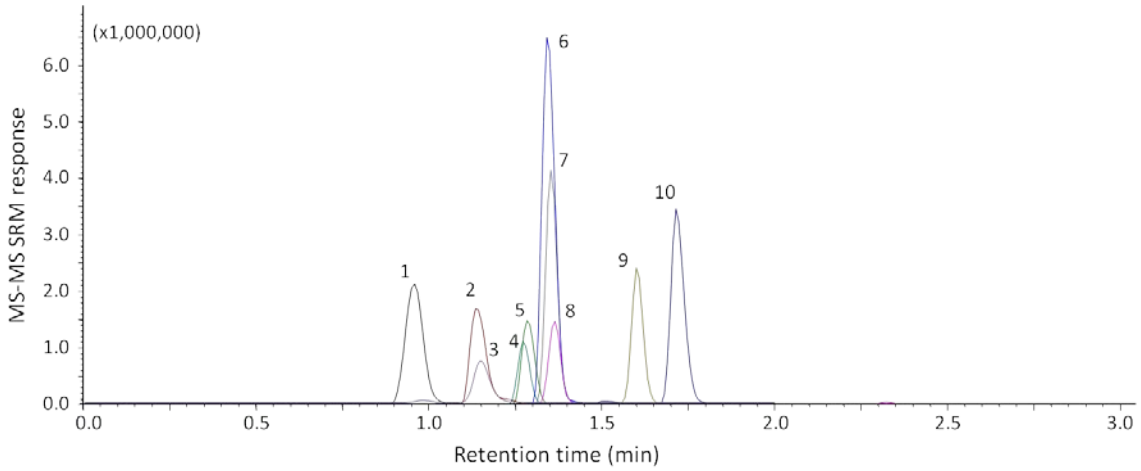

Figure 35. A 3-min UHPLC-MS/MS method for determining 10 metabolites of probe substrates for specific P450 enzymes. Metabolites: 1: Acetaminophen (1A2), 2: Desethylamodiaquine (2C8), 3: 6β-hydroxy-testosterone (3A4), 4: 6-Hydroxy-chlorzoxazone (2E1), 5: Dexthorphan (2D6), 6: Hydroxy-bupropion (2B6), 7: 4-Hydroxy-mephenytoin (2C19), 8: Hydroxy-coumarin (2A6), 9: Hydroxy-tolbutamide (2C9), 10: 1'-Hydroxy-midazolam (3A4)

Phenacetin *O*-deethylation by CYP1A2 was selected for the inhibition assay because of its superior specificity compared to other FDA-recommended substrates.[204] For CYP2A6, CYP2B6 and CYP2E1, coumarin-7-hydroxyation, bupropion-hydroxylation and chlorzoxazone 6-hydroxylation were selected based on the commercial availability of the

corresponding stable isotope-labeled metabolites for use as surrogate standards during UHPLC-MS/MS. For CYP2C8, amodiaquine *N*-deethylation by CYP2C8 was measured due to high solubility of amodiaquine. For CYP2C9 and CYP2D6, tolbutamide methyl-hydroxylation and dextromethorphan *O*-demethylation were used to measure interactions with CYP2C9 and CYP2D6, respectively. As a probe for CYP2C19, *S*-mephenytoin 4'-hydroxylation was used due to its high specificity as well as high sensitivity during UHPLC-MS/MS. For evaluation of CYP3A4/5 inhibition, the use of two structurally unrelated substrates have been recommended.[99,204] Therefore, midazolam 1-hydroxlyation and testosterone 6β-hydroxylation were used to probe inhibition of CYP3A4/5.[99] 7-Hydroxycoumarin, hydroxytolbutamide and 6-hydroxychlorzoxazone were measured using negative ion electrospray while the other seven metabolites were measured in positive ion mode (**Table 5**).

4.2.3.2 Inhibition of CYP Isoforms

Two concentrations (1 and 20 µg/mL) of *Glycyrrhiza glabra* ethanol extract were incubated with individual human cDNA-expressed recombinant enzymes and corresponding probe substrates. The relative amount of each metabolite that was formed was calculated as a percentage of control based on the control reactions where solvent was added instead of extract. As shown in **Figure 36**, the licorice extracts showed significant inhibition of CYP2B6, CYP2C8, CYP2C9, CYP2C19, and CYP3A4 that increased as extract concentration increased from 1 µg/mL to 20 µg/mL. Experiments with other cytochrome P450 isoforms showed little inhibition by licorice extracts. Among

those isozymes inhibited by licorice extract, CYP2C8, CYP2C9 and CYP2C19 were inhibited the most, with more than 80% inhibition at the 20 µg/mL level while CYP2B6 and CYP3A4 were inhibited by approximately 60% at the 20 µg/mL level. As shown in **Figure 36**, the CYP2C family was inhibited significantly by the licorice extracts while CYP2B6 and CYP3A4 were modestly inhibited.

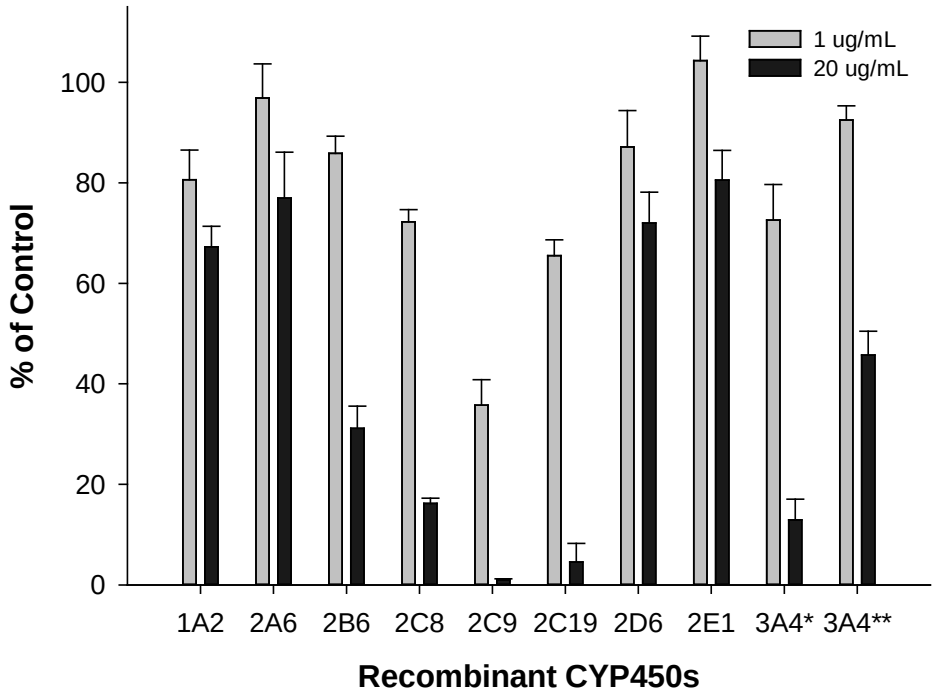

Figure 36. Inhibition of CYP450 enzymes using two licorice extract concentrations. * Midazolam as substrate, ** Testosterone as substrate

Inhibition of CYP450 enzymes can be either reversible or time-dependent[225] where reversible inhibition results from rapid association-dissociation of ligands and enzymes, and time-dependent inhibition generally involves irreversible covalent binding or non-

covalent tight binding to the enzyme resulting in loss of enzyme activity. Sometimes, reversible inhibition by a metabolite produced *in situ* can lead to time-dependent inhibition. It was reported that licorice root extract and glabridin inhibited CYP3A4 in a time-dependent fashion while CYP2C9 was competitively inhibited by glabridin.[109] Glabridin was tested using a time-dependent inhibition assay with recombinant P450 enzymes (CYP3A4 and CYP2C9) and time-dependent inhibition of CYP3A4 was observed (**Figure 40** and **Figure 42**) while the inhibition of CYP3A4 was reversible. Time-dependent inhibition of CYP3A4 by licorice extract and glabridin and identification of potential potent inhibitors are discussed in Section 4.3.

4.2.3.3 IC50 Values of Licorice and Glabridin

Four-parameter (Max, Min, LogIC_{50}, Hill Slope) sigmoidal curve fitting was used to analyze the data. The IC_{50} curves of licorice extract and glabridin for inhibition of CYP450 enzymes 2B6, 2C8, 2C9, 2C19, and 3A4 are shown in **Figure 37** and **Figure 38**, respectively. The IC_{50} results are summarized in **Table 6**, and the data are expressed as mean ± SD. Among the enzymes inhibited by licorice extract and glabridin, CYP2C9 showed the most inhibition with IC_{50} values of 0.6 µg/mL for licorice extract and 2.2 µM for glabridin. The low IC_{50} value of licorice extract for inhibition of CYP2C9 indicates the possible existence of highly potent inhibitor(s) in the licorice extract other than glabridin (given the IC_{50} value of only 2.2 µM for glabridin).

A systematic approach was implemented to identify highly potent CYP2C9 inhibitor(s): 14 sub-fractions of the crude licorice extract were isolated and tested in a one-point (1

μg/mL) inhibition assay. UHPLC with high resolution mass spectrometry and tandem mass spectrometry were used to characterize of components within each fraction that showed significant CYP2C9 inhibition. Diligent database searching and dereplication of known licorice compounds were used to determine possible chemical structures of the most inhibitory (CYP2C9) licorice components. Details are discussed in Section 4.4.

7-benzyloxy-trifluromethlcoumarin (7BFC) O-debenzylation activity was used for assessment of CYP3A4 inhibition by Kent et al[109], where 6.9 μg/mL licorice root extract inhibited 55% of enzyme activity after 15 minutes incubation and 3 μM glabridin led to 50% enzyme activity loss under same incubation condition. Kent et al also reported the concentration of glabridin required to obtain half-maximal inactivation of CYP2B6 and CYP2C9 were 12 μM and 100 μM, respectively (based on O-deethylation activity of 7-ethoxy-4-(trifluoromethyl)coumarin).[109] Although no IC_{50} data were reported by Kent et al, the inhibition results are comparable to those in **Table 6**, with an exception of CYP2C9 (2.5 μM compared to 100 μM by Kent et al). The difference is believed to result from the assays used for assessing enzyme inhibition.

TABLE VI. IC_{50} VALUES OF LICORICE EXTRACT AND GLABRIDIN FOR INDIVIDUAL CYP450 ISOZYMES

	CYP2B6	CYP2C8	CYP2C9	CYP2C19	CYP3A4[1]	CYP3A4[2]
Licorice (**μg/mL**)	6.2 ± 1.3	2.9 ± 0.4	0.6 ± 0.1	2.0 ± 0.2	13.4 ± 1.4	26.6 ± 1.7
Glabridin (**μM**)	6.3 ± 1.2	6.5 ± 1.1	2.2 ± 0.2	2.5 ± 0.2	4.8 ± 1.4	5.6 ± 1.2
Known Inhibitor[3] (**μM**)	0.2 ± 0.1	1.3 ± 0.2	0.2 ± 0.1	1.0 ± 0.1	0.2 ± 0.1	Not Tested

Data expressed as mean ± SD
[1]Midazolam as substrate
[2]Testosterone as substrate

[3]Known inhibitors: CYP2B6 – ticlopidine, CYP2C8 – quercetin, CYP2C9 – sulfaphenazole, CYP2C19 – ticlopidine, CYP3A4/5 - ketoconazole

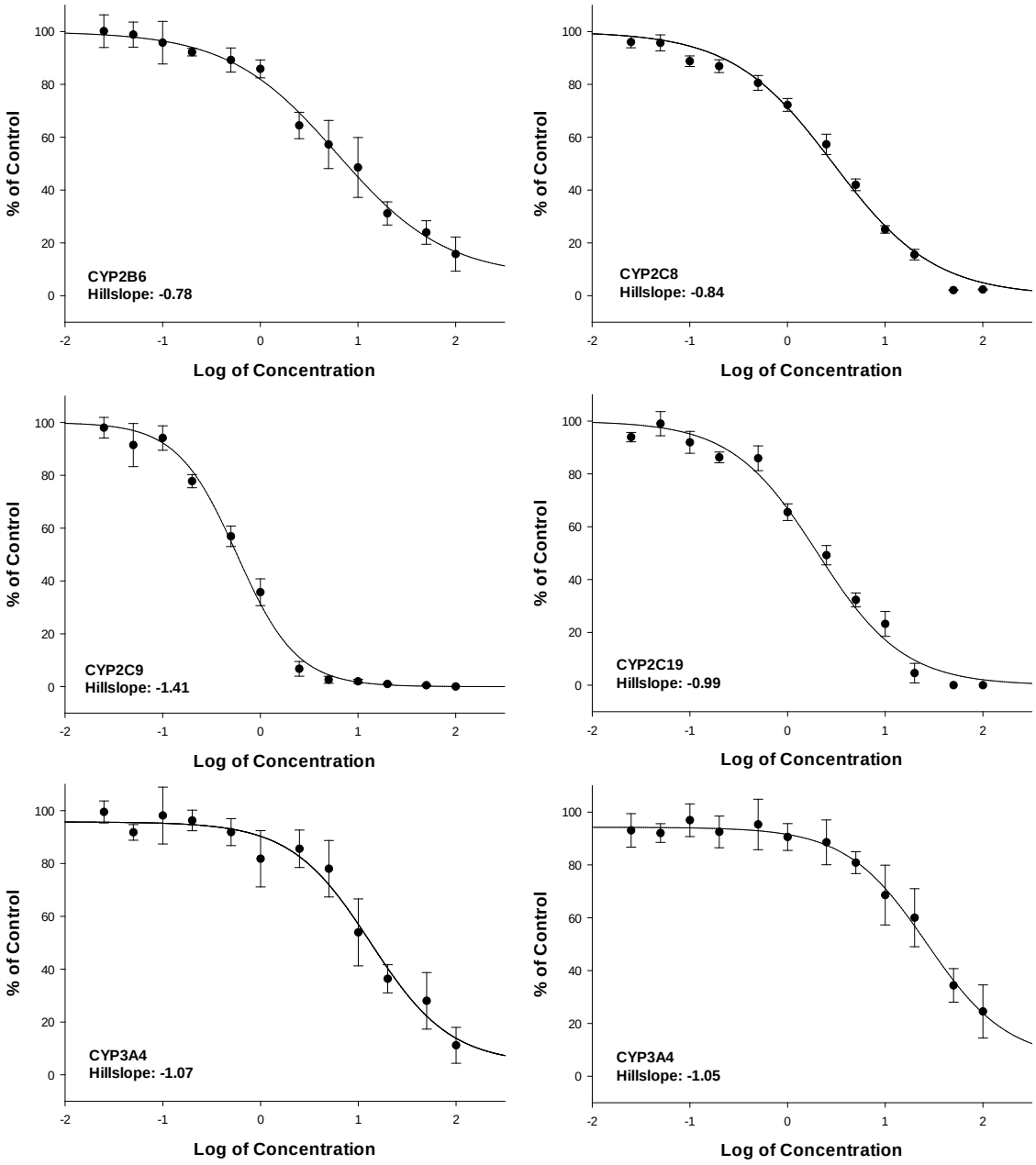

Figure 37. IC_{50} curves of licorice extract for inhibition of CYP2B6, 2C8, 2C9, 2C19, and 3A4.

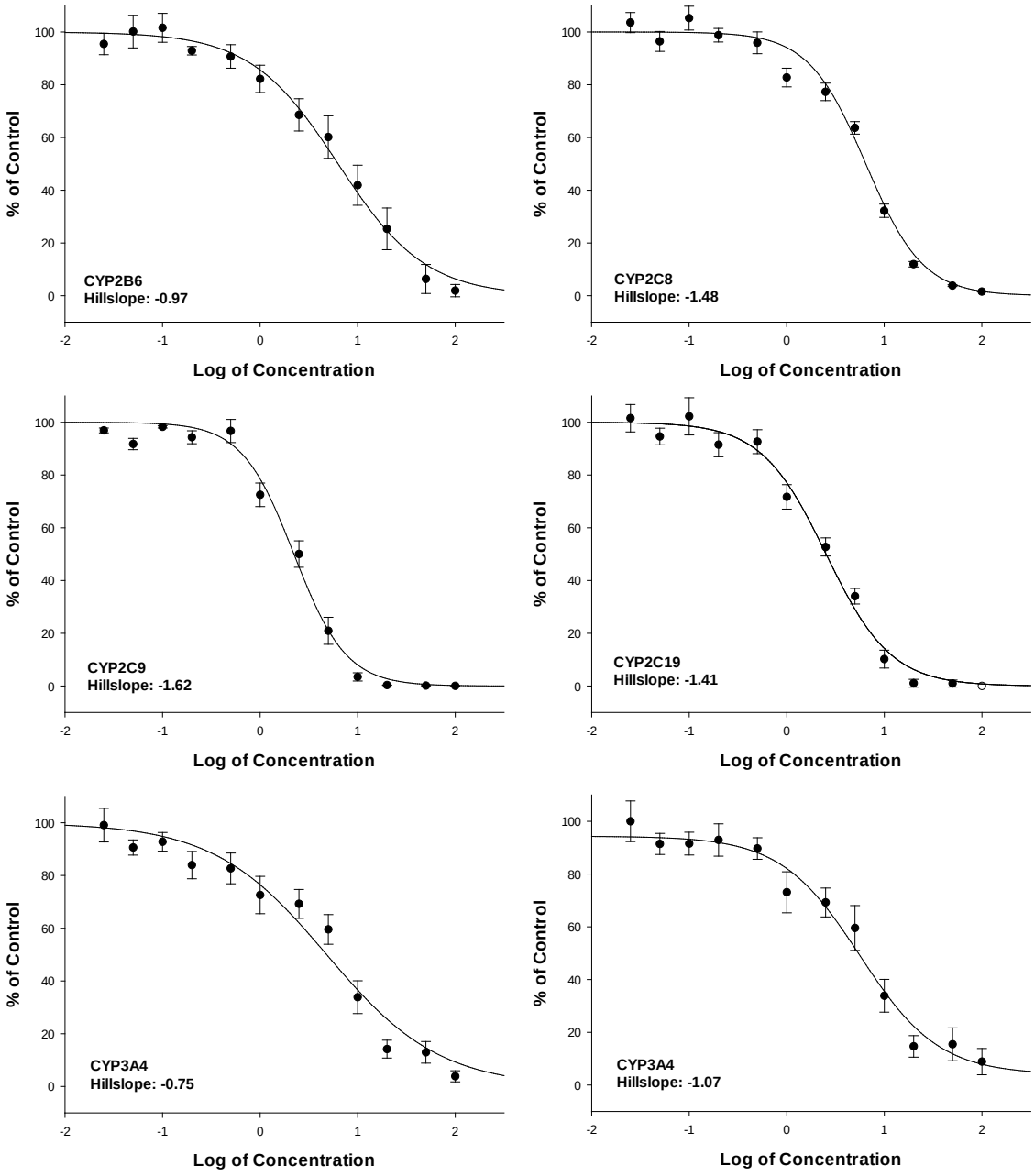

Figure 38. IC_{50} curves of glabridin for inhibition of CYP2B6, 2C8, 2C9, 2C19, and 3A4.

4.3 Time-Dependent Inhibition of CYP3A4 by Licorice and Sub-fractions

4.3.1 Background and Research Rationale

Although *Glycyrrhiza glabra* and *Glycyrrhiza uralensis* have been reported to inhibit cytochrome P450 3A4, the mechanism is unknown.[109-111] It has been reported that an alcoholic extract of licorice moderately inhibited CYP3A4 and its flavonoid glabridin inhibited the activities of CYP2B6, CYP2C9 and CYP3A4,[109] but FDA suggested probe substrates (such as midazolam and testosterone) were not used to investigate inhibition of specific CYP isoforms. No further studies have been reported to determine if other licorice compounds might inhibit CYP enzymes or if any constituents cause time-dependent inhibition of CYP3A4.

As described above (Section 4.2), a rapid, selective, and sensitive assay using UHPLC-MS/MS was developed and used to monitor the appearance of marker metabolites of specific cytochrome P450 enzymes. The was an updated version of our previous LC-MS/MS assay.[204] Licorice extracts, 14 sub-fractions and glabridin were tested using a time-dependent inhibition assay. The sub-fractions showing significant (>50%) inhibition were further studied to identify compounds that contributed most to the time-dependent inhibition of CYP3A4 enzymes.

4.3.2 Materials and Methods

4.3.2.1 Materials

NADPH was purchased from Sigma-Aldrich (St. Louis, MO). Testosterone was obtained from Cerilliant Corporation (Round Rock, TX). 1'-Hydroxymidazolam-$^{13}C_3$ was purchased from BD Gentest (Woburn, MA). Pooled human liver microsomes (20 mg/mL, 150 donors) and cDNA-expressed recombinant P450 enzymes (CYP3A4) were purchased from BD Biosciences (Woburn, MA). All organic solvents were HPLC grade or better and were purchased from Thermo Fisher (Pittsburgh, PA). Water was prepared using an Elga Purelab Ultra (Siemens Water Technologies, Woodridge, IL) water purification system. Botanically authenticated and standardized *Glycyrrhiza glabra* (licorice) extracts examined during this study were provided by Dr. Charlotte Simmler of the UIC/NIH Center for Botanical Dietary Supplements Research. Briefly, licorice root was extracted with 90% ethanol, 5% isopropanol, 5% water (*v/v/v*) (weight root powder (g) / volume solvent (mL): 1:15), and 13 crude extract fractions were isolated as described previously.[226] A Corbel Cherry-One automated operating system (Cherry Instruments, Chicago, IL, USA) was paired with a High Speed Countercurrent Chromatography (HSCCC) Tauto-TBE-300B instrument (Tauto Biotech, Shanghai, China) and used for the separation of the licorice extract. The total coil volume was 300 mL. A solvent system composed of premixed hexanes, ethyl acetate, methanol, and water was run head to tail. Fractions were collected every 6.5 min and pooled according to their TLC profiles, yielding 13 fractions. Each fraction (K=1.2-1.5) was further

separated with a YMC-Pack-ODS-AQ (250 x10 mm, 5 µm) column, run on a Waters 600 HPLC instrument using a UV detector at 254 nm.

4.3.2.2 Microsomal Incubation

To test for time-dependent inactivation of the cytochrome P450 enzymes that had already been determined to be inhibited by licorice, recombinant CYP3A4 (300 pmol/mL) was pre-incubated with licorice extract or fractions (50 µg/mL) and test compound (10 µM) for 30 min at 37 °C in 100 mM potassium phosphate buffer (pH 7.4) with or without (control) NADPH (1 mM). At 0 min and after 30 min incubation, 5 µL aliquots of each mixture were transferred to secondary incubation mixtures containing a probe substrate (3 µM midazolam for CYP3A4) and 1 mM NADPH in a total volume of 100 µL. The secondary incubation was carried out as described in **Table 4**. Note that aliquots of the pre-incubation mixtures were diluted 20-fold with probe substrate at a saturating concentration (≥4-fold *Km*) to measure residual enzyme activities.[212] After incubation, each reaction was stopped by the addition of 20 µL water/acetonitrile/formic acid (92:5:3, v/v) containing the internal standards. The samples were vortex mixed for 30 s and centrifuged at 13,000 x *g* at 4°C for 10 min. After centrifugation, 5 µL aliquots of the supernatants were analyzed using UHPLC-MS/MS.

4.3.2.3 UHPLC-MS/MS

UHPLC-MS/MS analyses were carried out as described in 4.2.2.3.

4.3.3 Results and Discussion

Two *Glycyrrhiza glabra* extracts (with and without glabridin), glabridin, and 13 sub-fractions of *G. glabra* prepared by the UIC/NIH Center for Botanical Dietary Supplements Research were tested using a single point (30 min) CYP3A4 time-dependent inhibition assay, and the results are summarized in **Figure 34**. Fractions 1 to 14 had been isolated based on hydrophobicity and roughly represented different classes of compounds within the licorice extract (see Section 4.3.2.1 above). Licorice extracts, glabridin, and most factions showed time-dependent inhibition. Both licorice extracts (with and without glabridin) demonstrated modest and similar inhibitory activities indicating that the relatively small concentration of glabridin (2%) did not contribute much to the inhibition. Among the 13 fractions, fraction 3 showed the most inhibition (6% remaining activity, more inhibitory than any extract tested; **Figure 34**). Therefore, fraction 3 was selected for further compound isolation and characterization.

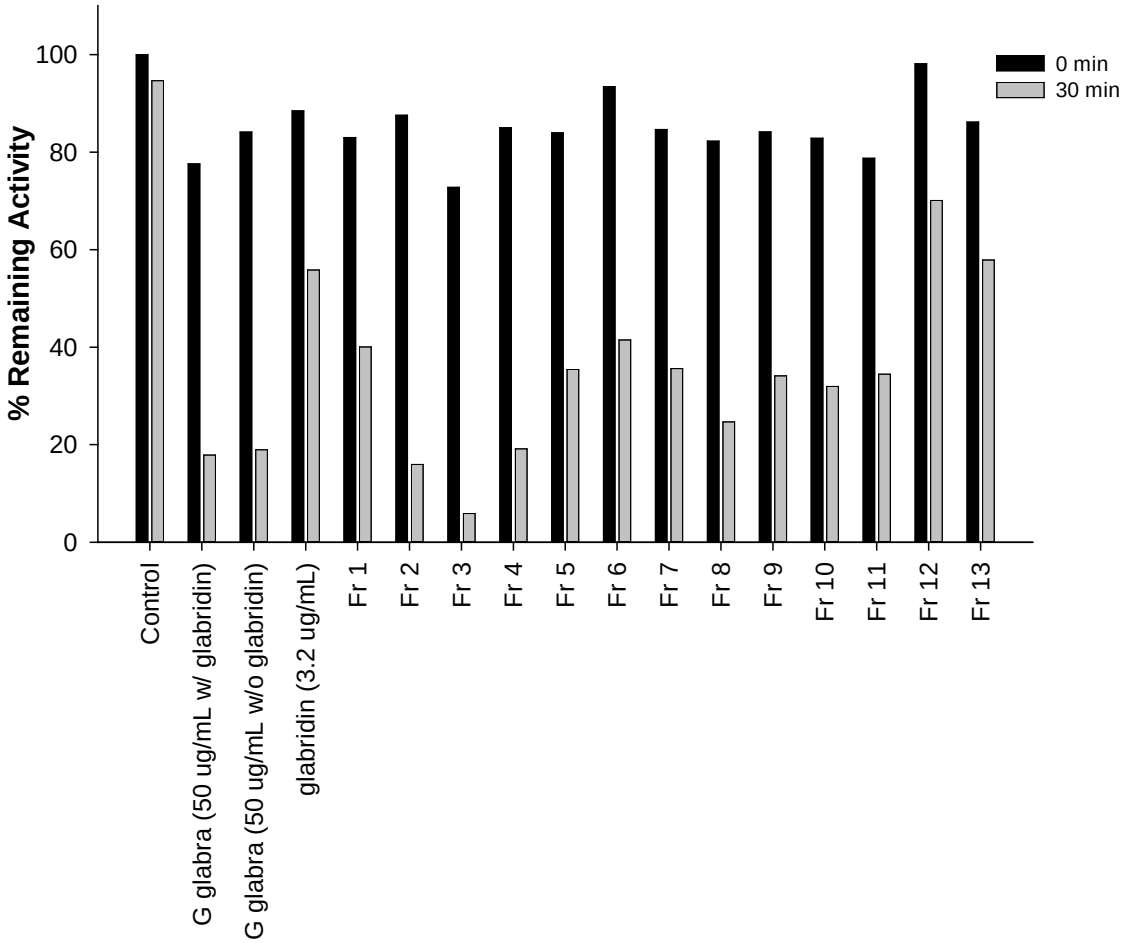

Figure 39. Remaining activity of cDNA-expressed recombinant CYP3A4 enzyme incubated with licorice extracts, glabridin, or fractions at 0 min and 30 min.

Four compounds (Compound 7, Compound 8, Compound 10, and Compound 14) were isolated from Fraction 3 by Dr. Charlotte Simmler at the UIC/NIH Center for Botanical Dietary Supplements Research (**Figure 40**, only structure of Compound 8 was disclosed). The structures of the isolates were determined by means of comprehensive 1D (^{1}H, ^{13}C) and 2D (gCOSY, HMBC, and HSQC) NMR analyses. Spectra were acquired on a Bruker

AVANCE 600.13 MHz spectrometer with a 5mm TXI cryoprobe (Billerica, MA, USA) and were consistent with previously published data.[227,228] These compounds were tested in parallel with Fraction 3 and the original licorice extract for time-dependent inhibition of CYP3A4 (**Figure 41**). Compound 10 showed the most potent time-dependent inhibition of CYP3A4 followed by Fraction 3. Compound 7, Compound 8, and Compound 14 were found to have time-dependent inhibition profiles that were similar to the licorice extract but less inhibitory than Fraction 3. These data suggest that multiple compounds in licorice might cause time-dependent inactivation of this enzyme. Note that when GSH was added to Fraction 3 (**Figure 41**), there was essentially no change in the time-dependent inactivation of CYP3A4, which indicated that formation of the enzyme-inhibitor complex is irreversible and GSH independent.

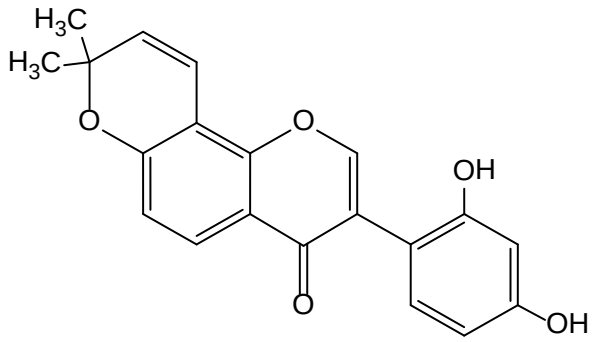

Figure 40. Proposed structure of Compound 8

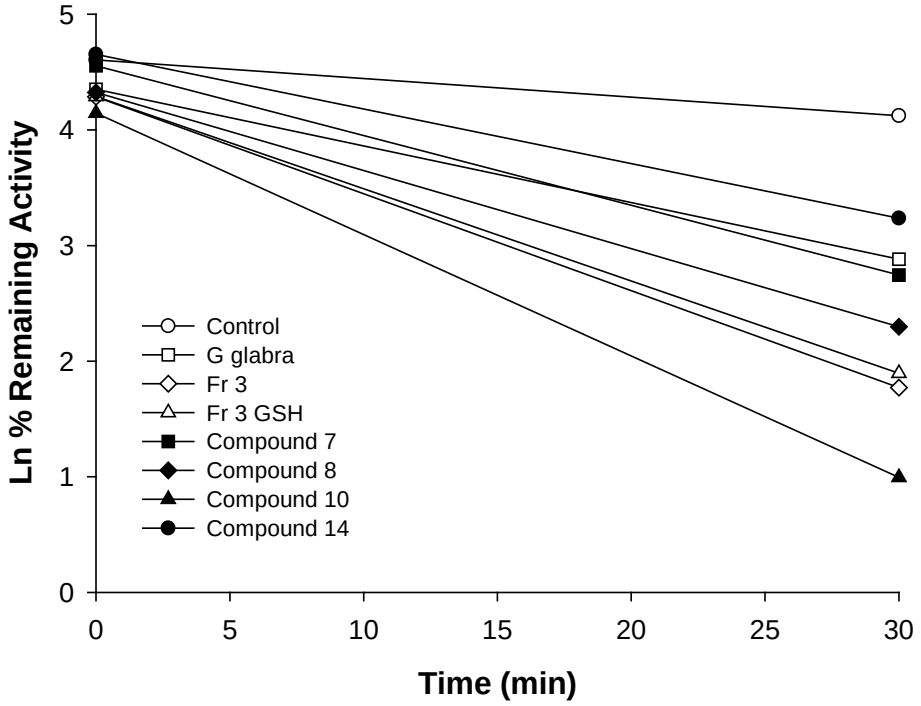

Figure 41. Time-dependent inhibition of cDNA-expressed recombinant CYP3A4 by licorice extract, Fraction 3, Compound 7, Compound 8, Compound 10, and Compound 14.

To determine whether Compound 10 inhibits CYP3A4 in a time-dependent manner, various concentrations of Compound 10 were incubated with recombinant CYP3A4 for different time periods. The residual CYP3A4 activity was measured by metabolism of the appropriate probe substrate (**Table 5**). The inactivation kinetics data was fit to the standard hyperbolic equation to determine k_{inact} of 0.132 min^{-1} and K_I of 13.7 μM. The data are comparable to the reported glabridin time-dependent inhibition where 7-benzyloxy-trifluromethylcoumarin was used as the probe substrate instead of the industry standard midazolam/testosterone.[109] However, it was recently determined that Compound

10 actually contains 3 different compounds. Therefore, additional work on "Compound 10" is required.

4.4 Identification of Potential Potent CYP2C9 Inhibitor in Licorice

4.4.1 Background and Research Rationale

Based on the results above (Section 4.2), among the major CYP isoforms, the *G. glabra* licorice extract inhibited CYP2C9 more than other cytochrome P450 enzymes with an IC_{50} value of 0.6 µg/mL. Given this relatively low IC_{50} value and the complexity of this licorice extract, the compounds that inhibit CYP2C9 most would have high potency (likely in the nM range). As a systematic approach to identify these CYP2C9 inhibitors, 14 sub-fractions of the crude licorice extract were isolated and tested in a one-point (1 µg/mL) inhibition assay as described in Section 4.2.2.2 above. Only the extracts that showed significant inhibition (> 90%) were selected for further analysis. UHPLC with high resolution mass spectrometry and tandem mass spectrometry were used to characterize of components within each fraction that showed significant CYP2C9 inhibition. Diligent database searching and dereplication of known licorice compounds were used to determine possible chemical structures of the most inhibitory (CYP2C9) licorice components. Due to lack of standards for these licorice compounds, the proposed chemical structures cannot be verified.

4.4.2 Materials and Methods

4.4.2.1 Materials

Tolbutamide and NADPH were purchased from Sigma-Aldrich. Hydroxytolbutamide and [d_9]-4-hydroxytolbutamide were obtained from Toronto Research Chemicals (Toronto, Canada). Pooled human liver microsomes (20 mg/mL, 150 donors) and cDNA-expressed recombinant P450 enzymes (CYP2C9) were purchased from BD Biosciences (Woburn, MA). All organic solvents were HPLC grade or better and were purchased from Thermo Fisher (Pittsburgh, PA). Water was prepared using an Elga Purelab Ultra (Siemens Water Technologies, Woodridge, IL) water purification system. Two alcoholic extracts of licorice roots (*Glycyrrhiza glabra*) were prepared from botanically authenticated plant material provided by Dr. Charlotte Simmler at the UIC/NIH Center for Botanical Dietary Supplements Research. The licorice root was extracted with 90% ethanol, 5% isopropanol, 5% water (*v/v/v*) (weight root powder (g) / volume solvent (mL): 1:15). Fourteen crude extract fractions were isolated from the crude extract at the UIC/NIH Center for Botanical Dietary Supplements Research.[229]

4.4.2.2 Incubation of Licorice Extract and Fractions with Recombinant CYP2C9 Enzyme

Incubation mixtures contained 2 pmol each of recombinant human CYP2C9, 1 mM NADPH, licorice extract or fraction (1 µg/mL), and cytochrome P450 substrate (**Table 4**)

in 100 mM potassium phosphate buffer at pH 7.4 in the total volume of 100 µL. After pre-incubation at 37 °C for 2 min, the reactions were initiated by the addition of NADPH. Enzymatic reactions were carried out under conditions (**Table 4**) shown to be linear with respect to time, microsomal protein concentration, and initial substrate concentration (within the range of reported *Km* in literature). After incubation, each reaction was terminated by the addition of acetonitrile/water/formic acid (86:10:4, v/v/v) containing the appropriate corresponding stable isotope-labeled internal standard (**Table 5**). The samples were vortexed for 2 min and centrifuged at 13,000 x *g* and 4 °C for 10 min. After centrifugation, 5 µL of each supernatant was injected onto the column for analysis using UHPLC-MS/MS. Incubations were carried out in duplicate.

4.4.2.3 HPLC-MS/MS

UHPLC-MS/MS analyses were carried out as described in 4.2.2.3 except for characterization of licorice components where LC-MS/MS was used with data-dependent product ion tandem mass spectrometric analysis on a Shimadzu IT-TOF mass spectrometer equipped with a Prominence UFLC XR system. HPLC separations were obtained using a Waters XTerra C_{18}, 2.1×100 mm, 3.5 µm, HPLC column. The mobile phase consisted of a 20.0 min linear gradient from 5% acetonitrile containing 0.05% formic acid 5 mM ammonium acetate to 100% acetonitrile containing 0.05% formic acid. The flow rate was 0.3 mL/min. Product ion scans were recorded over the range *m/z* 100 to 900 or based on the molecular mass of the compound.

4.4.3 Results and Discussion

Two alcoholic extracts and 13 sub-fractions of licorice prepared by Dr. Charlotte Simmler at the UIC/NIH Center for Botanical Dietary Supplements Research (Section 4.3.2.1 for preparation) were tested using a single point CYP2C9 inhibition assay. As shown in **Table 6**, the IC_{50} of the licorice extract was 0.6 µg/mL, therefore, 1 µg/mL extract would give more than 50% inhibition (less than 50% remaining activity) compared with control. The results of the inhibition assay of licorice extracts and sub-fractions are summarized in **Figure 42**. The two batches of alcoholic extracts prepared at different times showed remaining activities of 50% and 32%, respectively, which were consistent with previous results and can be used as assay controls. Among the 13 fractions, fractions 7 and 11 showed almost 100% inhibition (0% remaining activity). Therefore, fractions 7 and 11 were selected for further compound isolation and characterization.

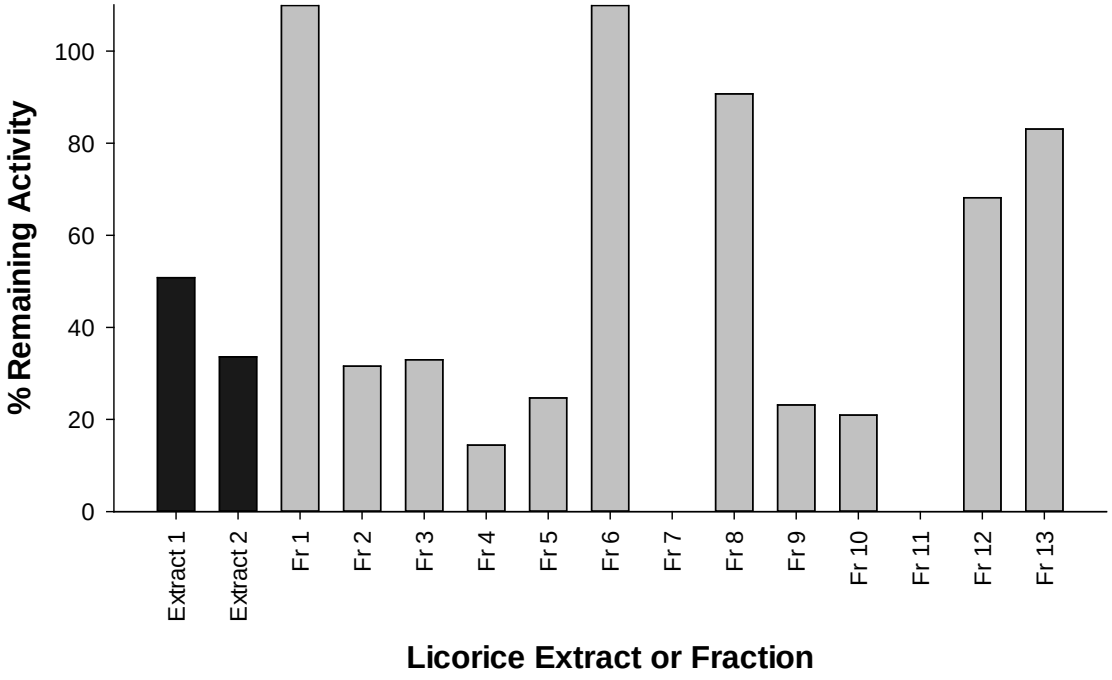

Figure 42. Remaining activity of recombinant CYP2C9 enzyme incubated with 1 µg/mL licorice extracts (black, Extract 1 and Extract 2) or fractions (grey, fractions (Fr) 1 to 14).

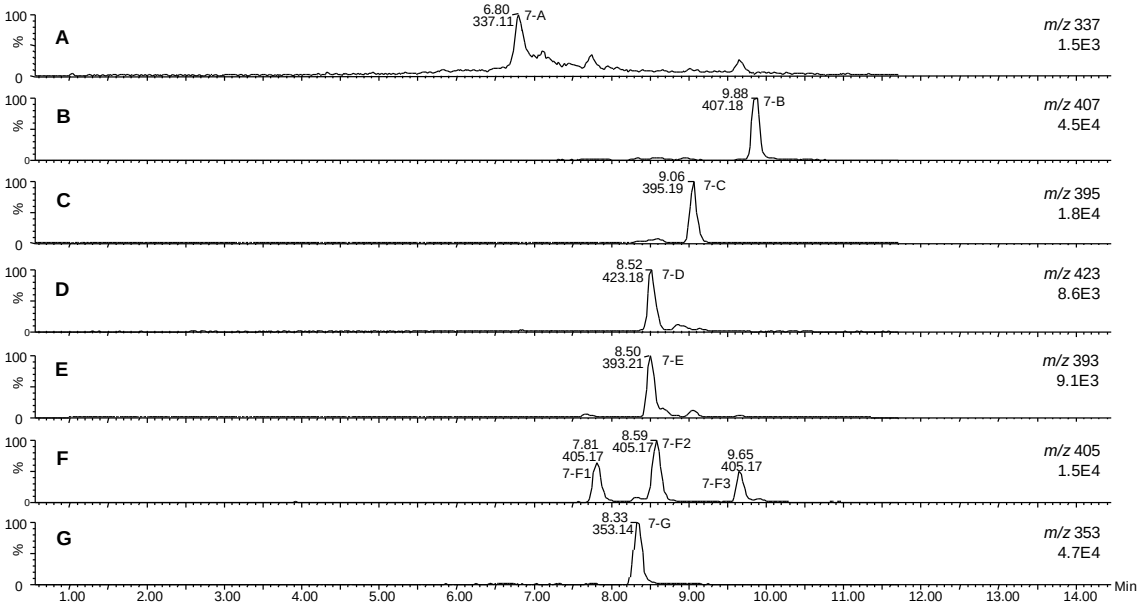

Figure 43. Negative ion LC-MS computer-reconstructed mass chromatograms of fraction 7 of a *G. glabra* licorice extract. Each peak is labeled with retention time (min), *m/z* value and peak designation (7-A, 7-B, 7-C, 7-D, 7-E, 7-F1, 7-F2, 7-F3, and 7-G).

In the negative ion computer-reconstructed mass chromatogram of fraction 7 of licorice extract (**Figure 43**), a total of 9 peaks were detected (7-A, 7-B, 7-C, 7-D, 7-E, 7-F1, 7-F2, 7-F3, and 7-G). Peak 7-G eluted at a retention time of 8.33 min, and accurate mass measurement indicated an elemental composition of $C_{21}H_{22}O_5$ (ΔM <3 ppm), which corresponded to the formula of glabridin with the addition of one carbon, two hydrogen atoms, and one oxygen atom.

High resolution negative ion product ion tandem mass spectra of compound 7-G (the accurate measured mass 353.1362 in **Figure 43**) and the reference licorice compound glabradin were obtained and compared (**Figure 44**). By comparing the accurate mass measurements and the MS/MS fragmentation patterns, the occurrence of the ions of *m/z* 201, *m/z* 187 and *m/z* 175 in both spectra indicated that the A-ring and C-ring of both glabridin and compound 7-G are identical. Therefore, 7-G differs from glabridin only in the B-ring. The two pairs of peaks (*m/z* 353/338 and *m/z* 165/150) in the tandem mass spectrum of 7-G (**Figure 44**) indicate the loss of CH_3. Based on this information and the literature, compound 7-G is proposed to be 3'-hydroxy-4'-O-methylglabridin, which is a known constituent of *G. glabra*.[230]

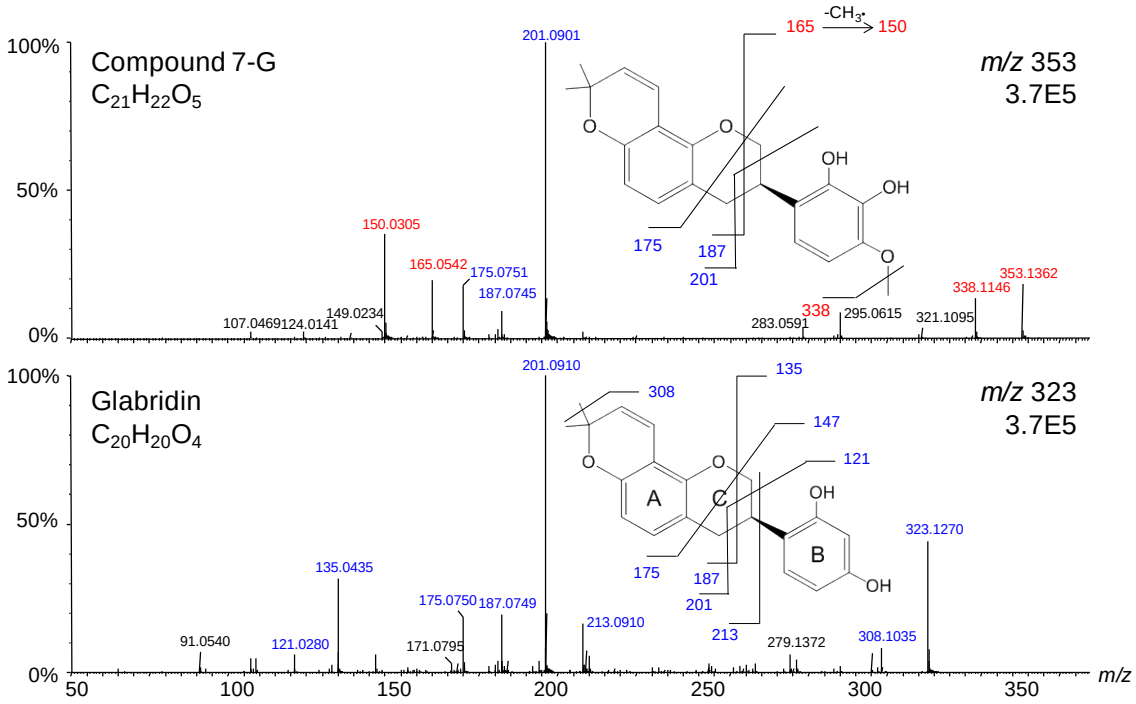

Figure 44. Negative ion LC-MS/MS product ion tandem mass spectra of compound 7-G (retention time 8.33 min in Figure 39) from fraction 7 of a *G. glabra* licorice extract with proposed structure and the similar licorice compound glabridin.

In **Figure 43B**, peak 7-B (retention time 9.88 min and the accurate measured mass 407.1852) had an elemental composition of $C_{25}H_{28}O_5$ (ΔM <3 ppm). The high resolution negative ion product ion tandem mass spectrum of compound 7-B was obtained (**Figure 45**). Based on the well-established tandem mass spectrometric fragmentation patterns of flavanoids and chalcones,[14,231,232] compound 7-B is proposed to be 2,3',4,4'-tetrahydroxy-3,5'-diprenylchalcone, which is a known constituent of *G. glabra* roots with PPAR-γ ligand-binding activity.[233] Given that chalcones can cyclize to the corresponding flavanones and that these two isomers produce nearly identical tandem mass spectra,[14,231,232] compound 7-B might be instead the corresponding flavanone (**Figure 45**,

structure on the left) depicted in **Figure 46**. The proposed fragmentation pathways during MS/MS with CID for the deprotonated molecule of compound 7-B is shown in **Figure 47**. Retro-Diels–Alder fragmentation of these compounds would produce fragment $^{1,3}B^-$ (*m/z* 203) which would further eliminate C_4H_7 to form *m/z* 148. Retro-Diels-Alder fragmentation (**Figure 47**) would also produce fragment $^{1,3}A^-$ (*m/z* 203) which would further lose CO_2 to form the ion of *m/z* 159. Because all of these fragment ions were observed (**Figure 45**), compound 7-B is probably either 2,3',4,4'-tetrahydroxy-3,5'-diprenylchalcone or its corresponding flavanone.

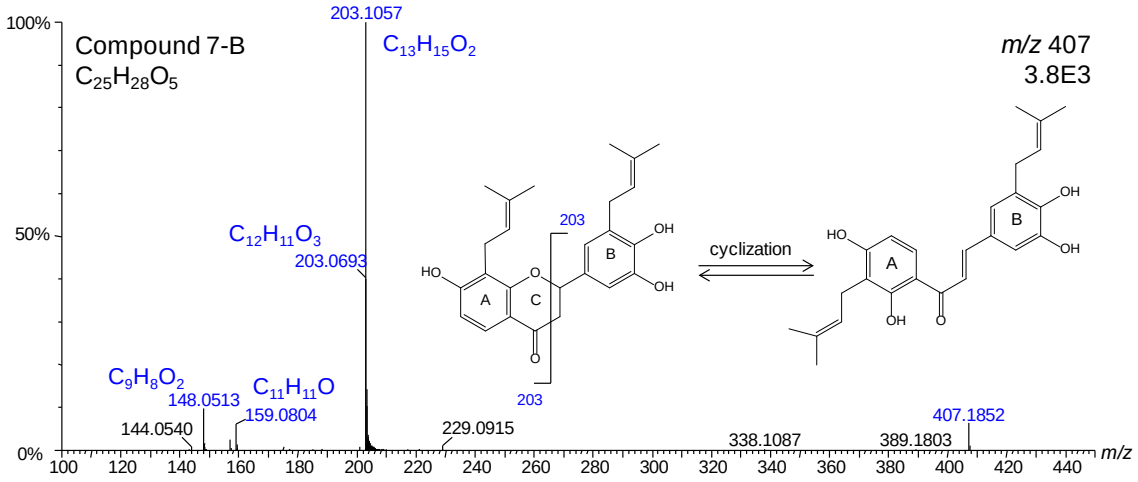

Figure 45. Negative ion LC-MS/MS tandem mass spectrum of compound 7-B eluting at 9.88 min in Figure 38 from fraction 7 of a *G. glabra* licorice extract with proposed structures.

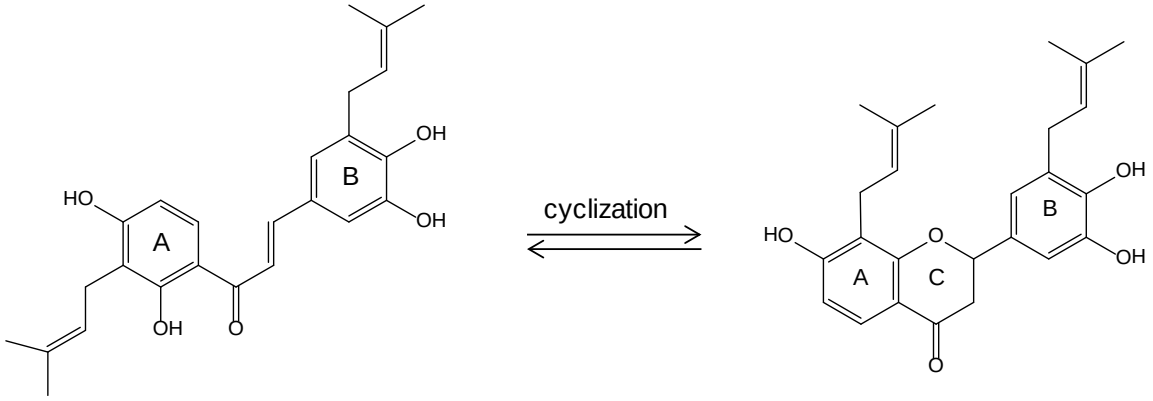

Figure 46. Cyclization of chalcone to flavanone

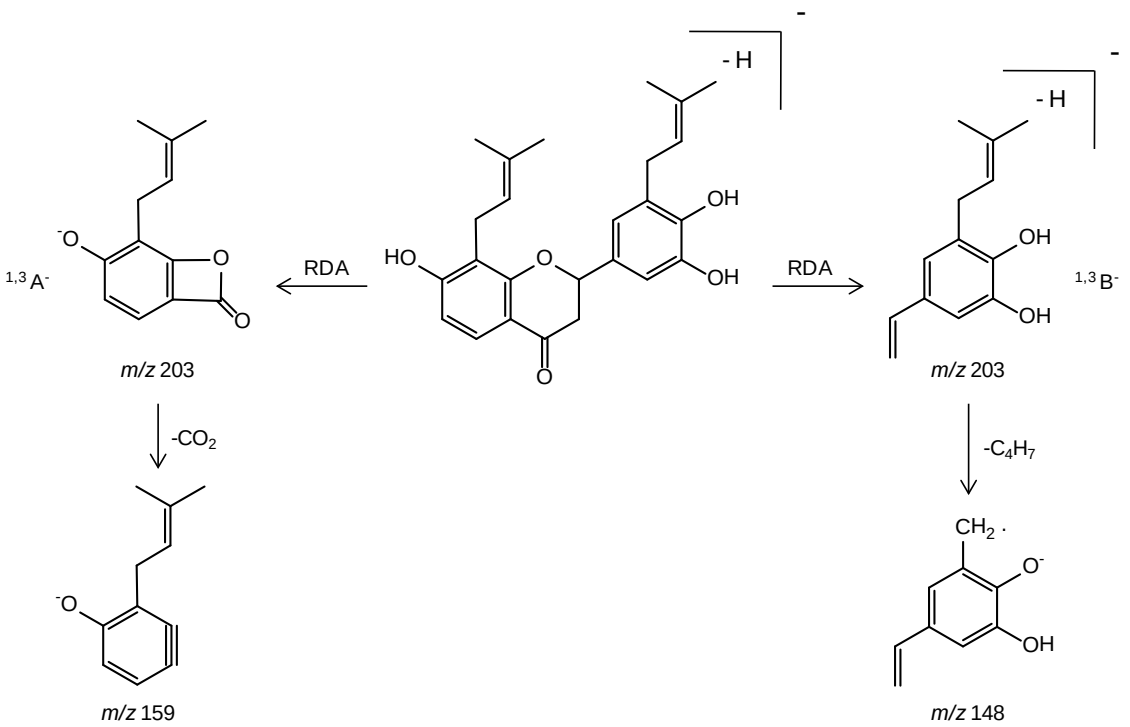

Figure 47. Proposed fragmentation pathways during MS/MS with CID for the deprotonated molecule of compound 7-B, which was tentatively identified as 2,3',4,4'-tetrahydroxy-3,5'-diprenylchalcone.

In **Figure 43E**, peak 7-E (retention time 8.50 min and the accurate measured mass 393.2053) was determined using accurate mass measurement to have an elemental

composition of $C_{25}H_{30}O_4$ (ΔM <5 ppm). The negative ion electrospray product ion tandem mass spectrum of compound 7-E was obtained (**Figure 48**) using accurate mass measurement. As discussed above for compound 7-B and based on established fragmentation patterns of glabridin, compound 7-E is proposed to be tenuifolin B (also known as kanzonol X) which has been isolated from roots of *Maackia tenuifolia.*[234] Kanzonol X has been reported previously to occur in *G. glabra*.[235]

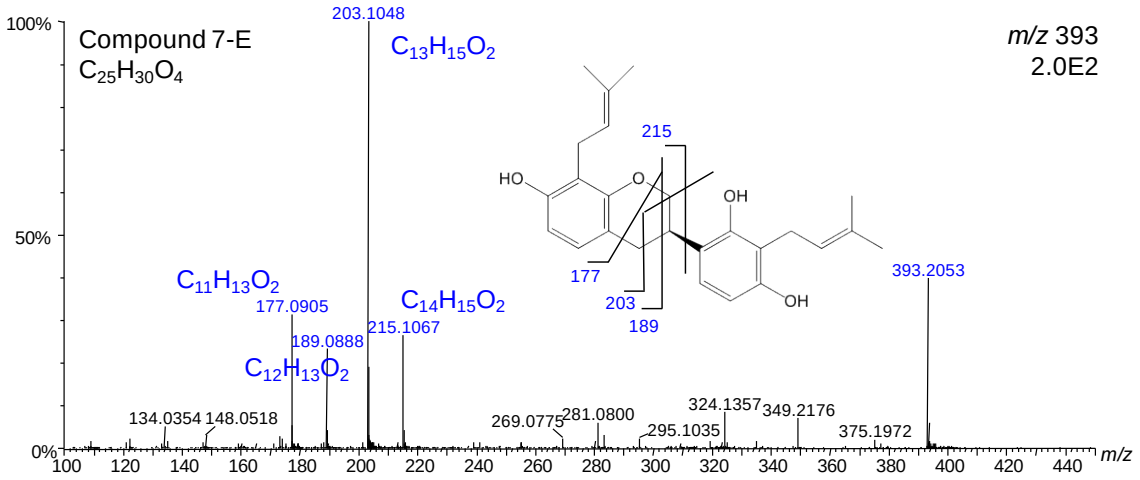

Figure 48. Negative ion electrospray product ion tandem mass spectrum of compound 7-E (retention time 8.50 min in Figure 39E) from fraction 7 of a *G. glabra* licorice extract. The proposed structure is consistent with that of tenuifolin B (kanzonol X) which has been isolated from roots of *Maackia tenuifolia.*[234]

In **Figure 43F**, three peaks were detected during LC-MS with retention times of 7.81 min, 8.59 min, and 9.65 min with the accurate measured mass 405.1691. Based on accurate mass measurements (ΔM <5 ppm of the elemental composition of $C_{25}H_{26}O_5$), these compounds, 7-F1, 7-F2, and 7-F3, were determined to be isomers. The negative ion

tandem mass spectra of all three isomers were obtained and are compared in **Figure 49**. Similar to compound 7-B, the fragmentation pattern of compound 7-F3 resembles that of a chalcone or flavanone. Dereplication and analysis of the product ion tandem mass spectrum indicates that compound 7-F3 corresponds to the chalcone glyinflanin C (or its flavanone form) which had been found in *Glycyrrhiza inflata* in 1992.[236] Although tandem mass spectra of compounds 7-F1 and 7-F2 were obtained (**Figure 49**), dereplication did not suggest similarities to any known natural products.

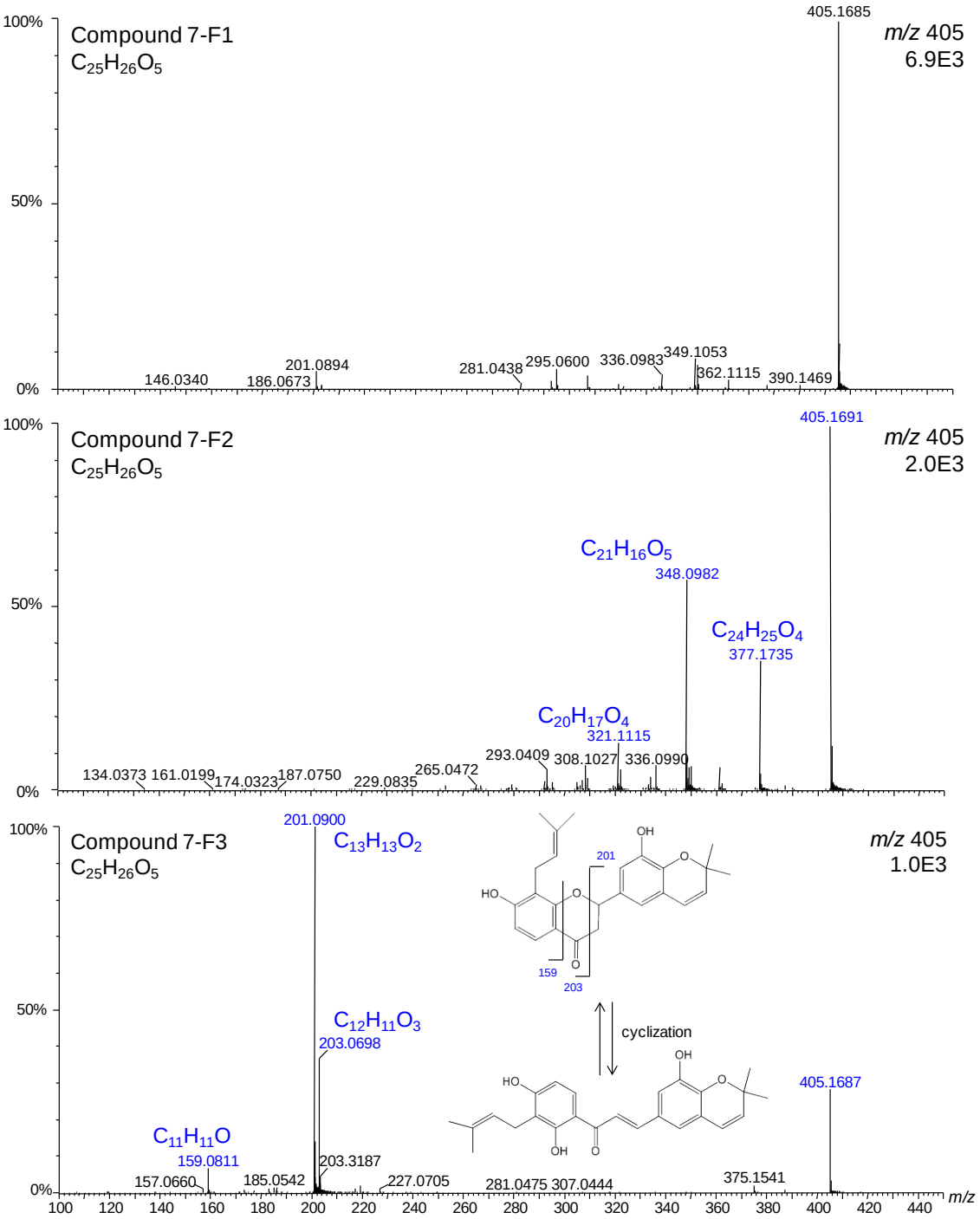

Figure 49. Negative ion electrospray product ion tandem mass spectra of isomeric compounds 7-F1, 7-F2 and 7-F3 from *G. glabra* fraction 7, which eluted at 7.81 min, 8.59 min and 9.65 min in LC-MS analysis (Figure 39). Based

on similarities in fragmentation to glabridin (Figure 39) compound 7-F3 is proposed to be glyinflanin C.

In **Figure 43C**, the peak with retention time 9.06 min and measured mass of 395.2192 was determined using accurate mass measurement to be within 5 ppm of the elemental composition of $C_{24}H_{28}O_5$. The negative ion product ion tandem mass spectrum of compound 7-C was obtained (**Figure 50**) using high resolution accurate mass measurement. No existing natural product compound has been identified to match this tandem mass spectrum. In **Figure 43A**, the peak with retention time 6.80 min with the accurate measured mass 337.11 was determined using accurate mass measurement to be within 5 ppm of the elemental composition of $C_{20}H_{18}O_5$. In **Figure 43D**, the peak with retention time 8.52 min with the accurate measured mass 423.1808 was determined using accurate mass measurement to be within 5 ppm of the elemental composition of $C_{25}H_{28}O_6$. No existing natural product compound has been identified to match these elemental compositions.

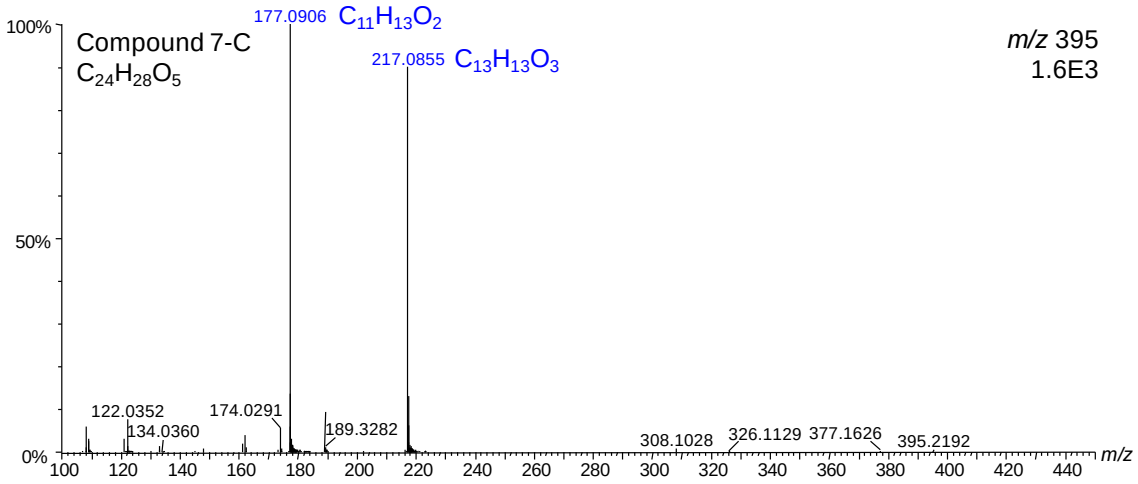

Figure 50. Negative ion electrospray product ion tandem mass spectrum of compound 7-C from fraction 7 of licorice extract, which eluted at 9.06 min in LC-MS analysis (Figure 39).

In the negative ion computer-reconstructed mass chromatogram of fraction 11 of licorice extract (**Figure 51**), a total of 8 peaks were detected (11-A1, 11-A2, 11-B1, 11-B2, 11-C, 11-D1, 11-D2, and 11-D3). Peak 11-A1 and Peak 11-A2 eluted at a retention time of 9.79 min and 10.49 min, respectively, and accurate measured mass 391.1889 indicated an elemental composition of $C_{25}H_{28}O_4$ (ΔM <5 ppm). The negative ion tandem mass spectra of both peaks were obtained and are compared in **Figure 52**.

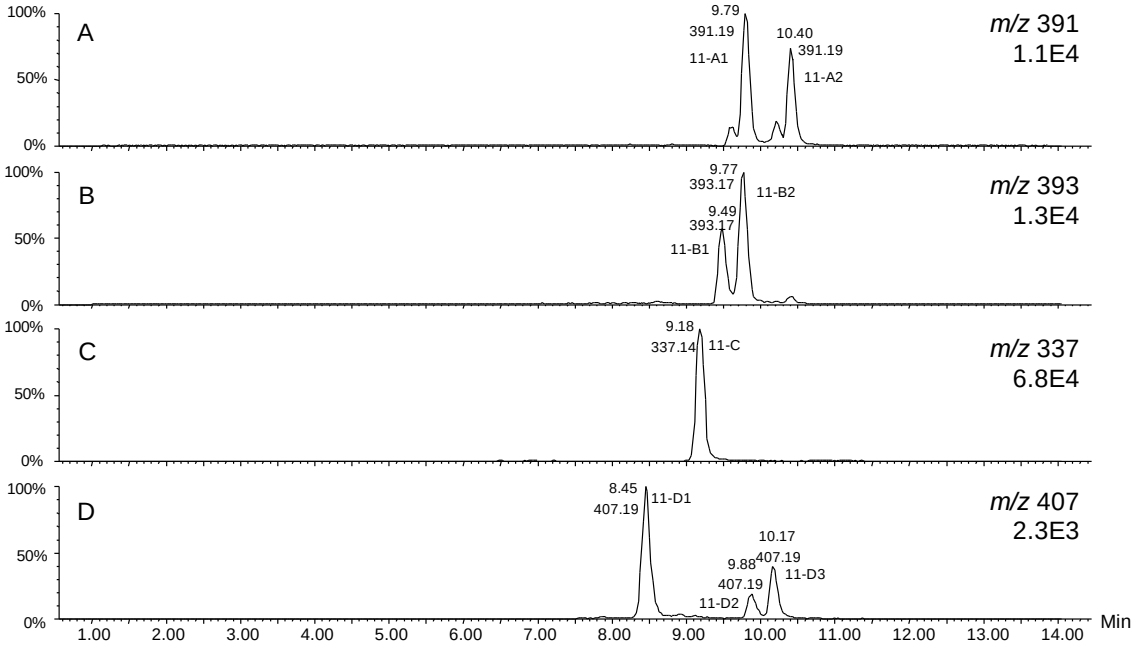

Figure 51. Negative ion LC-MS computer-reconstructed mass chromatograms of fraction 11 of a *G. glabra* licorice extract. Each peak is labeled with retention time (min), *m/z* value and peak designation (11-A1, 11-A2, 11-B1, 11-B2, 11-C, 11-D1, 11-D2, and 11-D3).

Compound 11-A1 showed a similar set of fragment ions as did glabridin (**Figure 44**): *m/z* 213, *m/z* 201, *m/z* 175 and loss of 15 (to *m/z* 376) which indicated that 11-A1 may share the same ring A and ring C with glabridin. Meanwhile, *m/z* 215, *m/z* 203 and *m/z* 189 are fragment ions that are 68 (C_5H_8) mass units higher than what was observed for glabridin (*m/z* 147, *m/z* 135 and *m/z* 121), pointing to the possibility that a prenyl group is attached to the glabridin B ring. Dereplication and further analysis of the product ion tandem mass spectrum suggest that compound 11-A1 is Hispaglabridin A which was first identified in *Glycyrrhiza glabra* in 1980.[237] Similar to compound 7-B and 7-F3, the fragmentation pattern of compound 11-A2 resembles that of a chalcone or flavanone. The fragments *m/z* 203 and *m/z* 159 are identical to those observed for 7-B while the MS/MS fragmentation from *m/z* 187 to *m/z* 132 is only 16 mass units lower than that of *m/z* 203 to *m/z* 148 observed in the 7-B tandem mass spectrum. Further dereplication and analysis of the product ion tandem mass spectrum suggests that compound 11-A2 corresponds to glabrol which was found in *Glycyrrhiza glabra* in 1976.[238]

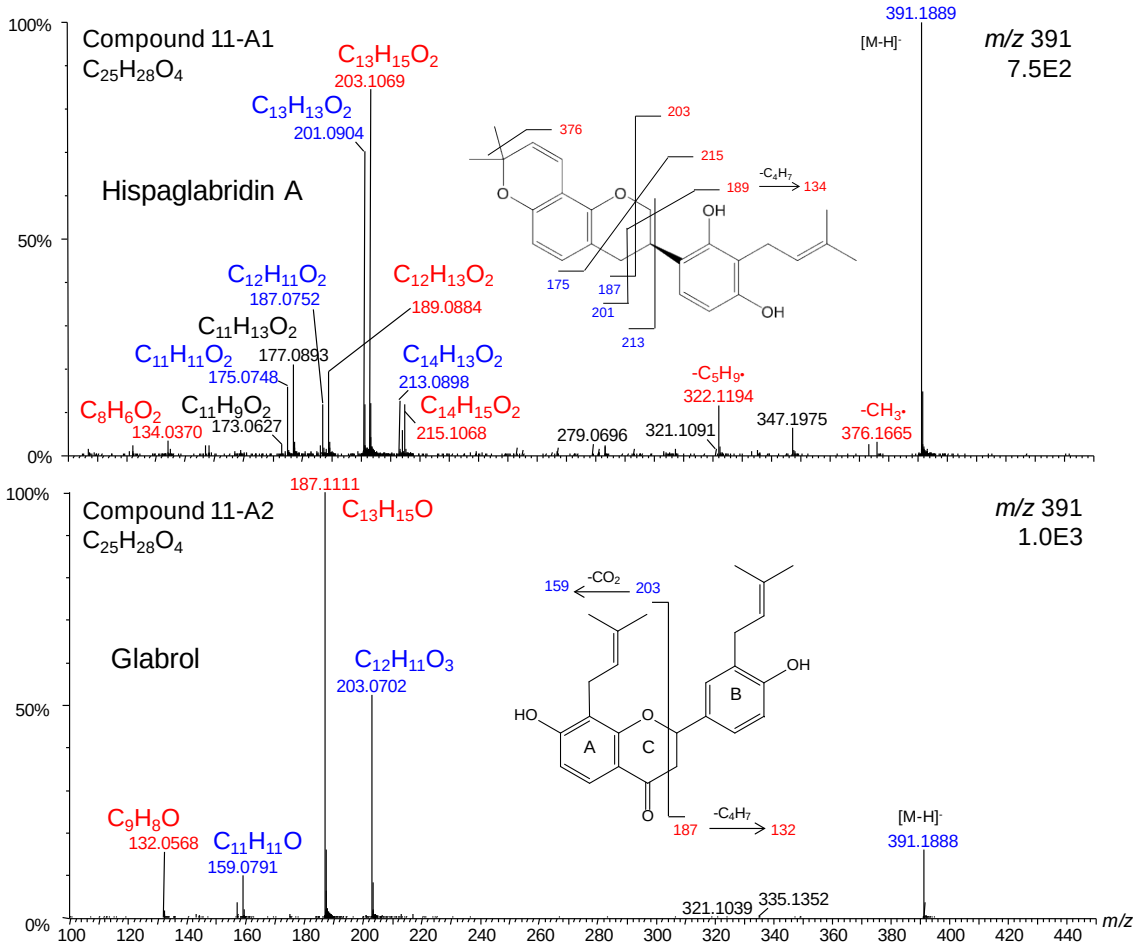

Figure 52. Negative ion electrospray product ion tandem mass spectra of isomeric compounds 11-A1 and 11-A2 from *G. glabra* fraction 11, which eluted at 9.79 min and 10.49 min in LC-MS analysis (Figure 51). Based on similarities in fragmentation to glabridin (Figure 39) compound 11-A1 and compound 11-A2 are proposed to be Hispaglabridin A and Glabrol, respectively.

Peak 11-B1 and Peak 11-B2 eluted at retention times of 9.49 min and 9.77 min, respectively, and isomeric accurate mass measurements of 393.1826 indicated an elemental composition of $C_{24}H_{26}O_5$ (ΔM <5 ppm). The negative ion tandem mass spectra of both peaks were obtained and are compared in **Figure 53**. The close retention time and the similarity of the two tandem mass spectra confirm that compound 11-B1 and

compound 11-B2 are isomers. The loss of 55 mass units from *m/z* 177 to *m/z* 122 indictes that these compounds may have a prenyl moiety. Although tandem mass spectra of compounds 11-B1 and 11-B2 were obtained, dereplication did not suggest similarities to any known natural products.

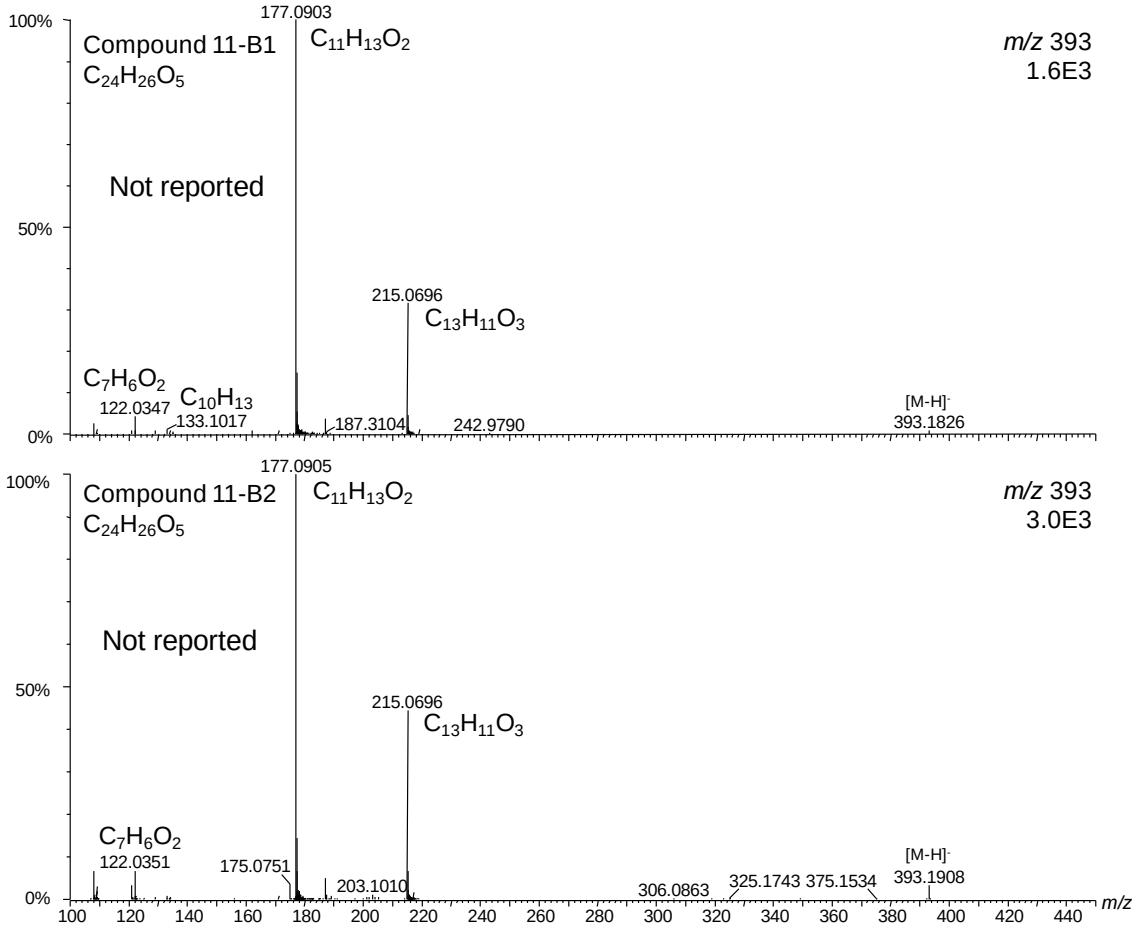

Figure 53. Negative ion electrospray product ion tandem mass spectra of isomeric compounds 11-B1 and 11-B2 from *G. glabra* fraction 11, which eluted at 9.49 min and 9.77 min during LC-MS analysis (Figure 51).

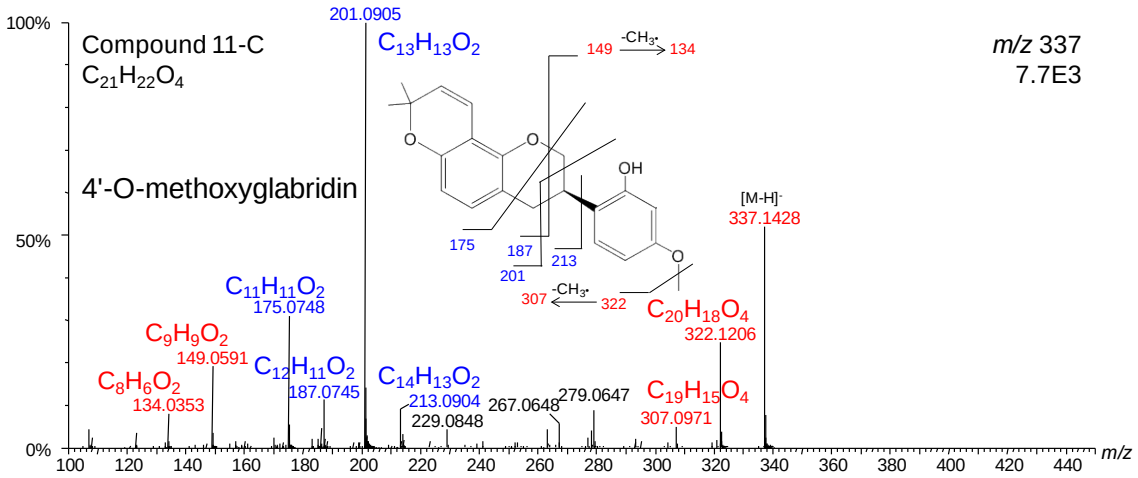

Figure 54. Negative ion electrospray product ion tandem mass spectrum of compound 11-C from fraction 11 of licorice extract, which eluted at 9.18 min during LC-MS analysis (Figure 51). Based on similarities in fragmentation to glabridin (Figure 39) compound 11-C is proposed to be 4'-O-methoxyglabridin.

Peak 11-C eluted at 9.18 min and accurate mass measurement of 337.1428 indicated an elemental composition of $C_{21}H_{22}O_4$ (ΔM <5 ppm). High resolution negative ion product ion tandem mass spectra of compound 11-C (**Figure 54**) is similar to those of Compound 7-G and glabridin: *m/z* 213, *m/z* 201, *m/z* 187 and *m/z* 175, suggesting they are structurally similar on one side of the glabridin molecule (ring A, ring C, and ring D). The fragment ions of *m/z* 337, *m/z* 322 (loss of 15 mass units), *m/z* 149, and *m/z* 134 are all 16 mass units less than those observed for Compound 7-G, indicating the other side of the Compound 11-C structure contains one fewer oxygen (hydroxyl) than Compound 7-G, 3'-hydroxy-4'-O-methylglabridin. Dereplication and analysis of the product ion tandem mass spectrum suggested that compound 11-C corresponds to 4'-O-methylglabridin which was first reported in *Glycyrrhiza glabra* in 1980.[237]

In **Figure 51D**, three peaks were detected during LC-MS analysis with retention times of 7.45 min, 9.88 min and 10.17 min and all with the same measured mass of 407.1789. Based on accurate mass measurements (ΔM <5 ppm of the elemental composition of $C_{25}H_{28}O_5$) and the similarity of tandem mass spectra (**Figure 55**), compounds 11-D1 and 11-D3 are probably isomers. Similar to compound 7-B, the fragmentation pattern of compound 11-D1 and compound 11-D3 resembles that of a chalcone or flavanone. Dereplication and analysis of the product ion tandem mass spectrum indicates that compound 11-D1 or 11-D3 corresponds to 3-hydroxy glabrol (or its flavanone form) which had been found in *Glycyrrhiza inflata* in 1976.[238] Although tandem mass spectra of compounds 11-D2 was obtained (**Figure 55**), dereplication did not suggest similarities to any known natural products.

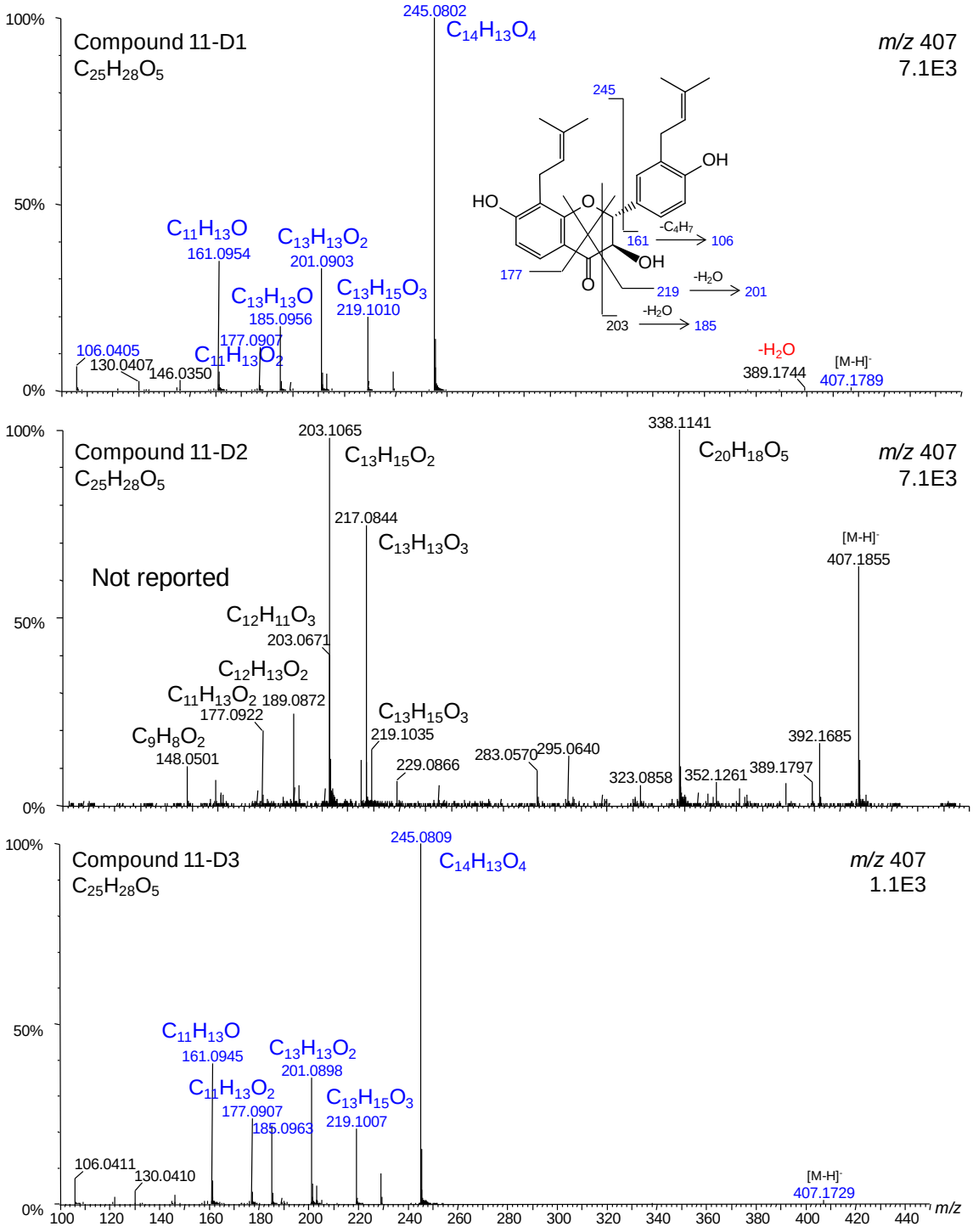

Figure 55. Negative ion electrospray product ion tandem mass spectra of isomeric compounds 11-D1, 11-D2 and 11-D3 from *G. glabra* fraction 11, which eluted at 8.45 min, 9.88 min and 10.17 min during LC-MS analysis (Figure 51).

4.5 Time-Dependent Inhibition by Hops

Section 4.5 in this work has been published previously in the *European Journal of Pharmaceutical Sciences* as part of an article with the title *Inhibition of human cytochrome P450 enzymes by hops (*Humulus lupulus*) and hop prenylphenols*:

Yuan Y, Qiu X, Nikolić D, Chen SN, **Huang K**, Li G, Pauli GF, van Breemen RB. Inhibition of human cytochrome P450 enzymes by hops (Humulus lupulus) and hop prenylphenols, *Eur. J. Pharmaceut. Sci.* **2014**, *53*, 55-61

4.5.1 Background and Research Rationale

The female flowers of hops (*Humulus lupulus* L.) are used in the brewing industry to add aroma and bitterness to beer. Although hop preparations are widely used as mild sedatives, most of the recent research has focused on their potential estrogenic and chemopreventive properties. Known active constituents of hops belong to the class of prenylphenols and may be divided into two groups: prenylated chalcones and prenylated flavanones. In hop cones, the most abundant prenylated chalcone is xanthohumol (XN; **Figure 56**), which is contained in amounts up to 1% of the dry weight.[239,240] Studied primarily for its chemoprevention properties, XN has shown anti-proliferative activity

against breast, colon and ovarian cancer cell lines[241,242] and is a potent inducer of quinone reductase.[243]

Among the prenylated flavanones, 8-prenylnaringenin (8-PN; **Figure 56**) has been identified as one of the most potent of the known phytoestrogens,[244] and its estrogenic properties have been confirmed in numerous *in vitro*[240-243,245,246] and *in vivo* assays.[239,240] Isoxanthohumol (IX; **Figure 56**), the 5-*O*-methyl derivative of 8-PN, has much weaker estrogenic activity.[247] However, several *in vitro* and *in vivo* studies have shown that IX can be metabolically converted into 8-PN, either by the action of cytochrome P450 (CYP) enzymes[232] or by the intestinal microbiome.[248,249] Therefore, IX may be considered a pro-phytoestrogen.

Previously at the UIC/NIH Center for Botanical Dietary Supplement Research, a hop extract and isolated prenylated phenols from hops were assayed for inhibition of the eight cytochrome P450 enzymes which are responsible for the metabolism of the vast majority of clinically useful drugs.[204] The four major prenylated compounds in hops (XN, IX, 6-PN, and 8-PN) were tested individually at 1 μM and 10 μM for inhibition of CYP enzymes. There was no significant inhibition of CYP3A4, CYP2D6 or CYP2E1 by the hop extract or any of the prenylated compounds isolated from hops. However, at 10 μM, all 4 prenylated compounds showed >60% inhibition of CYP2C8 and CYP2C9. The prenylated phenols IX and 8-PN, but not XN or 6-PN, were potent inhibitors (>90%) of CYP2C19. 8-PN was also a potent (>88%) inhibitor of CYP1A2. The hop extract at 5 μg/mL showed significant (≥70%) inhibition of CYP2C8, CYP2C9 and CYP2C19 but

only weak inhibition of CYP2B6 (36%) and CYP1A2 (27%). Extending this investigation, the possibility that this same hop extract and/or isolated hop prenylated phenols might cause time-dependent inactivation of the cytochrome P450 enzymes CYP1A2, CYP2B6, CYP2C8, CYP2C9, and CYP2C19 was investigated as part of this dissertation.

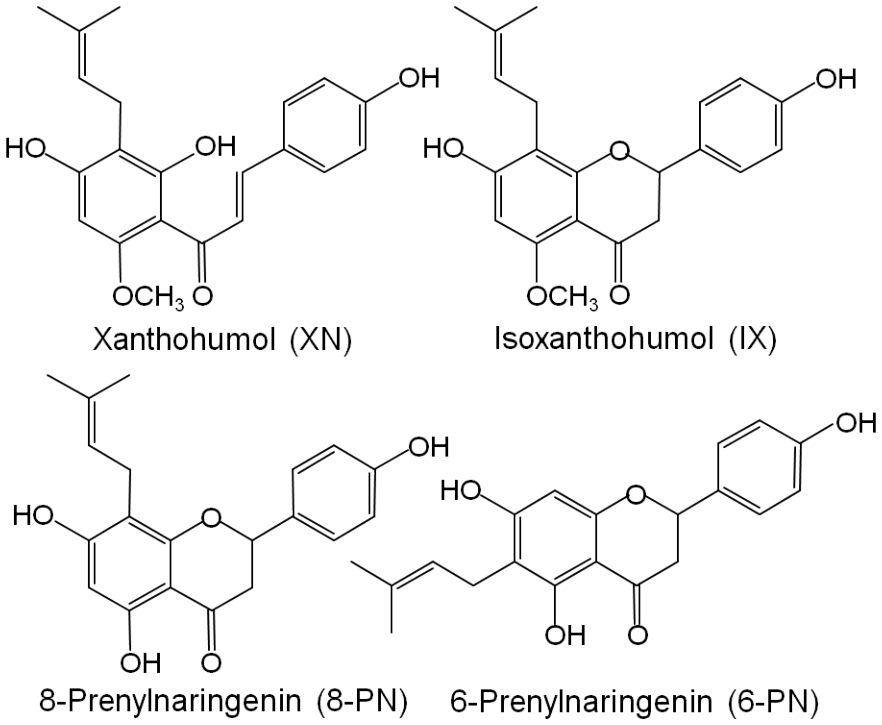

Figure 56. Structures of prenylated hop phenols XN, IX, 8-PN and 6-PN.

4.5.2 Materials and Methods

4.5.2.1 **Materials**

The hop extract examined during this study was developed at the UIC/NIH Center for Botanical Dietary Supplements Research for use in clinical studies of safety and efficacy. The extract was prepared from botanically authenticated hops provided by Hopsteiner (New York, NY) that had been depleted of bitter acids and then standardized chemically to contain 33.84% XN, 0.35% 8-PN, 1.77% 6-prenylnaringenin (6-PN), and 1.07% IX. The hop constituent XN was prepared and provided by Dr. Charlotte Simmler at the UIC/NIH Center for Botanical Dietary Supplements Research. XN was isolated from hops and purified as previously described[250] and the purity was determined to be >99.5% by qHNMR. IX (> 99.0% pure by qHNMR) was prepared by cyclization of XN as described previously.[250] 8-PN was synthesized chemically, and 6-PN was purified as previously reported.[251]

4.5.2.2 Microsomal Incubation

To test for time-dependent inactivation of the cytochrome P450 enzymes that were determined to be inhibited by hops, recombinant enzymes (300 pmol/mL) were pre-incubated with hop extract (50 μg/mL) or test compound (10 μM) for 30 min at 37 °C in 100 mM potassium phosphate buffer (pH 7.4) with or without (control) NADPH (1 mM). At 0 min and 30 min after incubation, 5 μL aliquots of each mixture were transferred to secondary incubation mixtures containing a probe substrate (85 μM phenacetin, 3.5 μM amodiaquine, 400 μM tolbutamide, or 85 μM S-(+)-mephenytoin for CYP1A2, CYP2C8, CYP2C9, or CYP2C19, respectively) and 1 mM NADPH in a total volume of 100 μL. The secondary incubation was carried out as described in **Table 4**. Note that aliquots of

the pre-incubation mixtures were diluted 20-fold with probe substrate at a saturating concentration (~*Km*) to measure residual enzyme activities. After incubation, each reaction was stopped by the addition of 20 µL water/acetonitrile/formic acid (92:5:3, v/v) containing the internal standards. The samples were vortex mixed for 30 s and centrifuged at 13,000 x *g* at 4°C for 10 min. After centrifugation, 5 µL aliquots of the supernatants were analyzed using UHPLC-MS/MS.

4.5.2.3 UHPLC-MS/MS

UHPLC-MS/MS analyses were carried out as described in 4.2.2.3.

4.5.3 Results and Discussion

Time-dependent enzyme inactivation experiments showed that the hop extract produced no irreversible inhibition of CYP2C8, CYP2C9 or CYP2C19 (**Figure 57**). However, pre-incubation of the hop extract with CYP1A2 did show partial inactivation (**Figure 58**). Although 8-PN had been reported inhibit CYP1A2,[16] pre-incubation with the enzyme showed no time-dependent inactivation. Instead, XN was found to produce time-dependent inactivation of CYP1A2 (**Figure 58**). However, the magnitude of CYP1A2 inactivation by the hop extract relative to that of XN alone (**Figure 58**) suggests that other compounds in hops might also cause time-dependent inactivation of this enzyme.

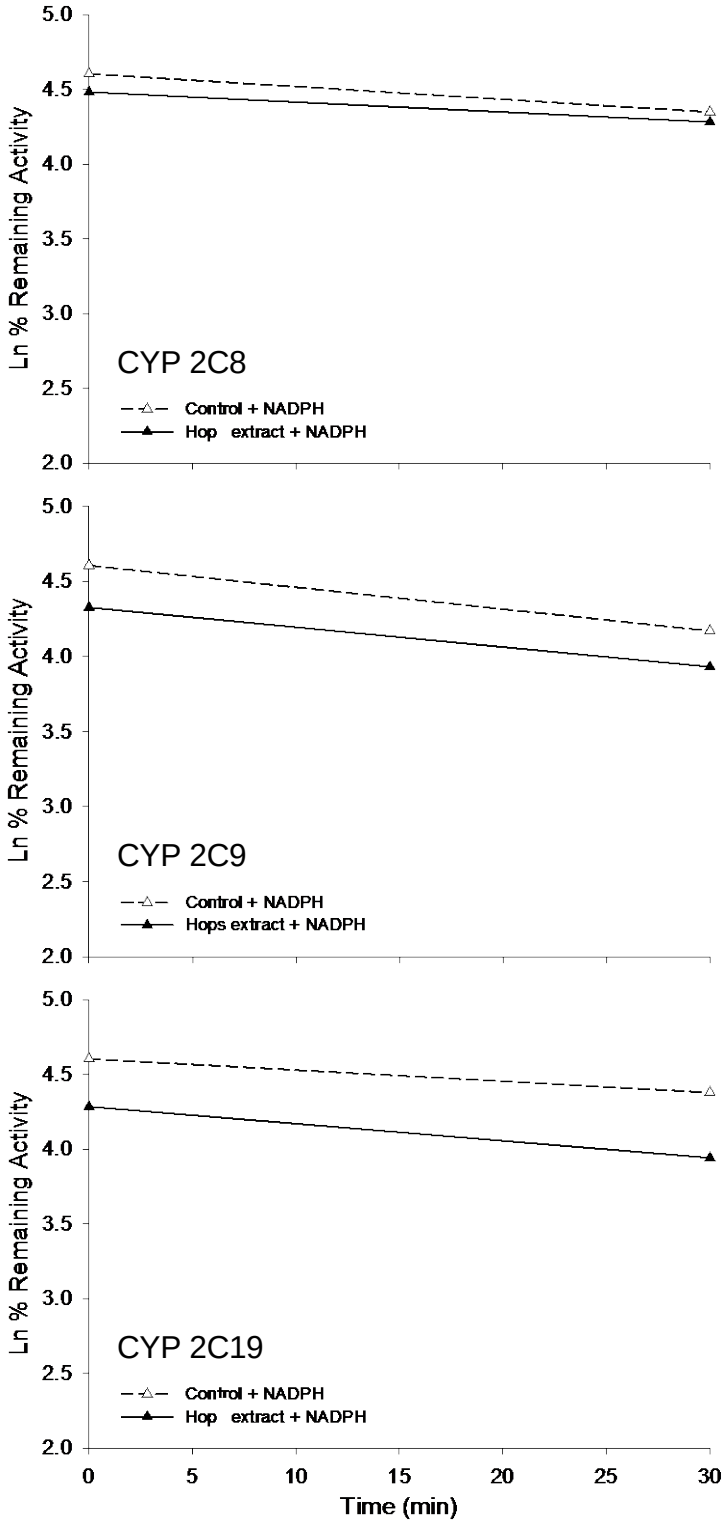

Figure 57. Time-dependent inhibition of cDNA-expressed recombinant CYP2C8, 2C9, 2C19 by a hop extract.

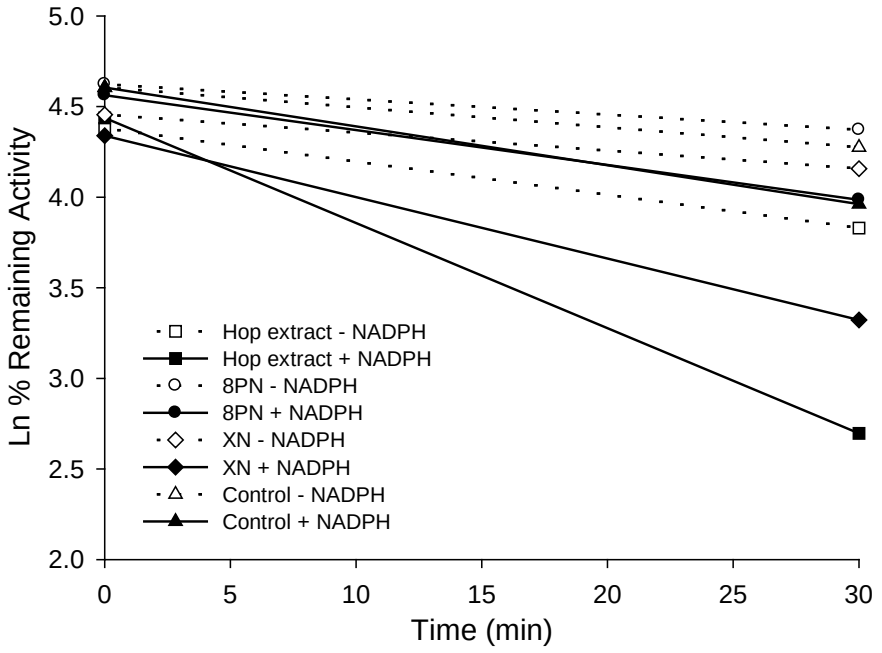

Figure 58. Time-dependent inhibition of cDNA-expressed recombinant CYP1A2 by a hop extract or the single hop compounds 8PN and XN.

According to **Figure 58**, the extent of hop extract time-dependent inactivation of CYP1A2 (15% remaining activity) was comparable to the inactivation of CYP3A4 (20% remaining activity). As hop extract contains 33% XN which exhibits relatively strong time-dependent inactivation of CYP1A2 (**Figure 58**), it was less imperative to study hop sub-factions for identification of other potent compounds for potential time-dependent inactivation. However, because no single compound in licorice extract comprises more than 13% weight of the extract,[252,253] it was reasonable to test sub-fractions and isolate and identify compounds of low concentrations that exhibit high inhibitory potency once CYP450 inhibition was observed for licorice extract.

Chapter 5 Conclusions and Future Directions

5.1 Glabridin Metabolism

The dried roots of licorice have been consumed for the past 6000 years as a flavoring and sweetening agent in the western world and in Asian countries for their anti-allergic and anti-inflammatory agent properties. Among the constituents identified in popular licorice species, few have been studied for metabolism by human cytochrome P450 enzymes.

Glabridin *in vitro* metabolism was studied with respect to metabolic stability, metabolite identification, and identification of metabolizing enzymes. Glabridin was metabolized with low hepatic clearance. In the incubations of glabridin with human liver microsomes and rat liver microsomes, six glabridin metabolites were observed. The D-ring diols formed via unstable epoxides were the major glabridin metabolites, and this finding was confirmed by treating glabridin treated with the epoxide-forming reagent *m*CPBA. Rat liver microsomes produced more diol metabolites but significantly less other products. Enzymatic kinetics study showed the two diol metabolites were produced at relatively similar rates but faster than other products. When compared to kinetics and other epoxide/diol formation, glabridin diol formation had lower *Km* values. Cytochrome P450 isozyme 1A2, 2C9, and 3A4 were found to be the major enzymes responsible for the formation of the diol metabolites while CYP3A4 and CYP2C9 were predominantly responsible for the other metabolites.

Future work on glabridin metabolism may include continued structural determination of all *in vitro* glabridin metabolites if corresponding synthetic standards are available. Given the phenolic structure of glabridin, studies of Phase II metabolism should provide important additional information regarding the metabolism of glabridin. Incubation with chemical inhibitors of specific P450 enzymes may be carried out to compare with the results from the incubation with cDNA expressed recombinant CYP enzymes.

A fast triple quadrupole mass spectrometer-based approach was developed that can detect positively and negatively charged GSH conjugates in a single analysis without the need for advance knowledge of the elemental compositions of potential conjugates and while avoiding false positives. This approach utilized UHPLC instead of HPLC to shorten separation time and enhance sensitivity, incorporated stable-isotope labeled GSH to avoid false positives, and used fast polarity switching electrospray MS/MS to detect GSH conjugates that form positive and/or negative ions. The method was used to study the bioactivation of a licorice extract from *Glycyrrhiza glabra*, which was found to form multiple GSH conjugates, including previously reported GSH conjugates with the chalcone isoliquiritigenin[189] as well as new conjugates with the isoflavan glabridin.

Glabridin is known to inactivate CYP3A4 and CYP2B6 in a time-dependent manner,[109] although no reactive metabolites have yet been reported. The immediate next step is to further research on the GSH conjugates formed with licorice extract and structural determination of GHS conjugates would help understand the formation of glabridin reactive metabolites. Other licorice species such as *Glycyrrhiza uralensis* and

Glycyrrhiza inflata should be screened next with this validated method to evaluate the risk of reactive metabolite formation.

5.2 Drug-Licorice Interactions

Licorice extract from *Glycyrrhiza glabra* has been found to inhibit CYP3A4, and in the same study glabridin was reported to inactivate CYP3A4 and CYP2B6 in a time- and concentration-dependent manner and to competitively inhibit CYP2C9.[109]

A rapid, selective, and sensitive assay using UHPLC-MS/MS was developed and used to monitor the appearance of marker metabolites of probe substrates of multiple CYP450 enzymes and to enhance the throughput of conventional drug-drug and drug-botanical inhibition assays. This was an updated assay based on HPLC-MS/MS that was developed and validated previously.[204] The licorice extracts showed significant inhibition of CYP2B6, CYP2C8, CYP2C9, CYP2C19, and CYP3A4 when the extract concentration was increased from 1 µg/mL to 20 µg/mL. Significant inhibition of CYP2C8, CYP2C9 and CYP2C19 was observed, while CYP2B6 and CYP3A4 were moderately inhibited. CYP2C9 was inhibited the most with IC_{50} values of 0.6 µg/mL for licorice extract and 2.2 µM for glabridin. The low IC_{50} value of CYP2C9 inhibition prompted us to search for highly potent inhibitor(s) in the licorice extract other than glabridin.

As a systematic approach to identify these CYP2C9 inhibitors, 13 sub-fractions of the crude licorice extract were tested in a one-point inhibition assay as. Fraction 7 and fraction 11 that showed significant inhibition were selected for further compound isolation and characterization. Diligent database searching and dereplication of known licorice compounds were used to determine possible chemical structures of the most potent inhibitors of CYP2C9. Due to lack of standards for these licorice compounds, the proposed chemical structures could not be identified at this time.

The same 13 sub-fractions were screened using a single point time assay to identify fractions that contributed most to the time-dependent inhibition of CYP3A4. Fraction 3 showed the most time-dependent inhibition and was selected for further compound isolation and characterization. Four compounds (Compound 7, Compound 8, Compound 10, and Compound 14) from Fraction 3 then were tested for time-dependent inhibition of CYP3A4. The most potent time-dependent inhibition of CYP3A4 was observed with “Compound 10” which was studied for time-dependent inhibition kinetics. Unfortunately, “Compound 10” was later determined to contain 3 separate components. These current data suggest that multiple compounds in licorice might contribute to the time-dependent inactivation of CYP3A4.

Future studies may be carried out to determine structures of highly potent CYP2C9 inhibitors and CYP3A4 time-dependent inhibitors when more reference standards become available.

REFERENCES

(1) U.S. Food and Drug Administration, *Dietary Supplements* http://www.fda.gov/Food/DietarySupplements Accessed Feburary 5, 2015.

(2) National Institutes of Health, *Using Dietary Supplements Wisely* http://nccih.nih.gov/health/supplements/wiseuse Accessed Feburary 1, 2015.

(3) Bailey RL, G. J., Miller PE, Thomas PR, Dwyer JT. *JAMA Intern. Med.* **2013**, *173*, 355-361.

(4) U.S. Food and Drug Administration, *Current Good Manufacturing Practices (cGMPs) for Dietary Supplements* http://www.fda.gov/Food/GuidanceRegulation/CGMP/ucm079496.htm Accessed Feburary 5, 2015.

(5) van Breemen, R. B.; Fong, H. H.; Farnsworth, N. R. *Am. J. Clin. Nutr.* **2008**, *87*, 509S-513S.

(6) The Washington Post, *GNC, Target, Wal-Mart, Walgreens accused of selling adulterated 'herbals'* http://www.washingtonpost.com/news/morning-mix/wp/2015/02/03/gnc-target-wal-mart-walgreens-accused-of-selling-fake-herbals Accessed Feburary 7, 2015.

(7) Little, D. P. *Genome* **2014**, *57*, 513-516.

(8) Heubl, G. *Planta Med.* **2010**, *76*, 1963-1974.

(9) Chadwick, L. R.; Pauli, G. F.; Farnsworth, N. R. *Phytomedicine* **2006**, *13*, 119-131.

(10) Guo, J.; Nikolic, D.; Chadwick, L. R.; Pauli, G. F.; van Breemen, R. B. *Drug Metab Dispos.* **2006**, *34*, 1152-1159.

(11) Gödecke, T.; Nikolic, D.; Lankin, David C.; Chen, S.-N.; Powell, Sharla L.; Dietz, B.; Bolton, Judy L.; van Breemen, Richard B.; Farnsworth, Norman R.; Pauli, Guido F. *Phytochem. Anal.* **2009**, *20*, 120-133.

(12) Choi, Y.; Jermihov, K.; Nam, S.-J.; Sturdy, M.; Maloney, K.; Qiu, X.; Chadwick, L. R.; Main, M.; Chen, S.-N.; Mesecar, A. D.; Farnsworth, N. R.; Pauli, G. F.; Fenical, W.; Pezzuto, J. M.; van Breemen, R. B. *Anal. Chem.* **2010**, *83*, 1048-1052.

(13) Dong, S.-H.; Nikolić, D.; Simmler, C.; Qiu, F.; van Breemen, R. B.; Soejarto, D. D.; Pauli, G. F.; Chen, S.-N. *J. Nat. Prod.* **2012**, *75*, 2168-2177.

(14) Nikolić, D.; van Breemen, R. B. *Curr. Anal. Chem.* **2013**, *9*, 71-85.

(15) Simmler, C.; Pauli, G. F.; Chen, S.-N. *Fitoterapia* **2013**, *90*, 160-184.

(16) Yuan, Y.; Qiu, X.; Nikolić, D.; Chen, S.-N.; Huang, K.; Li, G.; Pauli, G. F.; van Breemen, R. B. *Eur. J. Pharm. Sci.* **2014**, *53*, 55-61.

(17) Kondo, K.; Shiba, M.; Nakamura, R.; Morota, T.; Shoyama, Y. *Biol. Pharm. Bull.* **2007**, *30*, 1271-1277.

(18) Obolentseva, G. V.; Litvinenko, V. I.; Ammosov, A. S.; Popova, T. P.; Sampiev, A. M. *Pharm. Chem. J.* **1999**, *33*, 427-434.

(19) Tamir, S.; Eizenberg, M.; Somjen, D.; Izrael, S.; Vaya, J. *J. Steroid Biochem. Mol. Biol.* **2001**, *78*, 291-298.

(20) Fukai, T.; Marumo, A.; Kaitou, K.; Kanda, T.; Terada, S.; Nomura, T. *Life Sci.* **2002**, *71*, 1449-1463.

(21) Asl, M. N.; Hosseinzadeh, H. *Phytother. Res.* **2008**, *22*, 709-724.

(22) Isbrucker, R. A.; Burdock, G. A. *Regul. Toxicol. Pharmacol.* **2006**, *46*, 167-192.

(23) Rossum, T. G. J.; Vulto, A. G.; Hop, W. C. J.; Schalm, S. W. *Am. J. Gastroenterol.* **2001**, *96*, 2432-2437.

(24) Calò, L. A.; Zaghetto, F.; Pagnin, E.; Davis, P. A.; Mozzi, P. d.; Sartorato, P.; Martire, G.; Fiore, C.; Armanini, D. *J Clin Endocrinol Metab.* **2004**, *89*, 1973-1976.

(25) Omar, H. R.; Komarova, I.; El-Ghonemi, M.; Fathy, A.; Rashad, R.; Abdelmalak, H. D.; Yerramadha, M. R.; Ali, Y.; Helal, E.; Camporesi, E. M. *Ther. Adv. Endocrinol. Metab.* **2012**, *3*, 125-138.

(26) Chandler, R. *Can. Pharm. J.* **1985**, *118*, 420-424.

(27) Fiore, C.; Eisenhut, M.; Ragazzi, E.; Zanchin, G.; Armanini, D. *J. Ethnopharmacol.* **2005**, *99*, 317-324.

(28) *Glycyrrhiza glabra* Monograph **2005** *Altern. Med. Rev. 10*, 230-237.

(29) Murphy, S. C.; Agger, S.; Rainey, P. M. *Clin. Chem.* **2009**, *55*, 2093-2096.

(30) Vaya, J.; Belinky, P. A.; Aviram, M. *Free Radic. Biol. Med.* **1997**, *23*, 302-313.

(31) Hayashi, H.; Hattori, S.; Inoue, K.; Khodzhimatov, O.; Ashurmetov, O.; Ito, M.; Honda, G. *Chem. Pharm. Bull. (Tokyo)* **2003**, *51*, 1338-1340.

(32) Pompei, R.; Flore, O.; Marccialis, M. A.; Pani, A.; Loddo, B. *Nature* **1979**, *281*, 689-690.

(33) Partridge, M.; Poswillo, D. E. *Br. J. Oral Maxillofac. Surg.* **1984**, *22*, 138-144.

(34) Baba, M.; Shigeta, S. *Antiviral Res.* **1987**, *7*, 99-107.

(35) Ito, M.; Sato, A.; Hirabayashi, K.; Tanabe, F.; Shigeta, S.; Baba, M.; De Clercq, E.; Nakashima, H.; Yamamoto, N. *Antiviral Res.* **1988**, *10*, 289-298.

(36) Hattori, T.; Ikematsu, S.; Koito, A.; Matsushita, S.; Maeda, Y.; Hada, M.; Fujimaki, M.; Takatsuki, K. *Antiviral Res.* **1989**, *11*, 255-261.

(37) Crance, J. M.; Biziagos, E.; Passagot, J.; van Cuyck-Gandré, H.; Deloince, R. *J. Med. Virol.* **1990**, *31*, 155-160.

(38) Numazaki, K. E. I.; Umetsu, M.; Chiba, S. *Tohoku J. Exp. Med.* **1994**, *172*, 147-153.

(39) Rossum, T. G. V.; Vulto, A. G.; Hop, W. C.; Brouwer, J. T.; Niesters, H. G.; Schalm, S. W. *J. Gastroenterol. Hepatol.* **1999**, *14*, 1093-1099.

(40) Nishino, H.; Kitagawa, K.; Iwashima, A. *Carcinogenesis* **1984**, *5*, 1529-1530.

(41) Liu, W.; Kato, M.; Akhand, A. A.; Hayakawa, A.; Takemura, M.; Yoshida, S.; Suzuki, H.; Nakashima, I. *Int. J. Oncol.* **1998**, *12*, 1321-1326.

(42) Shiota, G.; Harada, K.-i.; Ishida, M.; Tomie, Y.; Okubo, M.; Katayama, S.; Ito, H.; Kawasaki, H. *Carcinogenesis* **1999**, *20*, 59-63.

(43) Tamir, S.; Eizenberg, M.; Somjen, D.; Stern, N.; Shelach, R.; Kaye, A.; Vaya, J. *Cancer Res.* **2000**, *60*, 5704-5709.

(44) Armanini, D.; Karbowiak, I.; Funder, J. W. *Clin. Endocrinol. (Oxf.)* **1983**, *19*, 609-612.

(45) Akamatsu, H.; Komura, J.; Asada, Y.; Niwa, Y. *Planta Med.* **1991**, *57*, 119-121.

(46) Hajirahimkhan, A.; Simmler, C.; Yuan, Y.; Anderson, J. R.; Chen, S.-N.; Nikolić, D.; Dietz, B. M.; Pauli, G. F.; van Breemen, R. B.; Bolton, J. L. *PLoS One* **2013**, *8*, e67947.

(47) Mersereau, J. E.; Levy, N.; Staub, R. E.; Baggett, S.; Zogric, T.; Chow, S.; Ricke, W. A.; Tagliaferri, M.; Cohen, I.; Bjeldanes, L. F.; Leitman, D. C. *Mol. Cell. Endocrinol.* **2008**, *283*, 49-57.

(48) Fujisawa, Y.; Sakamoto, M.; Matsushita, M.; Fujita, T.; Nishioka, K. *Microbiol. Immunol.* **2000**, *44*, 799-804.

(49) Shibata, S. *J. Pharm. Soc. Jpn.* **2000**, *120*, 849-862.

(50) Visavadiya, N. P.; Narasimhacharya, A. V. R. L. *Mol. Nutr. Food Res.* **2006**, *50*, 1080-1086.

(51) Shin, Y.-W.; Bae, E.-A.; Lee, B.; Lee, S. H.; Kim, J. A.; Kim, Y.-S.; Kim, D.-H. *Planta Med.* **2007**, *73*, 257,261.

(52) Somjen, D.; Katzburg, S.; Vaya, J.; Kaye, A. M.; Hendel, D.; Posner, G. H.; Tamir, S. *J. Steroid Biochem. Mol. Biol.* **2004**, *91*, 241-246.

(53) Somjen, D.; Knoll, E.; Vaya, J.; Stern, N.; Tamir, S. *J. Steroid Biochem. Mol. Biol.* **2004**, *91*, 147-155.

(54) Yamamura, Y.; Kawakami, J.; Santa, T.; Kotaki, H.; Uchino, K.; Sawada, Y.; Tanaka, N.; Iga, T. *J. Pharm. Sci.* **1992**, *81*, 1042-1046.

(55) Haraguchi, H.; Yoshida, N.; Ishikawa, H.; Tamura, Y.; Mizutani, K.; Kinoshita, T. *J. Pharm. Pharmacol.* **2000**, *52*, 219-223.

(56) Rosenblat, M.; Belinky, P.; Vaya, J.; Levy, R.; Hayek, T.; Coleman, R.; Merchav, S.; Aviram, M. *J. Biol. Chem.* **1999**, *274*, 13790-13799.

(57) Ofir, R.; Tamir, S.; Khatib, S.; Vaya, J. *J. Mol. Neurosci.* **2003**, *20*, 135-140.

(58) Veratti, E.; Rossi, T.; Giudice, S.; Benassi, L.; Bertazzoni, G.; Morini, D.; Azzoni, P.; Bruni, E.; Giannetti, A.; Magnoni, C. *Anticancer Res.* **2011**, *31*, 2209-2215.

(59) Chandrasekaran, C. V.; Deepak, H. B.; Thiyagarajan, P.; Kathiresan, S.; Sangli, G. K.; Deepak, M.; Agarwal, A. *Phytomedicine* **2011**, *18*, 278-284.

(60) Cui, Y.-M.; Ao, M.-Z.; Li, W.; Yu, L.-J. *Planta Med.* **2008**, *74*, 377-380.

(61) Ahn, J.; Lee, H.; Jang, J.; Kim, S.; Ha, T. *Food Chem. Toxicol.* **2013**, *51*, 439-445.

(62) Yengi, L.; Leung, L.; Kao, J. *Pharm. Res.* **2007**, *24*, 842-858.

(63) Arrowsmith, J.; Miller, P. *Nat. Rev. Drug Discov.* **2013**, *12*, 569-569.

(64) Chovan, L. E.; Black-Schaefer, C.; Dandliker, P. J.; Lau, Y. Y. *Rapid Commun. Mass Spectrom.* **2004**, *18*, 3105-3112.

(65) Pang, K. S.; Rowland, M. *J. Pharmacokinet. Biopharm.* **1977**, *5*, 625-653.

(66) Obach, R. S. *Drug Metab Dispos.* **1999**, *27*, 1350-1359.

(67) Detampel, P.; Beck, M.; Krähenbühl, S.; Huwyler, J. *Drug Metab. Rev.* **2012**, *44*, 253-265.

(68) Guengerich, F. P. *Chem. Res. Toxicol.* **2001**, *14*, 611-650.

(69) Ioannides, C.; V. Lewis, D. F. *Curr. Top. Med. Chem.* **2004**, *4*, 1767-1788.

(70) Rendic, S.; Carlo, F. J. D. *Drug Metab. Rev.* **1997**, *29*, 413-580.

(71) Wilkinson, G. R. *N. Engl. J. Med.* **2005**, *352*, 2211-2221.

(72) Cashman, J. R. *Chem. Res. Toxicol.* **1995**, *8*, 165-181.

(73) Tipton, K. F.; Boyce, S.; O'Sullivan, J.; Davey, G. P.; Healy, J. *Curr. Med. Chem.* **2004**, *11*, 1965-1982.

(74) Tukey, R. H.; Strassburg, C. P. *Annu. Rev. Pharmacol. Toxicol.* **2000**, *40*, 581-616.

(75) Negishi, M.; Pedersen, L. G.; Petrotchenko, E.; Shevtsov, S.; Gorokhov, A.; Kakuta, Y.; Pedersen, L. C. *Arch. Biochem. Biophys.* **2001**, *390*, 149-157.

(76) Hayes, J. D.; Flanagan, J. U.; Jowsey, I. R. *Annu. Rev. Pharmacol. Toxicol.* **2005**, *45*, 51-88.

(77) Guillouzo, A.; Morel, F.; Fardel, O.; Meunier, B. *Toxicology* **1993**, *82*, 209-219.

(78) Stringer, R. A.; Strain-Damerell, C.; Nicklin, P.; Houston, J. B. *Drug Metab Dispos.* **2009**, *37*, 1025-1034.

(79) Kalgutkar, A. S.; Dalvie, D. K.; Donnell, J. P.; Taylor, T. J.; Sahakian, D. C. *Curr. Drug Metab.* **2002**, *3*, 379-424.

(80) Evans, D. C.; Watt, A. P.; Nicoll-Griffith, D. A.; Baillie, T. A. *Chem. Res. Toxicol.* **2003**, *17*, 3-16.

(81) Walgren, J. L.; Mitchell, M. D.; Thompson, D. C. *Crit. Rev. Toxicol.* **2005**, *35*, 325-361.

(82) Zhou, S.; Chan, E.; Duan, W.; Huang, M.; Chen, Y.-Z. *Drug Metab. Rev.* **2005**, *37*, 41-213.

(83) Yang, C. S.; Brady, J. F.; Hong, J. Y. *FASEB J.* **1992**, *6*, 737-744.

(84) Zhou, S.; Koh, H. L.; Gao, Y.; Gong, Z. Y.; Lee, E. J. *Life Sci.* **2004**, *74*, 935-968.

(85) Hattori, M.; Sakamoto, T.; Yamagishi, T.; Sakamoto, K.; Konishi, K.; Kobashi, K.; Namba, T. *Chem. Pharm. Bull. (Tokyo)* **1985**, *33*, 210-217.

(86) Kim, D.-H.; Hong, S.-W.; Kim, B.-T.; Bae, E.-A.; Park, H.-Y.; Han, M. J. *Arch. Pharm. Res.* **2000**, *23*, 172-177.

(87) Zhao, K.; Ding, M.; Cao, H.; Cao, Z.-x. *J. Pharm. Pharmacol.* **2012**, *64*, 1445-1451.

(88) Guo, J.; Liu, D.; Nikolic, D.; Zhu, D.; Pezzuto, J. M.; van Breemen, R. B. *Drug Metab Dispos.* **2008**, *36*, 461-468.

(89) Wang, Q.; Qian, Y.; Wang, Q.; Yang, Y.-f.; Ji, S.; Song, W.; Qiao, X.; Guo, D.-a.; Liang, H.; Ye, M. *J. Pharm. Biomed. Anal.* **2015**, *115*, 515-522.

(90) Wang, Q.; Qiao, X.; Liu, C.-f.; Ji, S.; Feng, L.-m.; Qian, Y.; Guo, D.-a.; Ye, M. *J. Pharm. Biomed. Anal.* **2014**, *98*, 287-295.

(91) Wang, Q.; Qiao, X.; Qian, Y.; Liu, C.-f.; Yang, Y.-f.; Ji, S.; Li, J.; Guo, D.-a.; Ye, M. *J. Chromatogr. B* **2015**, *983–984*, 39-46.

(92) Bailey, D. G.; Malcolm, J.; Arnold, O.; David Spence, J. *Br. J. Clin. Pharmacol.* **1998**, *46*, 101-110.

(93) Wenk, M.; Todesco, L.; Krähenbühl, S. *Br. J. Clin. Pharmacol.* **2004**, *57*, 495-499.

(94) Wienkers, L. C.; Heath, T. G. *Nat. Rev. Drug Discov.* **2005**, *4*, 825-833.

(95) Meier, P. J.; Eckhardt, U.; Schroeder, A.; Hagenbuch, B.; Stieger, B. *Hepatology* **1997**, *26*, 1667-1677.

(96) Inui, K.-I.; Masuda, S.; Saito, H. *Kidney Int.* **2000**, *58*, 944-958.

(97) Kusuhara, H.; Sugiyama, Y. *NeuroRx* **2005**, *2*, 73-85.

(98) The International Transporter, C. *Nat. Rev. Drug Discov.* **2010**, *9*, 215-236.

(99) U.S. Food and Drug Administration, *Guidance for Industry: Drug Interaction Studies-Study Design, Data Analysis, Implications for Dosing, and Labeling Recommendations* http://www.fda.gov/downloads/Drugs/GuidanceComplianceRegulatoryInformation/Guidances/UCM292362.pdf Accessed December 9, 2013.

(100) Zhou, S.; Gao, Y.; Jiang, W.; Huang, M.; Xu, A.; Paxton, J. W. *Drug Metab. Rev.* **2003**, *35*, 35-98.

(101) Lin, J.; Lu, A. H. *Clin. Pharmacokinet.* **1998**, *35*, 361-390.

(102) Dresser, G.; Spence, J. D.; Bailey, D. *Clin. Pharmacokinet.* **2000**, *38*, 41-57.

(103) Gurley, B. J.; Gardner, S. F.; Hubbard, M. A.; Williams, D. K.; Gentry, W. B.; Cui, Y.; Ang, C. Y. W. *Drugs Aging* **2005**, *22*, 525-539.

(104) Gurley, B. J.; Gardner, S. F.; Hubbard, M. A.; Williams, D. K.; Gentry, W. B.; Cui, Y.; Ang, C. Y. W. *Clin. Pharmacol. Ther.* **2002**, *72*, 276-287.

(105) Wang, Z.; Gorski, J. C.; Hamman, M. A.; Huang, S.-M.; Lesko, L. J.; Hall, S. D. *Clin. Pharmacol. Ther.* **2001**, *70*, 317-326.

(106) Gurley, B. J.; Swain, A.; Williams, D. K.; Barone, G.; Battu, S. K. *Mol. Nutr. Food Res.* **2008**, *52*, 772-779.

(107) Xie, R.; Tan, L. H.; Polasek, E. C.; Hong, C.; Teillol-Foo, M.; Gordi, T.; Sharma, A.; Nickens, D. J.; Arakawa, T.; Knuth, D. W.; Antal, E. J. *J. Clin. Pharmacol.* **2005**, *45*, 352-356.

(108) Schwarz, U. I.; Hanso, H.; Oertel, R.; Miehlke, S.; Kuhlisch, E.; Glaeser, H.; Hitzl, M.; Dresser, G. K.; Kim, R. B.; Kirch, W. *Clin. Pharmacol. Ther.* **2007**, *81*, 669-678.

(109) Kent, U. M.; Aviram, M.; Rosenblat, M.; Hollenberg, P. F. *Drug Metab Dispos.* **2002**, *30*, 709-715.

(110) Pandit, S.; Ponnusankar, S.; Bandyopadhyay, A.; Ota, S.; Mukherjee, P. K. *Phytother. Res.* **2011**, *25*, 1429-1434.

(111) Tsukamoto, S.; Aburatani, M.; Yoshida, T.; Yamashita, Y.; El-beih, A. A.; Ohta, T. *Biol. Pharm. Bull.* **2005**, *28*, 2000-2002.

(112) Li, H. Y.; Xu, W.; Su, J.; Zhang, X.; Hu, L. W.; Zhang, W. D. *Pharmacology* **2010**, *86*, 287-292.

(113) He, W.; Wu, J.-J.; Ning, J.; Hou, J.; Xin, H.; He, Y.-Q.; Ge, G.-B.; Xu, W. *Toxicol. In Vitro* **2015**, *29*, 1569-1576.

(114) Kim, S. J.; Kim, S. J.; Hong, M.; Choi, H. G.; Kim, J. A.; Lee, S. *Xenobiotica* **2016**, *46*, 857-861.

(115) Qiao, X.; Ji, S.; Yu, S.-w.; Lin, X.-h.; Jin, H.-w.; Duan, Y.-k.; Zhang, L.-r.; Guo, D.-a.; Ye, M. *AAPS J.* **2014**, *16*, 101-113.

(116) Belinky, P. A.; Aviram, M.; Mahmood, S.; Vaya, J. *Free Radic. Biol. Med.* **1998**, *24*, 1419-1429.

(117) Wu, N.; Clausen, A. M. *J. Sep. Sci.* **2007**, *30*, 1167-1182.

(118) McLuckey, S. A.; Wells, J. M. *Chem. Rev.* **2001**, *101*, 571-606.

(119) John, P. S.; Mutlib, A. E. In *Drug Metabolizing Enzymes*; Informa Healthcare, 2003, pp 33-86.

(120) Peterman, S.; Duczak, N.; Kalgutkar, A.; Lame, M.; Soglia, J. *J. Am. Soc. Mass Spectrom.* **2006**, *17*, 363-375.

(121) Ramanathan, R.; McKenzie, D. L.; Tugnait, M.; Siebenaler, K. *J. Pharm. Biomed. Anal.* **2002**, *28*, 945-951.

(122) Zhu, M.; Ma, L.; Zhang, D.; Ray, K.; Zhao, W.; Humphreys, W. G.; Skiles, G.; Sanders, M.; Zhang, H. *Drug Metab Dispos.* **2006**, *34*, 1722-1733.

(123) Hopfgartner, G.; Husser, C.; Zell, M. *J. Mass Spectrom.* **2003**, *38*, 138-150.

(124) Levsen, K.; Schiebel, H.-M.; Behnke, B.; Dötzer, R.; Dreher, W.; Elend, M.; Thiele, H. *J. Chromatogr. A* **2005**, *1067*, 55-72.

(125) Mitchell, J. R.; Jollow, D. J.; Potter, W. Z.; Gillette, J. R.; Brodie, B. B. *J. Pharmacol. Exp. Ther.* **1973**, *187*, 211-217.

(126) Ma, S.; Zhu, M. *Chem. Biol. Interact.* **2009**, *179*, 25-37.

(127) Nikolic, D.; Fan, P. W.; Bolton, J. L.; van Breemen, R. B. *Comb. Chem. High T. Scr.* **1999**, *2*, 165-175.

(128) Kalgutkar, A. S.; Soglia, J. R. *Expert Opin. Drug Metab. Toxicol.* **2005**, *1*, 91-142.

(129) Haroldsen, P. E.; Reilly, M. H.; Hughes, H.; Gaskell, S. J.; Porter, C. J. *Biol. Mass Spectrom.* **1988**, *15*, 615-621.

(130) Murphy, C. M.; Fenselau, C.; Gutierrez, P. L. *J. Am. Soc. Mass Spectrom.* **1992**, *3*, 815-822.

(131) Youdim, K. A.; Lyons, R.; Payne, L.; Jones, B. C.; Saunders, K. *J. Pharm. Biomed. Anal.* **2008**, *48*, 92-99.

(132) Kozakai, K.; Yamada, Y.; Oshikata, M.; Kawase, T.; Suzuki, E.; Haramaki, Y.; Taniguchi, H. *Drug Metab. Pharmacokinet.* **2012**, *27*, 520-529.

(133) Dinger, J.; Meyer, M.; Maurer, H. *Anal. Bioanal. Chem.* **2014**, *406*, 4453-4464.

(134) Qin, C.-Z.; Ren, X.; Tan, Z.-R.; Chen, Y.; Yin, J.-Y.; Yu, J.; Qu, J.; Zhou, H.-H.; Liu, Z.-Q. *Biomed. Chromatogr.* **2014**, *28*, 197-203.

(135) Liu, L.-Y.; Han, Y.-L.; Zhu, J.-H.; Yu, Q.; Yang, Q.-J.; Lu, J.; Guo, C. *Biomed. Chromatogr.* **2015**, *29*, 437-444.

(136) Yu, C.; Shin, Y.; Chow, A.; Li, Y.; Kosmeder, J.; Lee, Y.; Hirschelman, W.; Pezzuto, J.; Mehta, R.; van Breemen, R. *Pharm. Res.* **2002**, *19*, 1907-1914.

(137) Zhang, D.; Luo, G.; Ding, X.; Lu, C. *Acta Pharmaceutica Sinica B* **2012**, *2*, 549-561.

(138) Simmler, C.; Pauli, G. F.; Chen, S.-N. *Fitoterapia* **2013**, *90*, 160-184.

(139) Xu, L.; Klunk, L. J.; Prakash, C. In *Mass Spectrometry in Drug Metabolism and Disposition*; John Wiley & Sons, Inc., 2011, pp 291-319.

(140) Anari, M. R.; Baillie, T. A. *Drug Discov. Today* **2005**, *10*, 711-717.

(141) Iwatsubo, T.; Hirota, N.; Ooie, T.; Suzuki, H.; Shimada, N.; Chiba, K.; Ishizaki, T.; Green, C. E.; Tyson, C. A.; Sugiyama, Y. *Pharmacol. Ther.* **1997**, *73*, 147-171.

(142) Lu, C.; Li, P.; Gallegos, R.; Uttamsingh, V.; Xia, C. Q.; Miwa, G. T.; Balani, S. K.; Gan, L.-S. *Drug Metab Dispos.* **2006**, *34*, 1600-1605.

(143) Aoki, F.; Nakagawa, K.; Kitano, M.; Ikematsu, H.; Nakamura, K.; Yokota, S.; Tominaga, Y.; Arai, N.; Mae, T. *J. Am. Coll. Nutr.* **2007**, *26*, 209-218.

(144) Aoki, F.; Nakagawa, K.; Tanaka, A.; Matsuzaki, K.; Arai, N.; Mae, T. *J. Chromatogr. B* **2005**, *828*, 70-74.

(145) Cheel, J.; Tůmová, L.; Areche, C.; Van Antwerpen, P.; Nève, J.; Zouaoui-Boudjeltia, K.; San Martin, A.; Vokřál, I.; Wsól, V.; Neugebauerová, J. *Acta Physiologiae Plantarum* **2013**, *35*, 1337-1349.

(146) Li, G.; Nikolic, D.; van Breemen, R. B. *J. Agric. Food Chem.* **2016**, *64*, 8062-8070.

(147) Rodriguez, E. B.; Rodriguez-Amaya, D. B. *J. Food Sci.* **2009**, *74*, C674-C682.

(148) Marquissolo, C.; Fátima, Â. d.; Kohn, L. K.; Ruiz, A. L. T. G.; Carvalho, J. E. d.; Pilli, R. A. *Bioorg. Chem.* **2009**, *37*, 52-56.

(149) Robinson, A.; Aggarwal, V. K. *Org Biomol Chem.* **2012**, *10*, 1795-1801.

(150) Muñoz, J.; Garcia-Molina, F.; Varon, R.; Rodriguez-Lopez, J. N.; García-Ruiz, P. A.; García-Cánovas, F.; Tudela, J. *J. Agric. Food Chem.* **2007**, *55*, 920-928.

(151) Rodionov, P. V.; Veselova, I. A.; Shekhovtsova, T. N. *Anal. Bioanal. Chem.* **2014**, *406*, 1531-1540.

(152) Tung, E. W. Y.; Philbrook, N. A.; Belanger, C. L.; Ansari, S.; Winn, L. M. *Mutat Res Genet Toxicol Environ Mutagen.* **2014**, *760*, 64-69.

(153) Einaudi, L.; Courbiere, B.; Tassistro, V.; Prevot, C.; Sari-Minodier, I.; Orsiere, T.; Perrin, J. *Hum. Reprod.* **2014**, *29*, 548-554.

(154) Boysen, G.; Hecht, S. S. *Mutat. Res.* **2003**, *543*, 17-30.

(155) Müller, C. S.; Knehans, T.; Davydov, D. R.; Bounds, P. L.; von Mandach, U.; Halpert, J. R.; Caflisch, A.; Koppenol, W. H. *Biochemistry* **2015**, *54*, 711-721.

(156) Kerr, B. M.; Thummel, K. E.; Wurden, C. J.; Klein, S. M.; Kroetz, D. L.; Gonzalez, F. J.; Levy, R. *Biochem. Pharmacol.* **1994**, *47*, 1969-1979.

(157) Nakamura, H.; Nakasa, H.; Ishii, I.; Ariyoshi, N.; Igarashi, T.; Ohmori, S.; Kitada, M. *Drug Metab Dispos.* **2002**, *30*, 534-540.

(158) Snider, N. T.; Kornilov, A. M.; Kent, U. M.; Hollenberg, P. F. *J. Pharmacol. Exp. Ther.* **2007**, *321*, 590-597.

(159) Barbosa-Sicard, E.; Markovic, M.; Honeck, H.; Christ, B.; Muller, D. N.; Schunck, W.-H. *Biochem. Biophys. Res. Commun.* **2005**, *329*, 1275-1281.

(160) Obach, R. S. *Drug Metab Dispos.* **2001**, *29*, 1057-1067.

(161) Piver, B.; Fer, M.; Vitrac, X.; Merillon, J.-M.; Dreano, Y.; Berthou, F.; Lucas, D. *Biochem. Pharmacol.* **2004**, *68*, 773-782.

(162) Yilmazer, M.; Stevens, J. F.; Deinzer, M. L.; Buhler, D. R. *Drug Metab Dispos.* **2001**, *29*, 223-231.

(163) Fujino, T.; Park, S. S.; West, D.; Gelboin, H. V. *Proc. Natl. Acad. Sci. U. S. A.* **1982**, *79*, 3682-3686.

(164) Gelboin, H. V.; Krausz, K. *J. Clin. Pharmacol.* **2006**, *46*, 353-372.

(165) Gelboin, H. V.; Krausz, K. W.; Gonzalez, F. J.; Yang, T. J. *Trends Pharmacol. Sci.*, *20*, 432-438.

(166) Khojasteh, S.; Prabhu, S.; Kenny, J.; Halladay, J.; Lu, A. H. *Eur. J. Drug Metab. Pharmacokinet.* **2011**, *36*, 1-16.

(167) Brandon, E. F. A.; Raap, C. D.; Meijerman, I.; Beijnen, J. H.; Schellens, J. H. M. *Toxicol. Appl. Pharmacol.* **2003**, *189*, 233-246.

(168) Emoto, C.; Murayama, N.; Rostami-Hodjegan, A.; Yamazaki, H. *Curr. Drug Metab.* **2010**, *11*, 678-685.

(169) Zhang, H.; Davis, C. D.; Sinz, M. W.; Rodrigues, A. D. *Expert Opin. Drug Metab. Toxicol.* **2007**, *3*, 667-687.

(170) Rodrigues, A. *Biochem. Pharmacol.* **1999**, *57*, 465-480.

(171) Sohl, C. D.; Isin, E. M.; Eoff, R. L.; Marsch, G. A.; Stec, D. F.; Guengerich, F. P. *J. Biol. Chem.* **2008**, *283*, 7293-7308.

(172) Lanza, D. L.; Yost, G. S. *Drug Metab Dispos.* **2001**, *29*, 950-953.

(173) Draper, A. J.; Hammock, B. D. *Arch. Biochem. Biophys.* **2000**, *376*, 199-205.

(174) Prueksaritanont, T.; Gorham, L. M.; Ma, B.; Liu, L.; Yu, X.; Zhao, J. J.; Slaughter, D. E.; Arison, B. H.; Vyas, K. P. *Drug Metab Dispos.* **1997**, *25*, 1191-1199.

(175) Ma, S.; Subramanian, R. *J. Mass Spectrom.* **2006**, *41*, 1121-1139.

(176) Baillie, T. A.; Davis, M. R. *Biol. Mass Spectrom.* **1993**, *22*, 319-325.

(177) Dieckhaus, C. M.; Fernández-Metzler, C. L.; King, R.; Krolikowski, P. H.; Baillie, T. A. *Chem. Res. Toxicol.* **2005**, *18*, 630-638.

(178) Yan, Z.; Caldwell, G. W. *Anal. Chem.* **2004**, *76*, 6835-6847.

(179) Wen, B.; Ma, L.; Nelson, S. D.; Zhu, M. *Anal. Chem.* **2008**, *80*, 1788-1799.

(180) Zhu, M.; Ma, L.; Zhang, H.; Humphreys, W. G. *Anal. Chem.* **2007**, *79*, 8333-8341.

(181) Ruan, Q.; Zhu, M. *Chem. Res. Toxicol.* **2010**, *23*, 909-917.

(182) Yan, Z.; Zhong, H. M.; Maher, N.; Torres, R.; Leo, G. C.; Caldwell, G. W.; Huebert, N. *Drug Metab Dispos.* **2005**, *33*, 1867-1876.

(183) Tang, W.; Stearns, R. A.; Bandiera, S. M.; Zhang, Y.; Raab, C.; Braun, M. P.; Dean, D. C.; Pang, J.; Leung, K. H.; Doss, G. A.; Strauss, J. R.; Kwei, G. Y.; Rushmore, T. H.; Chiu, S.-H. L.; Baillie, T. A. *Drug Metab Dispos.* **1999**, *27*, 365-372.

(184) Zhu, X.; Kalyanaraman, N.; Subramanian, R. *Anal. Chem.* **2011**, *83*, 9516-9523.

(185) Li, A. P.; Hartman, N. R.; Lu, C.; Collins, J. M.; Strong, J. M. *Br. J. Clin. Pharmacol.* **1999**, *48*, 733-742.

(186) Johnson, B. M.; van Breemen, R. B. *Chem. Res. Toxicol.* **2003**, *16*, 838-846.

(187) Johnson, B. M.; Bolton, J. L.; van Breemen, R. B. *Chem. Res. Toxicol.* **2001**, *14*, 1546-1551.

(188) Johnson, B. M.; Qiu, S. X.; Zhang, S.; Zhang, F.; Burdette, J. E.; Yu, L.; Bolton, J. L.; van Breemen, R. B. *Chem. Res. Toxicol.* **2003**, *16*, 733-740.

(189) Cuendet, M.; Guo, J.; Luo, Y.; Chen, S.; Oteham, C. P.; Moon, R. C.; van Breemen, R. B.; Marler, L. E.; Pezzuto, J. M. *Cancer. Prev. Res.* **2010**, *3*, 221-232.

(190) Kaufman, D. W.; Kelly, J. P.; Rosenberg, L.; Anderson, T. E.; Mitchell, A. A. *J. Am. Med. Assoc.* **2002**, *287*, 337-344.

(191) Huang, S.-M.; Lesko, L. J. *J. Clin. Pharmacol.* **2004**, *44*, 559-569.

(192) Neary, J. T.; Bu, Y. *Brain Res.* **1999**, *816*, 358-363.

(193) Teyssier, C.; Guenot, L.; Suschetet, M.; Siess, M.-H. *Drug Metab Dispos.* **1999**, *27*, 835-841.

(194) Tsukamoto, S.; Tomise, K.; Miyakawa, K.; Cha, B.-C.; Abe, T.; Hamada, T.; Hirota, H.; Ohta, T. *Biorg. Med. Chem.* **2002**, *10*, 2981-2985.

(195) Nguyen, T. D.; Villard, P. H.; Barlatier, A.; Elsisi, A. E.; Jouve, E.; Duc, N. M.; Sauze, C.; Durand, A.; Lacarelle, B. *Planta Med.* **2000**, *66*, 714-719.

(196) Doostdar, H.; Burke, M. D.; Mayer, R. T. *Toxicology* **2000**, *144*, 31-38.

(197) Jeong, H. G. *Toxicol. Lett.* **1999**, *105*, 215-222.

(198) Ueng, Y.-F.; Jan, W.-C.; Lin, L.-C.; Chen, T.-L.; Guengerich, F. P.; Chen, C.-F. *Drug Metab Dispos.* **2002**, *30*, 349-353.

(199) Bailey, D. G.; Dresser, G. K.; Kreeft, J. H.; Munoz, C.; Freeman, D. J.; Bend, J. R. *Clin. Pharmacol. Ther.* **2000**, *68*, 468-477.

(200) Ducharme, M. P.; Warbasse, L. H.; Edwards, D. J. *Clin. Pharmacol. Ther.* **1995**, *57*, 485-491.

(201) He, K.; Iyer, K. R.; Hayes, R. N.; Sinz, M. W.; Woolf, T. F.; Hollenberg, P. F. *Chem. Res. Toxicol.* **1998**, *11*, 252-259.

(202) Dubuisson, J. G.; Dyess, D. L.; Gaubatz, J. W. *Cancer Lett.*, *182*, 27-32.

(203) Jang, M.; Cai, L.; Udeani, G. O.; Slowing, K. V.; Thomas, C. F.; Beecher, C. W. W.; Fong, H. H. S.; Farnsworth, N. R.; Kinghorn, A. D.; Mehta, R. G.; Moon, R. C.; Pezzuto, J. M. *Science* **1997**, *275*, 218-220.

(204) Qiu, X.; Yuan, Y.; Nikolic, D.; van Breemen, R. B. *Proceedings of the 60th ASMS Conference on Mass Spectrometry and Allied Topics, Vancouver, Canada, May 20-24,* **2012**.

(205) Goodwin, B.; Moore, L. B.; Stoltz, C. M.; McKee, D. D.; Kliewer, S. A. *Mol. Pharmacol.* **2001**, *60*, 427-431.

(206) Moore, L. B.; Goodwin, B.; Jones, S. A.; Wisely, G. B.; Serabjit-Singh, C. J.; Willson, T. M.; Collins, J. L.; Kliewer, S. A. *Proc. Natl. Acad. Sci. U. S. A.* **2000**, *97*, 7500-7502.

(207) Wentworth, J.; Agostini, M.; Love, J.; Schwabe, J.; Chatterjee, V. *J. Endocrinol.* **2000**, *166*, R11-R16.

(208) Sesardic, D.; Edwards, R. J.; Davies, D. S.; Thomas, P. E.; Levin, W.; Boobis, A. R. *Biochem. Pharmacol.* **1990**, *39*, 489-498.

(209) Tassaneeyakul, W.; Birkett, D. J.; Veronese, M. E.; McManus, M. E.; Tukey, R. H.; Quattrochi, L. C.; Gelboin, H. V.; Miners, J. O. *J. Pharmacol. Exp. Ther.* **1993**, *265*, 401-407.

(210) Venkatakrishnan, K.; Moltke, L. L. V.; Greenblatt, D. J. *J. Pharm. Sci.* **1998**, *87*, 1502-1507.

(211) Lin, Y.; Lu, P.; Tang, C.; Mei, Q.; Sandig, G.; Rodrigues, A. D.; Rushmore, T. H.; Shou, M. *Drug Metab Dispos.* **2001**, *29*, 368-374.

(212) Walsky, R. L.; Obach, R. S. *Drug Metab Dispos.* **2004**, *32*, 647-660.

(213) Shimada, T.; Yamazaki, H.; Guengerich, F. P. *Xenobiotica* **1996**, *26*, 395-403.

(214) Draper, A. J.; Madan, A.; Parkinson, A. *Arch. Biochem. Biophys.* **1997**, *341*, 47-61.

(215) Bourrié, M.; Meunier, V.; Berger, Y.; Fabre, G. *J. Pharmacol. Exp. Ther.* **1996**, *277*, 321-332.

(216) Jurima, M.; Inaba, T.; Kalow, W. *Drug Metab Dispos.* **1985**, *13*, 151-155.

(217) Hall, S. D.; Guengerich, F. P.; Branch, R. A.; Wilkinson, G. R. *J. Pharmacol. Exp. Ther.* **1987**, *240*, 216-222.

(218) Chiba, K.; Kobayashi, K.; Tani, M.; Manabe, K.; Ishizaki, T. *Drug Metab Dispos.* **1993**, *21*, 747-749.

(219) Kronbach, T. In *Methods Enzymol.*; Academic Press, 1991, pp 509-517.

(220) Peter, R.; Boecker, R.; Beaune, P. H.; Iwasaki, M.; Guengerich, F. P.; Yang, C. S. *Chem. Res. Toxicol.* **1990**, *3*, 566-573.

(221) Ghosal, A.; Satoh, H.; Thomas, P. E.; Bush, E.; Moore, D. *Drug Metab Dispos.* **1996**, *24*, 940-947.

(222) Gelboin, H. V.; Krausz, K. W.; Goldfarb, I.; Buters, J. T. M.; Yang, S. K.; Gonzalez, F. J.; Korzekwa, K. R.; Shou, M. *Biochem. Pharmacol.* **1995**, *50*, 1841-1850.

(223) Mei, Q.; Tang, C.; Assang, C.; Lin, Y.; Slaughter, D.; Rodrigues, A. D.; Baillie, T. A.; Rushmore, T. H.; Shou, M. *J. Pharmacol. Exp. Ther.* **1999**, *291*, 749-759.

(224) Shou, M.; Lu, T.; Krausz, K. W.; Sai, Y.; Yang, T.; Korzekwa, K. R.; Gonzalez, F. J.; Gelboin, H. V. *Eur. J. Pharmacol.* **2000**, *394*, 199-209.

(225) White, R. E. *Annu. Rev. Pharmacol. Toxicol.* **2000**, *40*, 133-157.

(226) Simmler, C.; Hajirahimkhan, A.; Lankin, D. C.; Bolton, J. L.; Jones, T.; Soejarto, D. D.; Chen, S.-N.; Pauli, G. F. *J. Agric. Food Chem.* **2013**, *61*, 2146-2157.

(227) Jirawattanapong, W.; Saifah, E.; Patarapanich, C. *Arch. Pharm. Res.* **2009**, *32*, 647-654.

(228) Kinoshita, T.; Tamura, Y.; Mizutani, K. *Nat. Prod. Lett.* **1997**, *9*, 289-296.

(229) Simmler, C.; Hajirahimkhan, A.; Lankin, D. C.; Bolton, J. L.; Jones, T.; Soejarto, D. D.; Chen, S.-N.; Pauli, G. F. *J. Agric. Food Chem.* **2013**, *61*, 10.1021/jf304445p.

(230) Kinoshita, T.; Kajiyama, K.; Hiraga, Y.; Takahashi, K.; Tamura, Y.; Mizutani, K. *Heterocycles* **1996**, *43*, 653-664.

(231) Nikolic, D.; Li, Y.; Chadwick, L. R.; Grubjesic, S.; Schwab, P.; Metz, P.; van Breemen, R. B. *Drug Metab Dispos.* **2004**, *32*, 272-279.

(232) Nikolic, D.; Li, Y.; Chadwick, L. R.; Pauli, G. F.; van Breemen, R. B. *J. Mass Spectrom.* **2005**, *40*, 289-299.

(233) Kuroda, M.; Mimaki, Y.; Honda, S.; Tanaka, H.; Yokota, S.; Mae, T. *Biorg. Med. Chem.* **2010**, *18*, 962-970.

(234) Jia-Feng, Z.; Guo-Lin, L.; Xin, X.; Da-Yuan, Z. *Phytochemistry* **1996**, *43*, 893-896.

(235) Fukai, T.; Sheng, C.-B.; Horikoshi, T.; Nomura, T. *Phytochemistry* **1996**, *43*, 1119-1124.

(236) Kajiyana, K.; Demizu, S.; Hiraga, Y.; Kinoshita, K.; Koyama, K.; Takahashi, K.; Tamura, Y.; Okada, K.; Kinoshita, T. *J. Nat. Prod.* **1992**, *55*, 1197-1203.

(237) Mitscher, L. A.; Park, Y. H.; Clark, D.; Beal, J. L. *J. Nat. Prod.* **1980**, *43*, 259-269.

(238) Saitoh, T.; Kinoshita, T.; Shibata, S. *Chem. Pharm. Bull. (Tokyo)* **1976**, *24*, 752-755.

(239) Stevens, J. F.; Ivancic, M.; Hsu, V. L.; Deinzer, M. L. *Phytochemistry* **1997**, *44*, 1575-1585.

(240) Stevens, J. F.; Page, J. E. *Phytochemistry* **2004**, *65*, 1317-1330.

(241) Colgate, E. C.; Miranda, C. L.; Stevens, J. F.; Bray, T. M.; Ho, E. *Cancer Lett.* **2007**, *246*, 201-209.

(242) Miranda, C. L.; Stevens, J. F.; Helmrich, A.; Henderson, M. C.; Rodriguez, R. J.; Yang, Y. H.; Deinzer, M. L.; Barnes, D. W.; Buhler, D. R. *Food Chem. Toxicol.* **1999**, *37*, 271-285.

(243) Dietz, B. M.; Kang, Y.-H.; Liu, G.; Eggler, A. L.; Yao, P.; Chadwick, L. R.; Pauli, G. F.; Farnsworth, N. R.; Mesecar, A. D.; van Breemen, R. B.; Bolton, J. L. *Chem. Res. Toxicol.* **2005**, *18*, 1296-1305.

(244) Milligan, S. R.; Kalita, J. C.; Heyerick, A.; Rong, H.; De Cooman, L.; De Keukeleire, D. *J Clin Endocrinol Metab.* **1999**, *84*, 2249-2249.

(245) Schaefer, O.; Hümpel, M.; Fritzemeier, K.-H.; Bohlmann, R.; Schleuning, W.-D. *J. Steroid Biochem. Mol. Biol.* **2003**, *84*, 359-360.

(246) Overk, C. R.; Yao, P.; Chadwick, L. R.; Nikolic, D.; Sun, Y.; Cuendet, M. A.; Deng, Y.; Hedayat, A. S.; Pauli, G. F.; Farnsworth, N. R.; van Breemen, R. B.; Bolton, J. L. *J. Agric. Food Chem.* **2005**, *53*, 6246-6253.

(247) Overk, C. R.; Guo, J.; Chadwick, L. R.; Lantvit, D. D.; Minassi, A.; Appendino, G.; Chen, S.-N.; Lankin, D. C.; Farnsworth, N. R.; Pauli, G. F.; van Breemen, R. B.; Bolton, J. L. *Chem. Biol. Interact.* **2008**, *176*, 30-39.

(248) Possemiers, S.; Heyerick, A.; Robbens, V.; De Keukeleire, D.; Verstraete, W. *J. Agric. Food Chem.* **2005**, *53*, 6281-6288.

(249) Possemiers, S.; Bolca, S.; Grootaert, C.; Heyerick, A.; Decroos, K.; Dhooge, W.; De Keukeleire, D.; Rabot, S.; Verstraete, W.; Van de Wiele, T. *J. Nutr.* **2006**, *136*, 1862-1867.

(250) Chadwick, L. R.; Nikolic, D.; Burdette, J. E.; Overk, C. R.; Bolton, J. L.; van Breemen, R. B.; Fröhlich, R.; Fong, H. H. S.; Farnsworth, N. R.; Pauli, G. F. *J. Nat. Prod.* **2004**, *67*, 2024-2032.

(251) Stevens, J. F.; Taylor, A. W.; Deinzer, M. L. *J. Chromatogr. A* **1999**, *832*, 97-107.

(252) Simmler, C.; Jones, T.; Anderson, J. R.; Nikolić, D. C.; van Breemen, R. B.; Soejarto, D. D.; Chen, S.-N.; Pauli, G. F. *Phytochemical analysis : PCA* **2014**, *25*, 378-388.

(253) Simmler, C.; Nikolić, D.; Lankin, D. C.; Yu, Y.; Friesen, J. B.; van Breemen, R. B.; Lecomte, A.; Le Quémener, C.; Audo, G.; Pauli, G. F. *J. Nat. Prod.* **2014**, *77*, 1806-1816.

CURRICULUM VITAE

WORK EXPERIENCE

Bristol-Myers Squibb **Syracuse, NY**

Scientist *– Biologics Development and Operation* *2014 – Current*

- Support biologics commercial manufacturing globally, lead 3 tech transfer sub-teams to expand manufacturing network internally and externally
- Prepare and/or verify CMC sections in INDs and BLAs, address comments from health authorities, support 3 successful pre-approval inspections (PAI) from FDA
- Drive change controls and perform risk assessments to ensure material quality, performance consistency, and compliance to cGMP and regulatory requirements
- Develop platform to enable raw material trending in biologics manufacturing across network, led a sub-team to investigate performance variability and identified key root causes
- Managed a multi-site task force to characterize a critical raw material from 4 different vendors within an accelerated timeline, key contributor to commercial manufacturing process validation

Amgen **Thousand Oaks, CA**

Graduate Intern *– Product and Process Development* *Summer 2012*

- Applied quality-by-design (QbD) principles to develop robust analytical methods as risk assessment tool during API manufacturing for a Phase II schizophrenia drug
- Worked with scientific software vendor to evaluate a new software package used in process development, drafted comprehensive review to support procurement's decision-making

Abbott Laboratories (now Abbvie) **Abbott Park, IL**

Graduate Intern *– Pharmaceutics, Preformulation* *Summer 2010*

- Proposed and developed a highly selective UHPLC-MS based method for solubility assay
- Aligned existing resources and implemented an automated software package to support physicochemical evaluations, leading to tripled productivity and $40k cost saving per year
- Studied and controlled matrix effects in buffer systems via designed analytical procedures

Bristol-Myers Squibb **New Brunswick, NJ**

Graduate Intern *– Analytical R&D* *Summer 2008*

- Designed analytical procedures based on ICH guidance to remove genotoxic impurities from API, ensuring product quality in manufacturing and patient safety in clinical trials
- Searched literature and built a FTIR model to optimize molecular imprinting conditions, applied optimal parameters to synthesize solid phase extraction matrices

EDUCATION

University of Illinois **Chicago, IL**

Ph.D. *in Medicinal Chemistry,* GPA: 3.8/4.0 *Expected 2016*

University of Minnesota **Minneapolis, MN**

M.S. *in Analytical Chemistry,* GPA: 3.6/4.0 *2008*

Peking University **Beijing, China**

B.S. *in Geochemistry,* GPA: 3.7/4.0 *2005*

PUBLICATIONS

- Hauck Z, **Huang K**, Li G, van Breemen R. Determination of bisphenol A-glucuronide in human urine using ultrahigh-pressure liquid chromatography/tandem mass spectrometry. *Rapid Commun. Mass Spectrom.* **2016**, *30(3)*, 400-406
- Li G, **Huang K**, Nikolić D, van Breemen R. High-throughput Cytochrome P450 Cocktail Inhibition Assay for Assessing Drug-Drug and Drug-Botanical Interactions. *Drug Metab. Dispos.* **2015**, *43*, 1670-1678
- **Huang K**, Huang L, van Breemen R. Detection of reactive metabolites using isotope-labeled glutathione trapping and simultaneous neutral loss and precursor ion scanning with ultra-high-pressure liquid chromatography triple quadruple mass spectrometry., *Anal Chem.* **2015**, *87*, 3646-3654
- Prins GS, Hu WY, Shi GB, Hu DP, Majumdar S, Li G, **Huang K**, Nelles J, Ho SM, Walker CL, Kajdacsy-Balla A, and Van Breemen RB. Bisphenol A Promotes Human Prostate Stem-Progenitor Cell Self-Renewal and Increases In Vivo Carcinogenesis in Human Prostate Epithelium. *Endocrinology* **2014**, *155(3), 805-817*
- Karalius VP, Harbison JE, Plange-Rhule J, van Breemen RB, Li G, **Huang K**, Durazo-Arvizu R, Mora N, Dugas LR, Vail L, Tuchman NC, Forrester T, Luke A. Bisphenol A (BPA) found in humans and water across three distinctly different levels of development. *Environmental Health Insights* **2014**, *8*, 1-3
- Yuan Y, Qiu X, Nikolić D, Chen SN, **Huang K**, Li G, Pauli GF, van Breemen RB. Inhibition of human cytochrome P450 enzymes by hops (Humulus lupulus) and hop prenylphenols, *Eur. J. Pharmaceut. Sci.* **2014**, *53*, 55-61
- Andreani A, Granaiola M, Leoni A, Locatelli A, Morigi R, Rambaldi M, Varoli L, Cervellati R, Greco E, Kondratyuk T, Park E-J, **Huang K**, van Breemen R, Pezzuto J. Chemopreventive and Antioxidant Activity of 6-Substituted Imidazo[2,1-b]thiazoles. *Eur. J. Med. Chem.* **2013**, *68*, 412-421
- Marler L, Conda-Sheridan M, Cinelli MA, Morrell AE, Cushman M, Chen L, **Huang K**, van Breemen R, Pezzuto JM. Cancer Chemopreventive Potential of Aromathecins and Phenazines, Novel Natural Product Derivatives, *Anticancer Res.* **2010**, *30*, 4873-4882

APPENDIX

Publication Permission from Analytical Chemistry

eic@anchem.acs.org 8:08 AM (10 hours ago)

to me

Dear Ke Huang,

You have my permission to use this article "**Detection of Reactive Metabolites Using Isotope-Labeled Glutathione Trapping and Simultaneous Neutral Loss and Precursor Ion Scanning with Ultra-High-Pressure Liquid Chromatography Triple Quadruple Mass Spectrometry**" in your thesis as long as the correct citations are made as directed in the ACS Thesis/Dissertation Policy and the ACS Journal Publishing Agreement.

Sincerely,

Prof. Jonathan V. Sweedler
Editor-in-Chief
Analytical Chemistry
Phone: 217-244-7359
Fax: 202-513-8699
Email: eic@anchem.acs.org